Nanoporous Thin Film Templates for the Fabrication of Nanowires and Nanotubes

Ph.D. Thesis

NanoSYD, Mads Clausen Institute

University of Southern Denmark

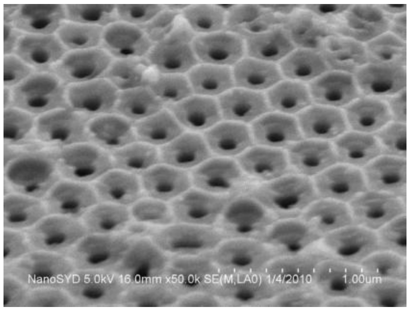

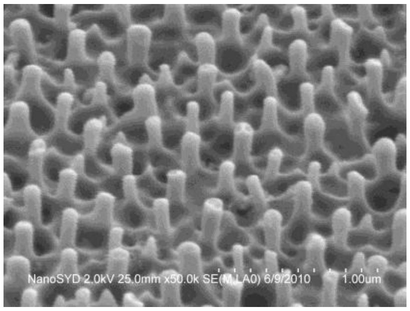

Kirill Bordo

November 30, 2011

Front side images:

Left: scanning electron microscopy image of a thin-film porous anodic alumina template

Right: scanning electron microscopy image of poly(3-hexylthiophene) nanostructures fabricated by template wetting

Preface

This thesis has been submitted as a partial fulfilment of the requirements to obtain the Ph.D. degree at the University of Southern Denmark (SDU). The main part of the work has been carried out at NanoSYD group at Mads Clausen Institute (MCI) in Sønderborg and a smaller part at the Institute for Materials and Surface Technology (IMST) in Kiel, Germany. The project has been supervised by Prof. Dr. Habil. Horst-Günter Rubahn as main supervisor, Dr. Manuela Schiek as project supervisor and Prof. Dr. Habil. Mohammed Es-Souni as co-supervisor. Apart from this thesis, a few other publications have been prepared during the course of this work. They are stated in Appendix A.

I would like to acknowledge several people for their help and support during this project.

First, I would like to thank my advisor Prof. Horst-Günter Rubahn for supervising me in the course of this project as well as for his permanent attention to all aspects of this work. I thank Dr. Manuela Schiek for planning the project activities and for helping me to study new experimental methods and techniques. I am grateful to Prof. Mohammed Es-Souni for supervising me as well as for his support during my work at IMST.

Furthermore, I would like to thank Frank Balzer for supporting the optical measurements on organic nanostructures, Kasper Thilsing-Hansen for help with the AFM measurements and the deposition of thin films as well as Morten Madsen and Michal Radziwon for valuable discussions.

I am grateful to all NanoSYD members (in particular, Jakob Kjelstrup-Hansen, Luciana Tavares, Roana de Oliveira Hansen, Xuhai Liu, Christian Maibohm, Mogens Melskens Petersen, Reiner Hübel, Martin Nørgaard, Jacek Fiutowski) for their help and cooperation in a friendly and creative environment. I would like to thank all members of IMST, especially Salah Habouti, Claus-Henning Solterbeck and Matthias Dietze, for their help and collaboration.

Last but not least, I am grateful to my parents for their enormous support and patience without which making this work would have been impossible.

November 30, 2011

Kirill Bordo

NanoSYD
Mads Clausen Institute (MCI)
University of Southern Denmark
Alsion 2
DK-6400 Sonderborg
Denmark

Abstract

The method of template wetting allows one to fabricate highly ordered arrays of upright standing nanowires or nanotubes from different materials in a controllable manner. In this method, a porous template is filled by an appropriate solution or melt. After selective removal of the template, arrays of nanowires or nanotubes are obtained. Such arrays can be subsequently integrated into e.g. solar cells and other electronic devices.

This thesis is focused on the fabrication of thin-film porous anodic alumina (PAA) templates on different substrates. The fabrication of organic nanowires and nanotubes via melt- or solution-assisted wetting of PAA templates is also studied.

Supported PAA templates were obtained by anodization of thin Al films. Thin Al films produced by evaporation of Al onto different substrates were studied by SEM and AFM. It has been found that the structure and surface morphology of these films depend strongly on the deposition rate, temperature and type of the substrate. In general, maintaining low deposition rate, low substrate temperature and low residual gas pressure allows the fabrication of smooth Al films with low grain size.

The formation of thin PAA films on different substrates (silicon, glass, ITO-glass, mica) and in different electrolytes (oxalic, sulphuric and phosphoric acid) was also systematically studied. It has been found that the structure of such films depends strongly on the structure and morphology of the initial thin Al films as well as on the anodization conditions. Anodization of smooth Al films at optimum conditions leads, in turn, to the formation of highly ordered PAA structures which can be successfully used as templates for the growth of organic nanowires and nanotubes.

A novel method for the fabrication of thin-film PAA templates on free-standing thin-film substrates was developed. The method involves the use

of water-soluble NaCl release layer produced by means of e-beam evaporation in high vacuum. The PAA templates are fabricated via anodization of thin Al films supported by thin layers of e-beam evaporated silicon oxide or aluminum oxide.

The prepared thin-film PAA templates were directly used for the fabrication of poly(3-hexylthiophene) (P3HT) nanotubes by means of melt-assisted wetting. Different architectures of solar cells based on P3HT nanotube arrays and thin films of PCBM were considered.

Additionally, 1D nanostructures from P3HT, poly(9,9-dioctylfluorene-2,7-diyl) (PF8), 2,7-diphenylcarbazole (DPC), zinc phthalocyanine (ZnPc) and perylene-tetracarboxydiimide (PTCDI) were obtained by melt- and/or solution-assisted wetting of commercial PAA membranes (Anodisc^{TM}). Since DPC nanowires were fabricated for the first time by this technique, their morphology and optical properties are discussed in detail.

Dansk Resumé

Skabelon-wettingsmetoden tillader fremstilling af højt ordnede rækker af opretstående nanotråde eller nanotuber af forskellige materialer. I denne metode fyldes en nanoporøs skabelon (template) med en passende opløsning eller smeltemasse. Efter en selektiv fjernelse af skabelonen opnås rækker af stående nanotråde eller nanorør. Denne slags rækker kan dernæst integreres i fx solceller eller andet elektronisk udstyr.

Denne phd-afhandling sætter fokus på fremstillingen af porøse anodiseret aluminium (PAA) tyndfilm skabeloner på forskellige substrater. Fremstillingen af organiske nanotråde og nanorør gennem smeltemasse- eller opløsning-assisteret wetting af PAA-skabeloner er også blevet undersøgt.

Assisterede PAA-skabeloner blev skaffet ved hjælp af anodisering af tynde Al-film. De tynde Al-film der blev produceret via Al pådampning på forskellige substrater blev undersøgt med SEM og AFM. Det blev fundet, at disse films struktur og overflademorfologi afhænger væsentligt af pådampningsrate, temperatur samt substrat-type. Generelt set muliggøres fremstillingen af glatte Al-film med en lille kornstørrelse ved at holde en lav pådampningsrate, en lav substrat-temperatur, samt et lavt resterende gastryk.

PAA-filmdannelse på forskellige substrater (silicium, glas, ITO-glas, mica) med anvendelse af forskellige elektrolytter (oxalsyre, svovlsyre fosforsyre) er også blevet systematisk undersøgt. Det blev fundet, at disse films struktur afhænger betydeligt af de initiale tynde Al-films struktur og morfologi, samt anodiseringsvilkår. Anodiseringen af glatte Al-film under optimale vilkår fører til dannelsen af højt ordnede PAA-strukturer, der med succes kan anvendes som skabeloner til dyrkning af organiske nanotråde og nanotuber.

En ny metode til fremstilling af tyndfilms PPA-skabeloner på fritstående tyndfilms-substrater er blevet udviklet. Denne metode inddrager anvendelsen af et vandopløseligt NaCl-frigørelseslag opnået

ved hjælp af e-beam-pådampning i højt vakuum. PPA-skabelonerne er fremstillet via tyndfilms anodisering assisteret med tynde lag af e-beam-pådampet silicium-oxid eller aluminum-oxid.

De fremstillede tyndfilms PPA-skabeloner blev direkte anvendt i fremstillingen af poly(3-hexylthiophene) (P3HT) nanorør ved hjælp af smeltemasse-assisteret wetting. Forskellige solcelle arkitekturer baseret på rækker af P3HT-nanorør og tynde PCBM-film blev taget i betragtning.

Endvidere blev 1D-nanostrukturer af P3HT, poly(9,9-dioctylfluorene-2,7-diyl) (PF8), 2,7-diphenylcarbazole (DPC), zinc phthalocyanine (ZnPc) samt perylene-tetracarboxydiimide (PTCDI) opnået ved hjælp af smeltemasse- eller opløsning-assisteret wetting af PAA-membraner (Anodisc^{TM}). Da DPC-nanotråde blev fabrikeret for første gang med anvendelsen af denne teknik, omtales deres morfologiske og optiske egenskaber i detaljer.

Contents

Chapter 5. Nanowires and Nanotubes from π-Conjugated Organic Materials Fabricated by Template Wetting 73

Chapter 6. Template Fabrication of Nanostructures for Bulk Heterojunction Solar Cells...95

Chapter 1. Introduction

1.1. ANODIZATION OF ALUMINUM

1.1.1. Anodization of thick Al foils

Anodic oxidation (or “anodization”) of aluminium has been widely used for several decades to produce protective and decorative coatings on its surface [1]. The development of electron microscopy techniques made it possible to observe the microstructure of the obtained alumina films [2].

It was found that, depending on the process conditions, two types of aluminium oxide may exist. If Al is anodized in neutral or basic solutions (pH > 5) a flat, non-porous, featureless insulating “barrier” oxide forms. When Al is anodized in an acidic electrolyte (usually sulphuric, oxalic or phosphoric acid), deep pores, having diameters from 5 to 100 nm and lengths of a few microns, are formed. This type of oxide is referred to as “porous anodic alumina” (PAA). The bottom of each pore also consists of a 10-100 nm thick “barrier layer” [2-6].

It has been known since 1960-s, that anodization of Al in common acidic electrolytes yielded PAA structures with approximately hexagonal pore arrangements. In 1995, Masuda and Fukuda [7] reported the two-step anodization of Al films which allowed the fabrication of highly-ordered PAA structures. In this procedure, the disordered PAA film formed during the first anodization step was etched away selectively to leave periodic concave features on the surface of the Al host. During the second anodization step carried out at the same conditions as the first step, the concave features acted as pore nucleation sites, and a highly-ordered PAA film could be obtained. The use of pre-patterning methods, such as nanoimprint lithography, allowed the fabrication of perfectly ordered nanopore arrays over large areas [8, 9].

Optionally, the Al host can be selectively dissolved in $HgCl_2$ solution and the barrier oxide which remains in the bottom of each pore can be dissolved in phosphoric acid. In such a case, a thick open-through PAA membrane is obtained [9-11]. Instead of wet etching, ion-beam sputtering can be used for the barrier layer removal [12, 13].

1.1.2. Anodization of thin Al films

During the last few years, the fabrication of PAA structures by anodization of thin Al films on different supports has been attracting great interest. In most cases, Si wafers are used as substrates for the deposition of thin Al films [14-26]. Depending on the purpose of the final PAA structures, intermediate (e.g. conductive) layers can be introduced [18, 19, 21]. Recently, thin PAA films on ITO-coated glass substrates were successfully fabricated [27-29].

Thin supported Al films are usually anodized at the same conditions which are applied for thick Al foils. However, for ultrathin (20-50 nm) Al films, it was found that applying the “common” anodization voltages leads to the breakdown of the formed alumina films [22, 26]. In such cases, lower voltages were applied. For example, the maximum applicable voltage for 30 nm thick Al films was 30 V in oxalic acid and 20 V in sulphuric acid.

1.1.3. PAA formation mechanism

To explain the fact of self-ordering in PAA structures during anodization, the so-called mechanical stress model has been proposed [6, 31-33]. The mechanism of the self-ordered PAA formation can be briefly described as follows.

At the beginning of the anodization, the “barrier” film which consists of non-conductive aluminium oxide covers the entire surface of the Al. At this stage, a drastic decrease of the current density is usually observed. The electric field is focused locally on the concave features of the surface. This leads to field-enhanced and/or temperature-enhanced dissolution of the formed oxide and to the growth of the pores. This stage is characterized by an increase of the current density. Some pores might stop growing due to the competition between the pores, and the current density slightly decreases again. Finally, the pores grow in a stable manner and the current density stays approximately constant. Due to the repulsive forces which appear between the neighbouring pores, self-organization occurs. The resulting PAA film has a characteristic hexagonal ordering of the pore channels.

1.1.4. Factors determining the morphology of PAA structures

The main process parameters which affect the morphology of PAA structures obtained by anodization of Al are the applied potential, the type and concentration of the electrlolyte and the temperature [5, 6, 9, 31-36].

It is known that interpore distance of the formed PAA structures is linearly proportional to the applied voltage with the proportionality constant being approximately 2.5-2.8 nm/V. The thickness of the barrier layer can be estimated as a half of the interpore distance [5, 9].

The choice of the electrolyte for the self-organized growth of PAAs is restricted. In most cases, sulphuric, oxalic and phosphoric acid are employed. Usually, sulphuric acid is used at relatively low voltages (15-30 V), oxalic acid is employed at intermediate voltages (30-60 V) and phosphoric acid is used at high voltages (160-195 V). The reason for this is the difference in conductivity and pH values of these electrolytes. For example, sulphuric acid has a rather high conductivity and the anodization of Al in sulphuric acid at voltages higher than about 30-40 V results in the breakdown of the oxide layer. The pore size is determined by the pH value of the electrolyte. The potential threshold for the field-enhanced dissolution at the pore tip decreases with a decrease of the pH value, which leads to smaller pore diameters. That explains the fact that the widest pores are obtained in phosphoric acid (which has the highest pH in this row), while in oxalic and sulphuric acid, pores with lower diameters are formed [5, 9, 34-36].

In order to prevent the formed oxide structure from being dissolved in the electrolyte, the temperature during the anodization is adjusted to be lower than 15°C (about 5°C for the anodization at high voltages). In addition, local heating at the bottom of the pores leads to inhomogeneous distribution of the electric field, which results in electrical breakdown of the oxide. The pore growth rate is also affected by the temperature, being lower at lower temperatures [9, 34].

There are a few other important issues related to the pore ordering in PAAs. The purity of the Al samples meant for anodization should be rather high (normally, about 99.99% grade Al is used). The Al samples are usually annealed at about 500°C for several hours to increase the grain size. The surface of Al is smoothened by electropolishing which is commonly performed in perchloric acid – ethanol mixture. Finally, the electrolyte is kept vigorously stirred during the anodization. Stirring allows more effective heat removal from the sample and also ensures more homogeneous diffusion of anions from the electrolyte into the pore channels [7, 9, 37, 38].

1.1.5. Applications of ordered PAA structures

The main application of PAAs in nanotechnology is their use as templates for the fabrication of nanowires and nanotubes (see Section 1.2.). If compared to macroporous silicon templates and track-etched polycarbonate membranes, PAA templates have better ordering of the pores. The size of the pores can be easily tuned by changing the electrolyte and the anodization voltage [39-41].

Another important application of PAA films is the production of nano-dot arrays on different substrates. Such arrays can be made using PAA films as masks; that provides a cheap alternative to traditional lithography techniques [14, 24, 42].

Potential use of highly ordered PAA structures in magnetic recording devices has attracted grate attention in the last few years [1, 40]. The possibility to use ordered PAA films in optical sensors has also been considered [43, 44].

1.2. TEMPLATE-BASED FABRICATION OF 1D NANOSTRUCTURES

Template-based synthesis of nanowires and nanotubes has been the main application of ordered PAAs during the last 15 years [39-41]. The main techniques which utilize PAA templates for the preparation of 1D nanostructures are electrochemical deposition, electrophoretic deposition and template wetting.

Electrochemical deposition involves oriented diffusion of charged reactive species through a solution when an external electric field is applied. The charged species are reduced at the deposition surface which also serves as an electrode. In general, this method is applicable for electrically conductive materials, such as metals alloys, semiconductors, electrically conductive polymers and oxides. As a template, either a free-standing PAA membrane with a conductive layer blocking one of its sides or a thin-film PAA template on a conductive support can be used [40]. This technique was employed to produce e.g. metallic nanowire arrays [21, 40, 45].

Electrophoretic deposition uses oriented motion of charged particles in a colloidal solution under an electrical field. If particles are positively charged, the deposition takes place at the cathode. Otherwise, it occurs on the anode. Templates for electrophoretic deposition are prepared in the same manner as the ones dedicated for electrochemical deposition [40]. By this method, nanostructures from e.g. phthalocyanines [46-49] and perylene derivatives [50] were fabricated.

In the method of template wetting, a PAA template is filled by a solution which contains the needed material, or a melt. Evaporation of the solvent (or solidification of the melt) results in the formation of nanowires or nanotubes in the template pores [51]. This technique has been used to produce 1D nanostructures from both polymers [52-56] and small organic molecules [57, 58].

The needed material can also be introduced into the template pores by vacuum evaporation [40]. In such a way, nanostructures from cabazole, naphthalene, phenanthrene, and anthracene were obtained [59].

Chapter 2. Thin Al Films: Microstructure and Surface Morphology

2.1. INTRODUCTION

In general, porous anodic alumina (PAA) templates can be obtained by anodization of either thick (tens of micrometers) Al foils or thin (from tens of nanometers to several micrometers) Al films deposited onto an appropriate substrate. It is known that during anodization of Al the pores are preferentially nucleated at concaves and grooves on the surface, where the local electric field appears to be higher [1, 6, 31-33]. Therefore it is important to ensure large areas on the Al surface which are flat and microscopically smooth (free from trenches, hillocks, etc.). In order to ensure good pore ordering and surface quality of the final PAA templates, standard pretreatments are employed, such as thermal annealing and electropolishing. Thermal annealing of Al foils allows formation of large grains and wide flat areas on the surface of Al [7, 9]. Electropolishing removes protruding features from the Al surface; in the case of optimal process parameters it allows formation of very smooth surface on a big scale [37, 38]. For thin (a few hundreds of nanometers) Al films such pretreatments are not applicable. Annealing of such films at high temperatures leads to the growth of hillocks [60]; electropolishing might remove too much material from the film and even dissolve it completely. Thus, the preferred way of improving the surface quality of thin Al films is the careful control over the deposition parameters which influence the film microstructure and surface morphology.

The properties of thin Al films produced by e-beam or thermal evaporation and DC- or RF-sputtering have been extensively studied by a number of research groups [60-78]. It is known that structural and therefore also electrical and optical properties of thin metallic films are affected by a few factors, namely by the type of the substrate [79-81], the thickness of the film [67, 68], the deposition rate [68, 69, 71, 80-82], the temperature of the substrate [64, 66, 71, 78, 81], the annealing conditions [65, 72, 75] and the background gas composition [63, 69].

The deposition rate is one of the most important parameters influencing the structure and surface morphology of the resulting thin films. In principle, this parameter can be readily controlled during the fabrication process. Semaltianos [68] studied thin Al films produced on quartz substrates by evaporation from a boat at rates from 0.1 to 2 nm/s. It was found that the root mean square (rms) roughness of the 22 nm thick Al films increases from about 3.2 to 5 nm with an increase of the rate from 0.2 to 1.5 nm/s. Qui et al. [69] investigated the influence of the deposition rate on the structure, composition and resistivity of thin Al films produced by e-beam evaporation on glass at two rates: 0.17 and 0.55 nm/s. The film prepared at higher deposition rate had larger grain size but lower roughness than the one made at lower rate. Higo et al. [71] did not observe any change in the surface roughness of 200 nm thick evaporated Al films on mica as the deposition rate increased from 0.5 to 2 nm/s. Data on the rate-dependent properties of thin evaporated Al films on silicon, as well as data for a wide range of deposition rates for glass and mica, are lacking so far in the literature.

In this chapter, different techniques for improving the surface quality of Al foils and thin Al films will be considered. The influence of mechanical and electrochemical polishing on the surface morphology of Al foils will be briefly discussed. Particular attention will be given to the influence of deposition rate and substrate temperature on the surface morphology of thin Al films.

2.2. EXPERIMENTAL DETAILS

2.2.1. Pretreatments of Al foils

Thick (0.1 mm) Al foils were purchased from Goodfellow. The foils were cleaned by ultrasonication in acetone for 15 min. After that, the foils were polished either mechanically or electrochemically.

Mechanical polishing was made with the help of a hand-held drilling machine fitted with wool polishing discs (pellets). Commercial diamond polishing pastes (particle size from 0.25 to 7 μm) were used. The polishing has been made manually, typically during a few minutes, until a mirror-like surface was obtained.

Electropolishing was performed in a perchloric acid - ethanol (1:4) solution in a commercial electropolishing setup (Struers LectroPol-5) at the voltage of 40 V at 10°C for 30-40 s (according to [37, 38]). Alternatively, electropolishing was made in a 15% Na_2CO_3 and 5% Na_3PO_4 ("Brytal") solution at the voltage of 2 V at 80-82°C for 30 min. in a lab-made setup consisting of two electrodes dipped into an electrolyte bath kept at constant temperature (according to [37, 83]).

2.2.2. Deposition of thin films

For the deposition of thin Al films, a conventional electron beam evaporation system (either Edwards Auto 500 or Cryofox 600 Explorer) equipped with an oil-free turbomolecular pumping system was used. The film thickness and deposition rate were controlled by a quartz microbalance. Aluminum films with a thickness ranging from 100 nm to 5 μm were deposited on silicon, glass, ITO-coated glass and mica substrates using a high-purity (99.99%) Al target placed into an intermetallic (BN-TiB_2) crucible liner. For some of the samples, Al was evaporated from a resistively heated molybdenum boat or a tungsten filament. Some of the films were also produced by RF-sputtering of a high-purity (99.999%) Al target in a conventional sputtering system (Cryofox 600 Explorer). The Ar pressure in the deposition chamber during sputtering was about 10^{-1} Pa.

For the investigation of the deposition rate effects on the film morphology, the films were produced at 5 different evaporation rates: 0.10 ± 0.02, 0.20 ± 0.02, 0.5 ± 0.1, 1.0 ± 0.1 and 2.0 ± 0.2 nm/s. The required evaporation rate was achieved by adjusting the e-beam current. The pressure in the chamber during deposition was better than $1 \cdot 10^{-3}$ Pa. The acceleration voltage of the electron gun was fixed at 4.76 kV and the e-beam current was kept in the range between 20 and 80 mA, depending on the required evaporation rate and the load of the crucible.

For the investigation of the deposition temperature effect on the film structure and morphology, the films were deposited in the range between room temperature (25°C) and (roughly) 450°C. In each case, the substrate was fixed on a flat copper plate which was kept in a firm contact with a resistively heated molybdenum plate. The temperature of the substrate for different values of the current was roughly estimated by placing very small (a fracture of mm in diameter) pieces of pure metals onto the substrate and fixing the values of current at which they started melting. For that purpose, the following metals were used: Sn (T_m = 232°C), Pb (T_m = 327.5°C) and Zn (T_m = 419.5°C).

Silicon (Si (100), *p*-type, resistivity 1-100 $\mathrm{Ohm \cdot cm^{-1}}$) and glass (BK7) substrates were prepared by sawing 1x1 or 2x2 $\mathrm{cm^2}$ square pieces from respective wafers in a commercial programmable wafer-sawing unit. Sometimes Si wafers were also cleaved manually with the help of a diamond tip. In some cases, microscope glass slides (from Thermo Scientific) were used instead of BK7 glass substrates. The substrates were pre-cleaned by ultrasonication in acetone and ethanol (5 min. in each solvent) followed by oxygen plasma etching (5 min. at 300 W, Branson IPC 3000 barrel plasma system). Muscovite mica substrates (grade V-3, Plano GmbH) were cleaved in air and transferred thereafter immediately into the deposition chamber.

For some of the substrates, a thin (typically 5-15 nm; 1-2 nm for the case of ITO-coated glass) Ti layer was applied to ensure good adhesion of Al film. The typical deposition rate for Ti was 0.05-0.1 nm/s. In order to improve the adhesion of thin Al films deposited onto ITO coated glass, post-depositional annealing was applied. The films were annealed at 150-200°C for 3-5 hours.

2.2.3. Characterization of thin films

The SEM imaging of the deposited thin Al films was performed in a commercial instrument (Hitachi S-4800) with an acceleration voltage of

2-3 kV. The ranges of grain size of the films were obtained by picking randomly 20 grains on each SEM image and estimating their Feret diameters along the horizontal direction.

The AFM characterization was performed using a Dimension 3100 AFM (Digital Instruments, Veeco, CA) operated in tapping mode. The topographic and phase images were recorded simultaneously using a standard silicon tip with radius 10 nm. The spring constant of the cantilever was between 20 and 100 N/m. Root mean square (rms) surface roughness values were determined for each sample on an area of 30 X 30 μm^2. Root mean square (rms) surface roughness values were calculated using free SPM analysis software (Gwyddion [84]).

2.3. RESULTS AND DISCUSSION

2.3.1. Mechanical polishing of Al foils

A top-view SEM image and an AFM scan of an untreated Al foil are shown in Fig. 2.1. It can be seen that the surface of the foil is very rough and exhibits a number of almost parallel grooves and ridges. The widths of the ridges range from several hundreds of nanometers to several micrometers. Probably these features appear during the rolling step of the foil manufacturing.

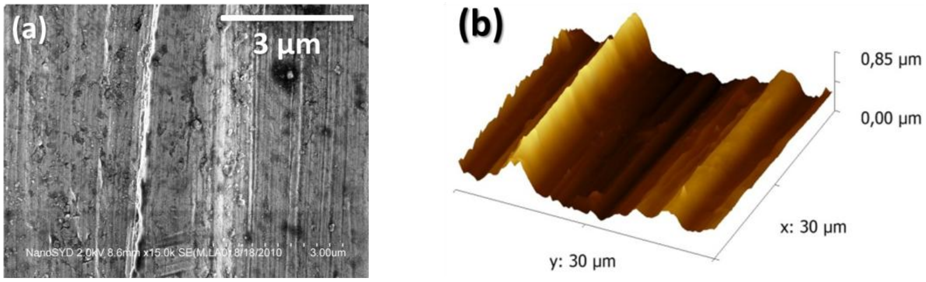

Figure 2.1. Top-view SEM image (a) and AFM scan (b) of untreated Al foil.

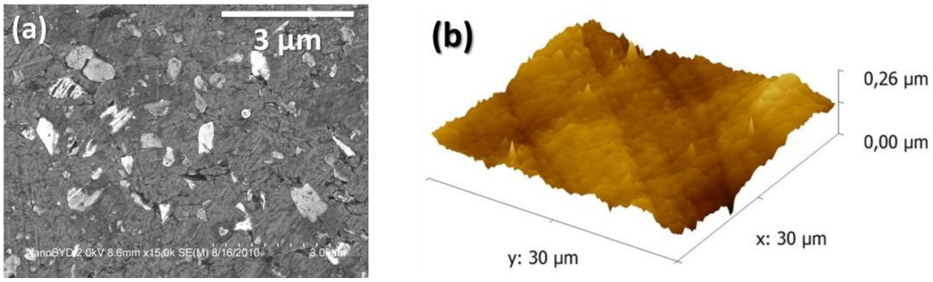

Figure 2.2. Top-view SEM image (a) and AFM scan (b) of Al foil mechanically polished with 2 diamond suspensions having different particle sizes: first 7 μm and then 1 μm.

Mechanical polishing allows significant smoothening of the ridges and trenches and decreasing of the overall surface roughness. For all diamond particle sizes, such polishing leads to a mirror-like surface. However, the result is not satisfactory at the micro-scale. The use of 7 μm large particles results in the formation of deep grooves all over the sample surface. Some of the particles get trapped on the Al surface. However, most of them can be easily removed by ultrasonication in acetone. If smaller particles (0.25 or 1 μm) are applied, most of them are trapped in the trenches at the initial stage of the polishing. The trapped particles cannot be removed even by prolonged ultrasonication. As can be seen from Fig. 2.2, the same takes place if the polishing with big particles (7 μm) is followed by polishing with smaller ones (1 μm).

It can be considered that a big number of incorporated dielectric particles will not allow the formation of a uniform PAA film during anodization. Thus mechanical polishing with the use of hard microparticle suspensions cannot be used for the smoothening of Al foils meant for the further anodization.

2.3.2. Electropolishing of Al foils

In the present work, Al foils were electropolished either in perchloric acid - ethanol (1:4) solution or in 15% Na_2CO_3 and 5% Na_3PO_4 (“Brytal”) solution.

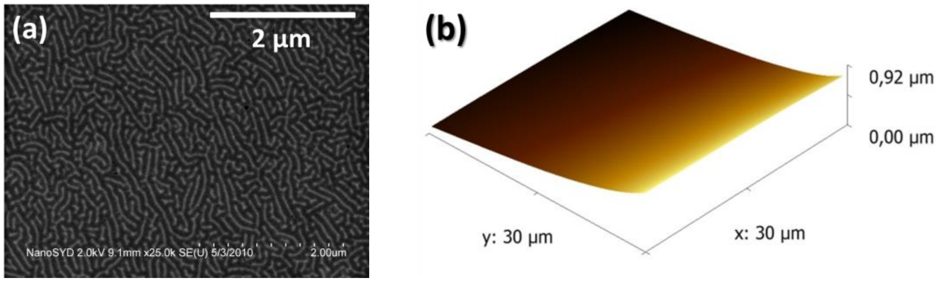

Figure 2.3. Top-view SEM image (a) and AFM scan (b) of an Al foil electropolished in perchloric acid - ethanol (1:4) solution at the voltage of 40 V at 10°C for 40 s.

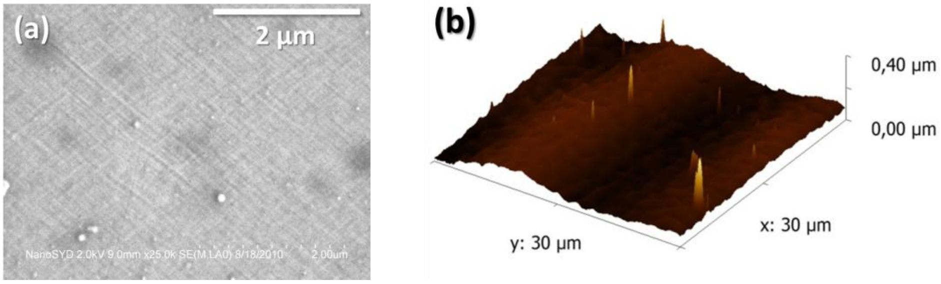

Figure 2.4. Top-view SEM image (a) and AFM scan (b) of an Al foil electropolished in Brytal solution at the voltage of 2 V at 80°C for 30 min.

As can be seen from Fig. 2.3a, electropolishing of Al in perchloric acid - ethanol solution results in the formation of periodic curved trenches having widths of about 100 nm. The formation of similar surface features at these electropolishing conditions has been observed previously [37, 38]. From a 30 X 30 μm^2 AFM scan (Fig. 2.3b) it can be seen that the Al surface is very smooth on a big scale. Here, the periodic trenches mentioned above cannot be seen because of a high scanning rate.

Electropolishing of Al in Brytal solution leads to strait trenches (or ridges) which are oriented along two directions (Fig. 2.4a). On the surface of the sample, small (about 1 µm in diameter) “bumps” can be noticed. As can be seen from a 30 X 30 μm^2 AFM scan (Fig. 2.4b), few-µm wide ridges still remain on the Al surface.

Perchloric acid - ethanol solution is known to be effective for electropolishing aluminum and is the most common electrolyte for such treatments in the lab practice [37, 38]. However, strong oxidizing properties of perchloric acid make the use of this mixture rather dangerous. The use of Brytal solution allows getting satisfactory results in terms of Al surface roughness while being much safer for handling. The use of this electrolyte can therefore be considered as a good alternative, especially when a commercial electropolishing device is not available.

2.3.3. Surface quality of different substrates for the deposition of thin Al films

In order to compare the surface morphology of the common substrates (glass, Si, mica) used for the deposition of thin Al films, AFM scans of these substrates were acquired. For each of the substrates, 5 scans of the same area (30 X 30 μm^2) and at the same scanning parameters were made.

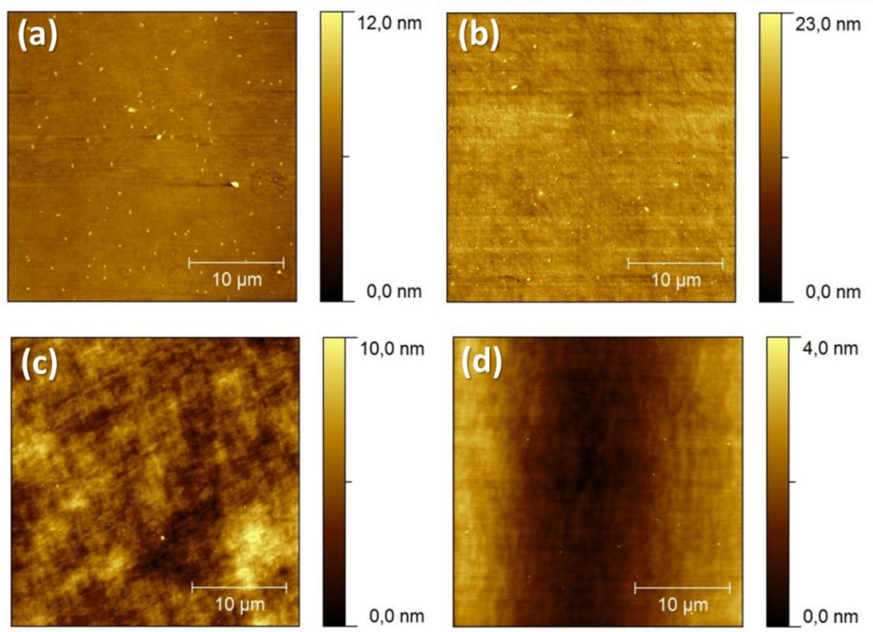

Figure 2.5. AFM scans of the bare substrates used for the deposition of thin Al films.

The surface of a microscope glass slide (Fig 2.5a) is rather smooth. However, a number of sub-μm sized particles can be seen on the surface. These might be some dirt particles which were not removed by ultrasonication and plasma treatment. On the surface of a BK7 glass substrate (Fig. 2.5b), randomly distributed grooves are seen. These grooves probably appear during the sawing of the wafer. The surface of a Si substrate (Fig. 2.5c) exhibits few-nm high features which are probably left after the industrial polishing. A cleaved mica sheet has an extremely smooth surface without any noticeable features (Fig. 2.5d).

The rms surface roughness values, obtained for all of the substrates from the AFM measurements, are presented in Table 2.1. It can be seen that both types of glass slides show almost similar roughness values (around 1 nm), while the roughness of Si substrates is a bit higher. Mica substrates show a significantly lower rms roughness (about 0.25 nm) which should also result in smoother Al films after deposition.

Table 2.1. Rms surface roughness (nm) of different substrates for Al thin film deposition.

Substrate	Rms roughness, nm
Microscope glass slide	0.98 ± 0.28
BK7 glass (sawed from a wafer)	1.06 ± 0.22
Si (sawed from a wafer)	1.24 ± 0.20
Mica	0.25 ± 0.05

From here onwards, BK7 glass slides will be called simply “glass slides”, since only this type of glass substrates was used for the deposition of Al.

2.3.4. Thin Al films: the influence of the deposition rate on the surface morphology

For the investigation of the deposition rate effects on the film morphology, 100 nm thick Al films were prepared. The Al films were fabricated on glass, Si and mica substrates at the following rates: 0.10 ± 0.02, 0.20 ± 0.02, 0.5 ± 0.1, 1.0 ± 0.1 and 2.0 ± 0.2 nm/s.

SEM imaging of thin evaporated Al films made it possible to observe the microstructure of the films as a function of deposition rate and to estimate the grain size. Fig. 2.6 shows representative SEM images of thin Al films evaporated onto Si substrates at rates from 0.1 to 2 nm/s.

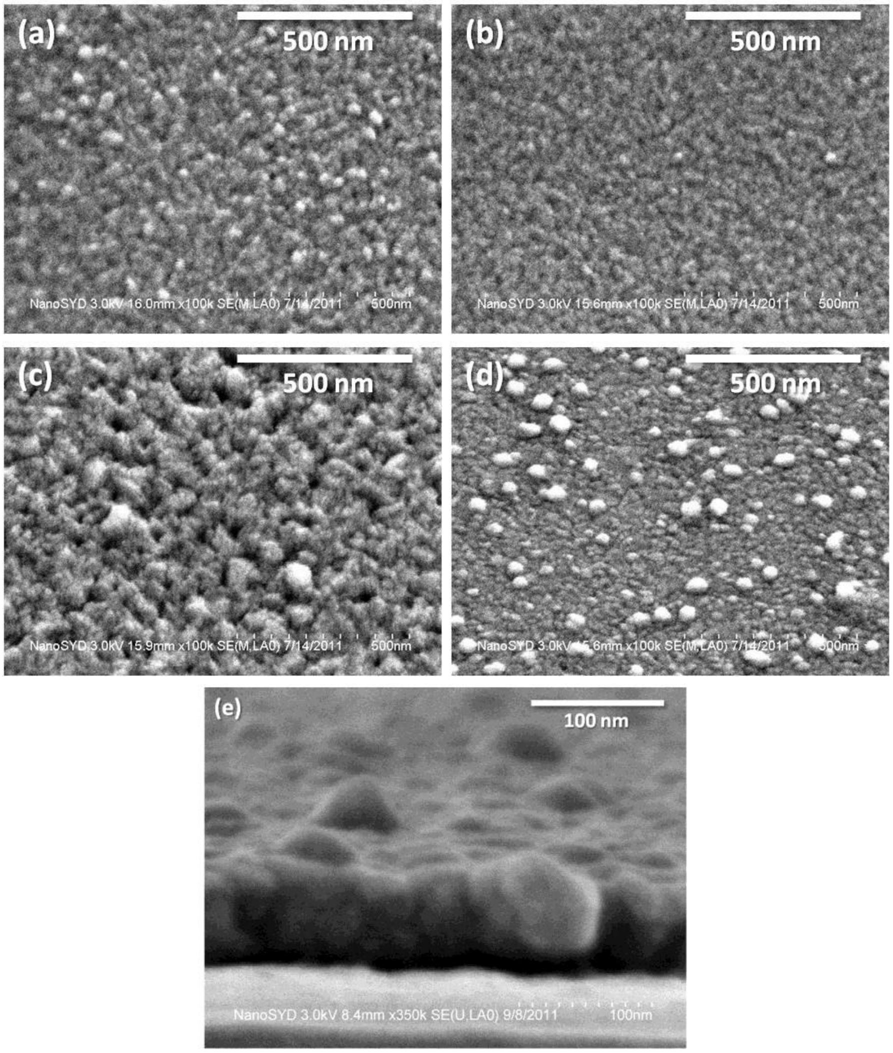

Figure 2.6. SEM images of thin Al films produced on Si substrates at different deposition rates: 0.1 nm/s (a), 0.5 nm/s (b), 1 nm/s (c) and 2 nm/s (d, e); (e) is the cross-sectional view of the film shown on (d).

In order to achieve a better contrast for the film structure, the top view images (Fig. 2.6, a-d) were obtained with the SEM stage being tilted by 45° with respect to the horizontal position. For all of the films, a grainy surface structure with well-defined individual grains and voids between them is observed. The films produced at the lower deposition rate (0.1 nm/s) exhibit a rather smooth grainy surface. The grains have spherical or oval shape and are almost uniform in size. The films produced at higher rates (1-2 nm/s) exhibit single outgrowths (hillocks) protruding out from the film surface. The density of the hillocks increases with an increase in the deposition rate.

The ranges of grain size (nm) of the deposited thin Al films, estimated from the SEM images, are presented in Table 2.2 (the grain sizes were estimated as Feret diameters of the grains along the horizontal direction).

Table 2.2. Ranges of grain size (nm) of thin Al films evaporated on glass, Si and mica substrates at different deposition rates, as estimated from SEM images.

Deposition rate, nm/s	Substrate		
	Glass	Si	Mica
0.1	20-40	15-30	15-30
0.2	20-40	15-40	15-30
0.5	20-50	20-40	20-40
1	30-70	20-70	30-70
2	40-100	30-80	40-100

It can be seen that the average grain size increases monotonically with increase in deposition rate. At low deposition rates (0.1-0.2 nm/s) the films consist of small grains with almost uniform size (in the range between 15 and 40 nm). At higher rates (1-2 nm/s) large hillocks having size of 50-100 nm appear on the film surface. At the same time, there are still a lot of smaller (20-50 nm) grains in the areas between the hillocks. Thus, the grain size distributions of the as-deposited Al films become wider with increase in deposition rate.

The surface morphology of the thin Al films on different substrates was investigated by tapping mode AFM as a function of deposition rate. Root mean square surface roughness values were determined on an area of 30 X 30 μm^2. For each of the samples, including bare glass, Si and mica substrates, 5 scans of the same area at the same scanning parameters were performed.

Fig. 2.7 shows typical AFM scans of 100 nm thick Al films evaporated onto Si substrates at two deposition rates: 0.5 nm/s and 2 nm/s. It can be seen that at the lower deposition rate of 0.5 nm/s (Fig. 2.7a) the Al film is rather smooth but exhibits a grainy morphology. For the higher deposition rate of 2 nm/s (Fig. 2.7b), the same kind of surface morphology is observed; however, the film consists of bigger grains and there are more big hillocks on the surface.

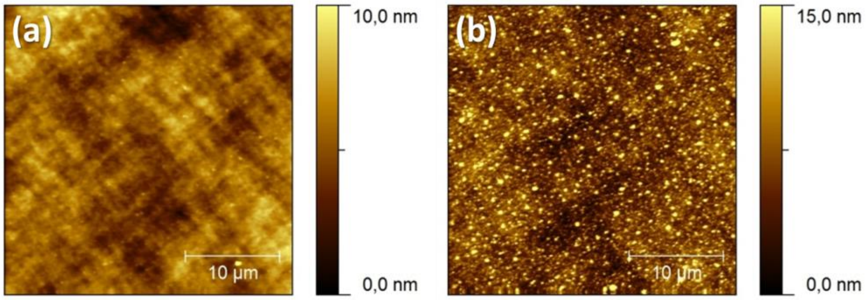

Figure 2.7. AFM images (30 X 30 μm^2) of 100 nm thick Al films evaporated on Si substrates at 0.5 nm/s (a) and 2 nm/s (b).

In Table 2.3, rms surface roughness for thin Al films, produced on different substrates at different deposition rates, are summarized.

As can be seen from the data presented, the rms roughness of as-produced Al films increases significantly as the deposition rate is increased from 0.1 to 2 nm/s. For low rates (0.1-0.2 nm/s) the roughness of the films correlates well with the roughness of the bare substrates. In particular, the films deposited on mica are much smoother than the ones evaporated on glass and Si.

Table 2.3. Rms surface roughness (nm) of thin Al films evaporated on glass, Si and mica substrates, as a function of deposition rate. The mean values are obtained from 5 scans of 30 X 30 μm^2 size on each sample.

Deposition rate, nm/s	Substrate		
	Glass	Si	Mica
0 (bare substrate)	1.06 ± 0.22	1.24 ± 0.20	0.25 ± 0.05
0.1	1.12 ± 0.09	1.25 ± 0.10	0.67 ± 0.11
0.2	1.23 ± 0.13	1.30 ± 0.18	1.10 ± 0.17
0.5	1.6 ± 0.5	1.51 ± 0.25	1.46 ± 0.15
1	2.0 ± 0.6	1.73 ± 0.19	1.8 ± 0.4
2	4.1 ± 0.7	3.6 ± 0.7	3.8 ± 0.6

In the present work, the microstructure of thin evaporated Al films was observed and evaluated by SEM and AFM. The former technique provides general information about the surface structure (shape and size of grains), while the latter technique allows quantitative characterization of the surface morphology, including e.g. the determination of surface roughness.

As can be seen from SEM images (Fig. 2.6), all the Al films exhibit a grainy structure with well-defined columnar grains separated by voids. This kind of structure was observed for many evaporated and sputtered films [85-89]. In order to describe it, the so-called structure zone model was proposed [85, 86]. According to this model, the film surface structure is dominated by the substrate temperature (T). There are 3 main structure zones with boundary temperatures $T_1 = 0.3T_m$ and $T_2 = 0.5T_m$, where T_m (K) is the melting point of the film material. At relatively low temperatures ($T < T_1$, zone 1), the surface diffusion of adatoms is too weak to ensure the filling of the shadowed surface regions (self-shadowing effect). That leads to the formation of the characteristic well-defined columnar structure. The films deposited at higher temperatures ($T_1 < T < T_2$, zone 2) exhibit much larger columns with domed tops. The surface diffusion of adatoms becomes sufficient which leads to surface recrystallization under these conditions. The films deposited at $T > T_2$

(zone 3) consist of big grains with flat and faceted faces [86].

In the present work, the Al films were deposited at room temperature (20°C, $T/T_m = 0.31$ for Al) which corresponds to the boundary between zone 1 and zone 2. Even if a slight heating of the substrates by radiation from the evaporation source takes place, that should not lead to any significant changes in the films structure, according to the zone model. Therefore, the observed difference in the structure and morphology of the films is most probably caused by deposition rate effects.

From the SEM images, the average grain size of the Al films prepared at different evaporation rates was estimated. The results are presented in Fig. 2.8. It can be seen that for all substrates the average grain size increases monotonically with increase in deposition rate. For films deposited onto different substrates at the same rate, the grain size ranges are approximately the same (see also Table 2.2).

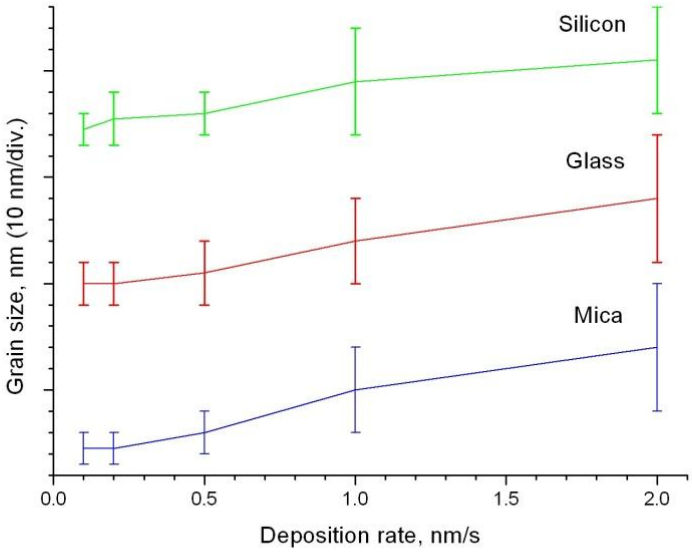

Figure 2.8. Range of grain size (estimated from SEM images) of thin Al films evaporated on glass, Si and mica substrates as a function of deposition rate.

The observed dependence of grain size on deposition rate is consistent with the results obtained by Semaltianos [68] for thin evaporated Al films on quartz and also with the results reported by Cai et al. [82] for thin evaporated Ti films on glass. This trend can be explained by considering the processes of surface diffusion of adatoms and nucleation and coalescence of metal clusters during deposition [89]. The Al atoms arriving onto the substrate surface can diffuse along the surface and form clusters which can in turn contribute to the formation of crystallites (grains). At low evaporation rates and low substrate temperatures, the surface diffusion of the Al atoms and formation of Al clusters is not prominent. Therefore the density of clusters (nuclei) which can potentially coalesce to form grains is small, resulting in a small grain size. At higher deposition rates, the number of Al atoms arriving onto the surface per unit time is higher. Consequently the number of nuclei formed on the surface is bigger which leads to the formation of bigger grains.

In addition to the mechanism described above, the residual gases such as oxygen are considered to affect the growth of the individual grains [69, 89]. The adsorbed oxygen and/or oxide precipitates, which accumulate on the surface of growing crystallites, can suppress the crystallite growth. The ratio of the number of residual gas atoms impinging on the substrate or the film surface to the number of film atoms arriving to the substrate or the film surface per time and area (in other words, the concentration of residual gas atoms in the film) is inversely proportional to the deposition rate [69]. Thus it can be assumed that at given temperature, pressure and residual gas composition, the concentration of residual gas atoms in the film decreases by a factor of 20 with increase in the deposition rate from 0.1 to 2 nm/s. Therefore increasing the deposition rate within the stated range should significantly weaken the influence of the residual gas atoms on the grain growth and allow the formation of bigger grains.

Surface roughness of metal thin films and coatings is known to influence their properties (such as wear and corrosion resistance, reflectivity, etc.) which are critical for practical applications. In the present work, the surface roughness of the thin evaporated Al films was determined from AFM data. For each of the samples 5 scans of the same area (30 X 30 μm^2) at the same scanning parameters were obtained. The dependence of the rms surface roughness on the deposition rate is shown in Fig. 2.9 (for uncertainties, refer to Table 2.3).

It can be seen that the rms roughness of the Al films on all substrates increases monotonically with increase of the deposition rate. These results agree with the data reported by Semaltianos [68] but they are not consistent with the data presented by Qui et al. [69] who observed a decrease in the roughness of Al films on glass from 2.5 to 1.5 nm with an increase of deposition rate from 0.17 to 0.55 nm/s. However in the latter study only single values of roughness were presented which were determined from very small areas (0.5 X 0.5 μm^2). In such a case the value of surface roughness on a bigger scale (tens of μm), arising from the large grains and hillocks formed at high deposition rates, might be underestimated.

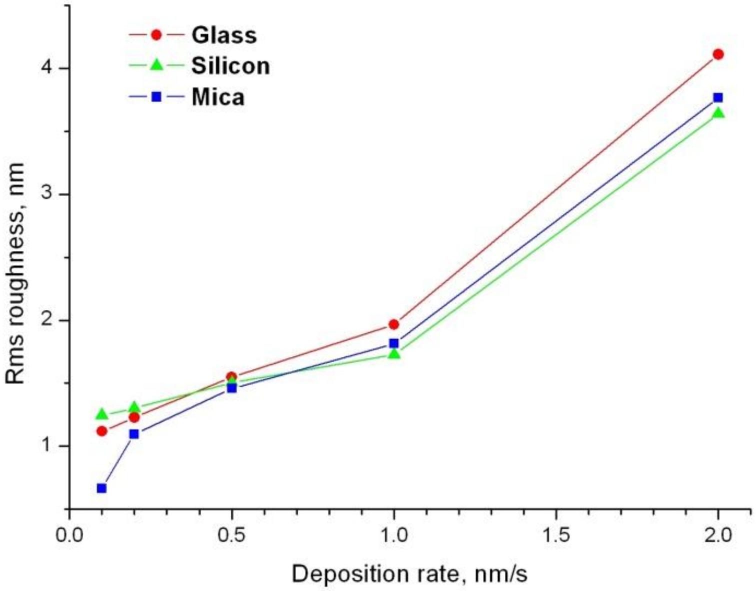

Figure 2.9. Rms surface roughness (obtained from 5 scans of 30 X 30 μm^2 size on each sample) of thin Al films evaporated on glass, Si and mica substrates, as a function of deposition rate.

It is known that the main factors contributing to the roughening of evaporated metal films are self-shadowing (mentioned above) and statistical roughening. The self-shadowing effect leads to the formation of the characteristic columnar structure of thin films in zone 1, according to the zone model [85, 86]. Statistical roughening is caused by the statistical fluctuation of the vapor flux. This phenomenon also causes the increase in surface roughness with an increase of film thickness [68, 89]. The increase of surface roughness for the Al films under investigation agrees well with the increase in average grain size estimated from the SEM images. At lower deposition rates (0.1-1 nm/s) the roughness is determined by the size of the columnar grains and the depths of the voids between them. At the higher rate of 2 nm/s the significant increase in roughness is apparently related to the big number of large hillocks protruding out from the film surface.

It should be noted that at low deposition rates (0.1-0.2 nm/s) the roughness of the Al films correlates well with the roughness of the bare substrates. In particular, the films deposited on mica are significantly smoother (rms roughness 0.25-0.67 nm) than the ones evaporated on glass and Si (rms roughness higher than 1 nm). At higher deposition rates (0.5-2 nm/s) the roughness of the films deposited on different substrates has very similar values for each rate. It is known [90] that a thin film can mimic some morphology features from the substrate. Apparently, for 100 nm thick Al films which are evaporated at low rates and consist of fine grains, this effect is rather prominent. At higher rates, the overall coarsening of the surface structure does not allow observing any correlation between the roughness values of the Al films and that of the bare substrates.

2.3.5. Thin Al films: the influence of the deposition temperature on the surface morphology

For the investigation of the substrate temperature effect on the film structure and morphology, thin Al films were deposited at different temperatures, ranging (roughly) from room temperature (about 25°C) to about 450°C.

Fig. 2.10 shows SEM images of thin Al films deposited onto Si at about 350°C (Fig. 2.10a) and about 450°C (Fig. 2.10b). Both films consist of very large (a few μm) grains and some of the grains exhibit well-define facets. Such a structure is a characteristic of the 3rd structure zone [85, 86]. Indeed, since the temperature of transition between zone 2 and zone 3 for Al is about 195°C, both samples should correspond to zone 3, according to the model considered above. The obtained results are in agreement with the data reported by Higo et al. [66, 71, 81] for thin Al films deposited on mica at different temperatures.

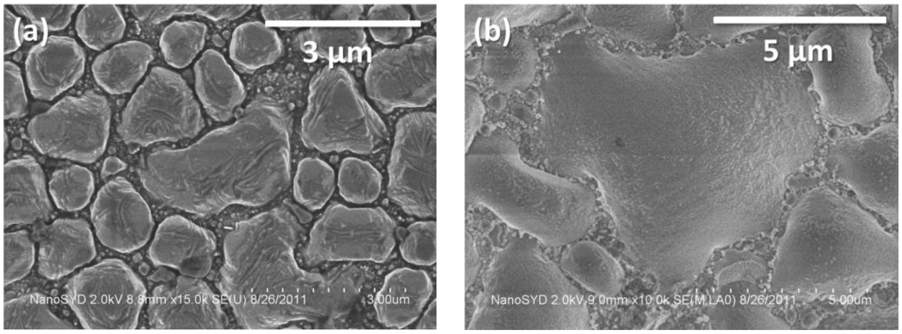

Figure 2.10. SEM images: 530 nm thick Al film on Si deposited at about 350°C (a), 750 nm thick Al film on Si deposited at about 450°C (b).

In fact, if the substrate is intensively heated by the evaporation source during deposition, the formation of Al films with similar morphology can also take place. For example, if the substrate is placed very close to the source (crucible or boat) and no external cooling is applied to the substrate, the deposition proceeds at elevated temperature. Fig. 2.11 shows Al films obtained on Si by evaporation from a resistively heated boat. The distance between the boat and the substrate was about 5 cm. It can be noticed that the 200 nm thick Al film (Fig. 2.11a) consists of small (less than 100 nm) grains with well-defined facets. The same applies to the 800 nm thick film (Fig. 2.11b), but here most of the grains are about 400-600 nm large. Such structure is again the characteristic of the 3rd zone. Thus it can be assumed that the temperature of the substrates during deposition was well above 200°C in both cases.

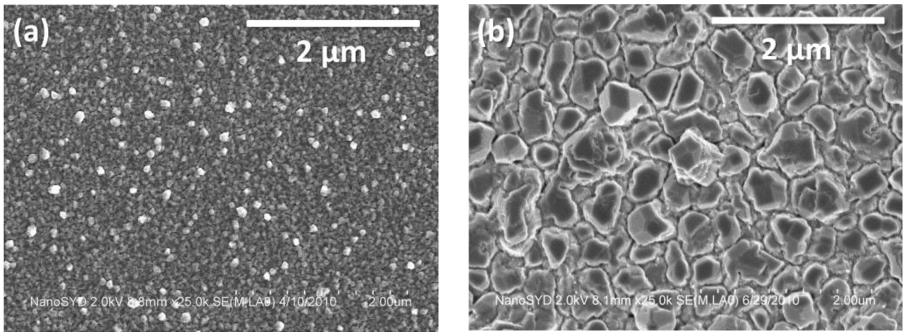

Figure 2.11. SEM images: 200 nm (a) and 800 nm (b) thick Al film on Si deposited under intensive heating from the evaporation source.

2.4. SUMMARY AND OUTLOOK

In the present chapter, different ways of improving the surface quality of Al foils and thin Al films, meant for further anodization, were considered.

Mechanical polishing with diamond suspensions cannot be used as a pretreatment for Al foils, since a lot of particles get trapped on the Al surface.

Electropolishing of Al foils in perchloric acid - ethanol solution or in Brytal solution results in rather smooth surfaces. Brytal solution can be used as an alternative to the perchloric acid - ethanol mixture and is advantageous in terms of safety.

The surface structure and morphology of thin Al films on glass, Si and mica substrates were investigated as a function of deposition rate within a wide range of rates: from 0.1 to 2 nm/s.

SEM imaging of the as-prepared films reveals a grainy structure, with the grain size and overall roughness being strongly dependent on the deposition rate. The films produced at higher rates (1-2 nm/s) exhibit outgrowths (hillocks) the density of which increases with increase in deposition rate. The mean grain size increases for Al films on all substrates from 20-30 to 50-70 nm with increase of deposition rate.

Quantitative AFM characterization reveals a strong dependence of the surface roughness of the deposited films on the evaporation rate. For all substrates, the root mean square surface roughness increases monotonically with increasing the deposition rate from 0.1 to 2 nm/s. For low rates (0.1-0.2 nm/s) the roughness of the films correlates well with the roughness of the bare substrates.

Three main factors are believed to be responsible for the observed dependence of the grain size and surface roughness on the deposition rate. They are: (1) the characteristic features of the island growth mode (surface diffusion of adatoms, nucleation and coalescence of Al clusters); (2) influence of the residual gases (in particular oxygen), which can be incorporated into the film during deposition, on the grain growth; (3) the surface morphology of the corresponding bare substrates.

Heating of the substrate up to 350-450°C during the evaporation of Al results in the formation of big faceted Al grains. A similar structure is obtained if the substrate is placed very close to the evaporation source and is intensively heated by the radiation from the source.

In general, maintaining low deposition rate, low substrate temperature and low residual gas pressure allows the fabrication of smooth Al films with low grain size. The influence of the structure of Al foils and thin Al films on the morphology of the subsequently obtained PAA templates will be considered in Chapter 3.

Chapter 3. Thin-Film Porous Anodic Alumina (PAA) Templates

3.1. INTRODUCTION

Porous anodic alumina (PAA) is commonly used as a template material for the synthesis of nanotubes and nanowires via template wetting and electrochemical deposition techniques [39-41]. The traditional method of PAA film fabrication which includes two-step anodization of thick aluminum foils or plates requires tedious pretreatments for initial substrates and several days of processing time. Since the films are fragile, it can be difficult to create free-standing PAA membranes of relatively low thickness. It is of great technological interest to develop PAA films on appropriate supports such as silicon wafers, glass slides, plastic sheets, etc. Having a PAA film on a silicon substrate facilitates the anodization procedure as well as the following treatments and allows one to integrate PAA-based devices with silicon-based electronics. A PAA film on an ITO-coated glass substrate can be used as a platform for the fabrication of a solar cell. In addition, supported PAA films show interesting properties which differ from those of porous alumina on aluminum hosts. The structure of the films depends strongly not only on anodization solution used, but also on the composition, structure and thickness of the initial aluminum film. In this respect, research is required with the aim to fabricate highly ordered PAA films having a pre-defined thickness, pore size and interpore distance, via anodization of supported thin aluminum films.

In this chapter, the formation of thin PAA films on different substrates, including Al foils, is described. The effect of the anodization conditions (electrolyte, voltage and temperature) and the Al microstructure on the final morphology of PAA films is discussed. The formation of PAA templates on conductive underlayers (such as Au and ITO) is also considered.

3.2. ANODIZATION SETUP

In the present work, a lab-made anodization setup was used. The schematic of this setup is shown in Fig. 3.1.

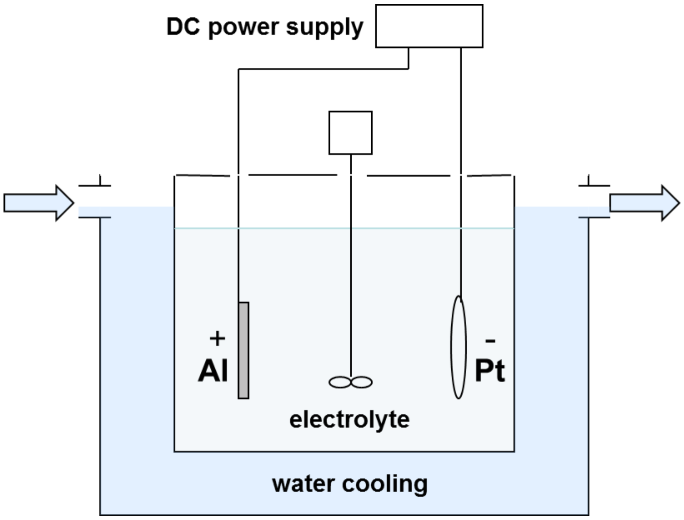

Figure 3.1. Setup for anodization of Al.

The main part of the setup was a home-built two-electrode electrochemical cell. The cell consisted of a cylindrical plastic tank closed with a rigid plastic cap from the top, two electrodes connected to a DC power supply and a mechanical stirrer.

The volume of the tank was 1000 ml. The electrolyte was placed into the tank so that the electrodes were fully dipped into it. The typical volume of the electrolyte was 600 ml.

The body of the anode was made from a transparent plastic cylinder and a rectangular rigid plastic sample holder glued onto it. The electrical contact between the Al sample to be anodized and the positive terminal of the power supply was made by a metallic wire put through the plastic cylinder. One end of the wire was fixed on the outer part of the sample holder by putting a stripe of adhesive Al tape onto it. The other end was fixed on the upper opening of the plastic tube and connected to the cord from the power supply terminal by a clamp. The Al sample to be anodized was placed onto the strip of Al tape and firmly attached to the sample holder with the use of scotch tape. The penetration of the electrolyte beneath the scotch tape was prevented by applying nail polish along the sides of the tape. For Al foils and thin Al films on Si substrates, the contact was made directly to the back side of the sample. For thin Al films on non-conductive supports, the contact was made via a narrow strip of Al foil. One end of this strip was glued to the top surface of the sample by silver paint while the other end was fixed on the strip of adhesive Al tape on the sample holder. The strip was covered by nail polish to prevent its oxidation by the electrolyte.

The body of the cathode was made from a plastic tube similar to the one used in the anode. The cathode was made from a 99.9% pure Pt wire, having length of 80 mm and diameter of 0.3 mm. The Pt wire was bent to form a circle and placed opposite to the Al sample. The end of the Pt wire was connected to a steel wire placed inside the plastic cylinder. The upper end of the steel wire was fixed on the upper opening of the plastic tube and connected to the cord from the power supply terminal by a clamp.

The bodies of both electrodes were led through the circular holes in the cap of the tank. The distance between the electrodes was about 6 cm. The rod of the mechanical stirrer was led through the third hole in the cap near its center.

The whole electrolytic cell was dipped into a water filled thermostat bath. The thermostat allowed cooling the electrolyte down to 5°C.

The DC power supply allowed working at voltages of up to 2000 V and currents of up to 60 mA. For both the voltage and the current, the upper limit could be pre-adjusted.

3.3. EXPERIMENTAL DETAILS

3.3.1. Anodization of Al foils

The schematic of the procedure for the fabrication of PAA films on Al substrates or free-standing PAA membranes is shown in Fig. 3.2.

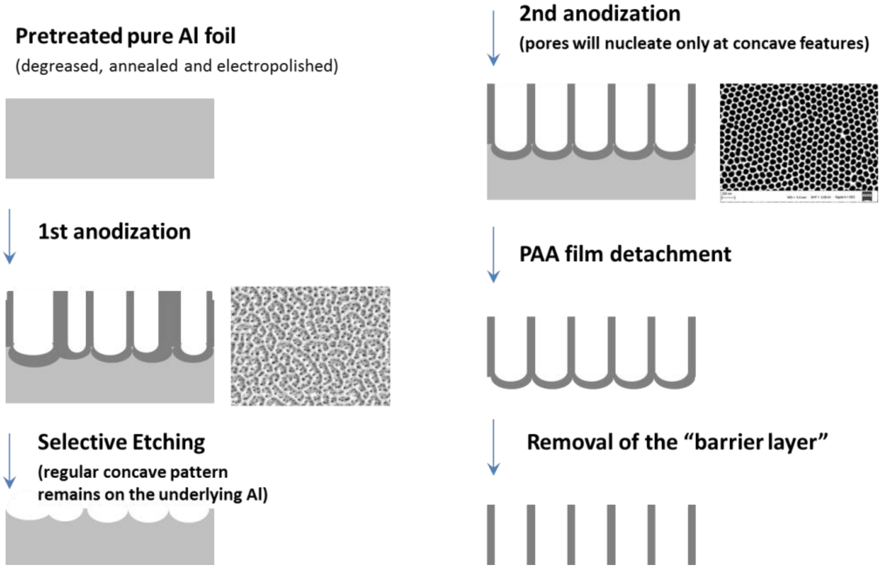

Figure 3.2. Fabrication of PAA films on Al or free-standing PAA membranes by two-step anodization of Al foils.

0.25 mm thick Al foils (99.999%, Goodfellow) were pre-treated as described in Section 2.2.1. The anodization of the Al foils was made either in 0.3M oxalic acid at 40 V or in 0.1M phosphoric acid at 170 V. The temperature of the electrolyte was typically 10-15°C for oxalic acid and 5°C for phosphoric acid. For most of the samples, the conventional two-step anodization procedure was applied. The first anodization lasted 8-12 hours. After the first anodization, the obtained disordered porous alumina film was removed by soaking the sample in a mixed phosphoric acid (5 wt. %) : chromic acid (1.8 wt. %) solution at 80°C for 10-12 hours. The second anodization lasted typically 12-24 hours. In some cases, the second anodization was stopped after 1-2 hours. For some of the samples, three- or four-step anodization was also performed. This procedure resulted in a thin Al film supported by Al foil.

For some of the samples, the Al host was removed and free-standing PAA membrane was obtained. In such cases, a layer of commercial nail polish was put onto the top surface of the PAA film after the second anodization. This layer protected the pores of the PAA from contamination during the further treatments. The remaining Al substrate was removed in a $CuCl_2$-based solution (50 ml of HCl (38%) + 50 ml of H_2O + 1.7 g of $CuCl_2 \cdot 2H_2O$) at room temperature for 10-30 min. For some of the samples, the Al substrate was just partly removed and a thin Al “frame” left around the PAA film which made it easier to handle. The precipitate of metallic Cu formed during the etching process was removed by several rinses in deionized water. After that the sample was soaked in a 5% phosphoric acid solution at 35°C for 30 min in order to dissolve the barrier alumina layer on the bottom of each pore. Finally the nail polish layer was peeled off by tweezers and a free-standing PAA membrane was obtained.

3.3.2. Anodization of thin Al films

The schematic of the procedure for the fabrication of thin PAA films by anodization of thin supported Al films is shown in Fig. 3.3.

Figure 3.3. Fabrication of thin-film PAAs by anodization of thin Al films.

Thin Al films on different substrates (Si, Si with thin Au film on top, glass, ITO-coated glass, mica) were prepared as described in Section 2.2. For the anodization of thin Al films the following electrolytes were used: sulphuric acid (10%) at 15-20 V, oxalic acid (0.3M) at 30-60 V and phosphoric acid (0.1M) at 160-190 V. The temperature of the electrolyte during anodization was around 5°C and the electrolyte was constantly stirred. For the PAA films fabricated on Au layers supported by Si or on ITO-coated glass slides, the pores were widened and the barrier layer was penetrated by etching in 5% phosphoric acid at room temperature for 45-50 min under stirring. Finally, the PAA films were rinsed several times in deionized water and dried on a hotplate at 150°C for 15 min.

The morphology of the obtained PAA structures was observed by SEM (Hitachi S-4800) operating at acceleration voltage of 2-20 kV.

3.4. RESULTS AND DISCUSSION

3.4.1. PAA films on Al substrates and free-standing PAA membranes by anodization of Al foils

The common procedure for the fabrication of PAAs by two-step anodization includes pretreatments for the Al foils, such as thermal annealing and electropolishing [7, 9, 36-38]. Thermal annealing enlarges the Al crystal grains and allows the fabrication of big PAA domains with perfect pore ordering. Electropolishing smoothens the Al surface, which leads to a better surface quality of the fabricated PAA films. If a perfect pore ordering is not critical, these pretreatment steps can be skipped.

Fig. 3.4a shows the top surface of a PAA film obtained by anodizing an untreated Al foil in 0.1M phosphoric acid at 170 V for 12 hours (the image is slightly distorted because of charging effects). Before the anodization, the foil was only degreased by ultrasonication in acetone for 5 min. As can be seen from the picture, the first anodization gave a PAA film with pores of about 100 nm in diameter. The pores are grouped along the parallel grooves which existed initially on the surface of the Al foil (see Fig. 2.1). On the other hand, the interpore distance of 200-300 nm, which is typical for the applied anodization conditions [9], is also preserved.

After the first anodization, the formed PAA film was etched away selectively by soaking the sample in H_3PO_4-H_2CrO_4 mixture at 80°C for 10 hours. The resulting morphology of the Al surface can be seen on Fig. 3.4b. The first anodization produces a regular array of concaves which should act as pore nucleation sites during the second anodization [7, 9].

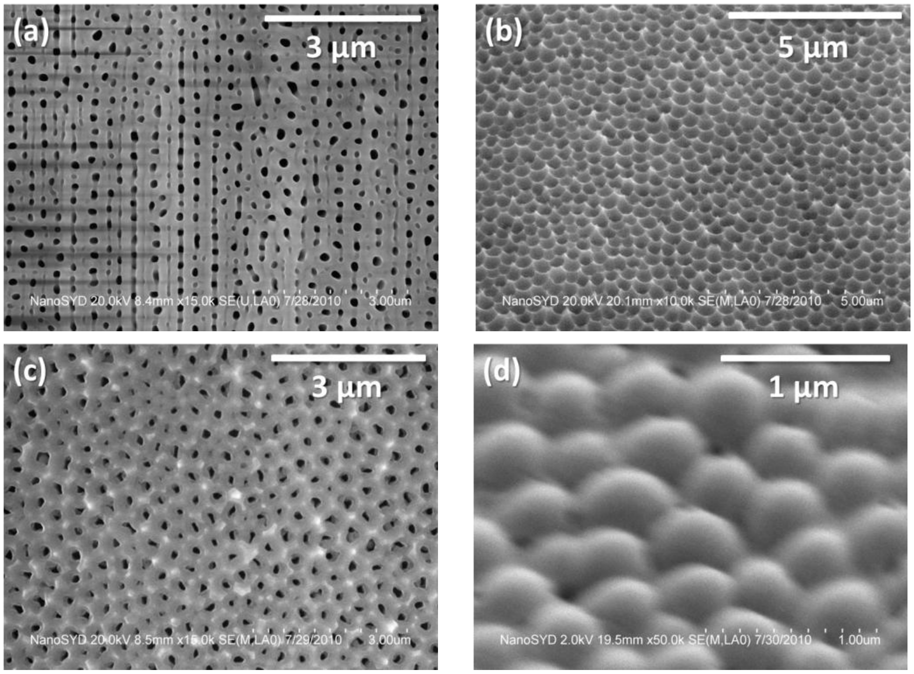

Figure 3.4. SEM images: PAA film obtained by single anodization of untreated Al foil (a), periodic concave pattern left on the Al surface after selective removal of this PAA film (b), PAA film obtained during the second anodization under the same conditions (c), the bottom-view of the barrier layer formed during the second anodization (d).

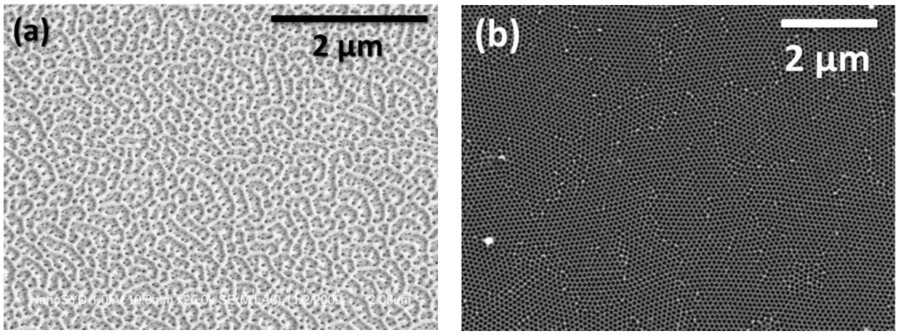

Figure 3.5. PAA structures obtained after the first anodization (a) and after the second anodization (b) of Al foils in 0.3M oxalic acid at 40 V. *Image (b) is made by S. Habouti (IMST).*

The second anodization of the so-structured Al foil gives a PAA with a much better pore ordering (Fig. 3.4c). The pores are about 100 nm wide and have irregular shapes. In principle, the pores could be widened and rounded by etching in 5% phosphoric acid at room temperature [7, 9-11]. Such a PAA film supported by the Al host can be further used as a template for the fabrication of 1D nanostructures, as described in Chapter 5. As an alternative, a free-standing PAA membrane can be made. In that case the PAA film is detached from the PAA host by soaking the sample in $CuCl_2$/HCl solution [11]. After that, the top surface of the detached PAA film is covered by nail polish for protection and the barrier oxide layer (shown in Fig. 3.4d) is removed from the bottom of each pore by etching in phosphoric acid [10].

If a good pore ordering is required, the Al foils should be pre-treated according to the common procedure, i.e. annealed and electropolished. In the present work, highly ordered open-through PAA membranes and thin PAA films on Al supports were obtained by two-step anodization of pretreated Al foils in 0.3M oxalic acid at 40 V, according to the common procedure [7, 9-11].

The Al foils were annealed at 500°C for 5 hours under nitrogen flow and electropolished in perchloric acid - ethanol solution according to [7, 9]. During the first anodization, a disordered PAA film was obtained (Fig. 3.5a). The surface of the PAA film shows the “scallop” features which are also observed for the initial Al surface (see Fig. 2.3). These concave features are typical for the applied electropolishing conditions and believed to act as nucleation sites during the first-step anodization [9]. The formed PAA film was dissolved in H_3PO_4-H_2CrO_4 mixture and the second anodization was performed under the same conditions. The image of the obtained highly-ordered PAA film (after pore widening) is shown in Fig. 3.5b. As can be seen from the picture, the PAA film consists of few-micrometer large domains with almost perfect hexagonal arrangement of the pores. The pores are round and the mean pore diameter is about 80 nm. Such PAA films were also used for the template-based fabrication of nanostructures. This approach is described in detail in Chapter 6.

3.4.2. Thin PAA films on Si by anodization of thin evaporated Al films in different electrolytes

In the present work, thin PAA films were fabricated on several types of substrates. Since Si substrates are very smooth, easy to prepare and provide a good adhesion for Al films, the morphology of thin PAA films in most cases was studied for the structures made on Si substrates.

It is known [9, 36] that the morphology of PAAs depends strongly on the anodization conditions, in particular on the electrolyte and anodization voltage. In the present work, the anodization of thin Al films was studied for the three most common electrolytes: sulphuric acid, oxalic acid and phosphoric acid.

Sulphuric acid

The top-view SEM images of thin PAA films, obtained by anodization of 500 nm thick Al on Si in 10% sulphuric acid, are shown in Fig. 3.6. The anodization was performed at 10°C at two different voltages: 15 V (Fig. 3.6a) and 20 V (Fig. 3.6b). As can be seen from the picture, the formed PAA films consist of nanotubes having diameters of about 15-20 nm. The tube wall thickness is about 20 nm. Since the diameters of the nanotubes are close to the resolution limit of the SEM at the used imaging conditions, it is hard to see any difference between the two samples. In general, it is known [9, 36] that at higher anodization voltages the pore diameters and interpore distances in PAAs are higher. Thus one should expect that the diameters of the nanotubes are a little bit higher for the sample obtained at 20 V (Fig. 3.6b).

The formation of alumina nanotubes under similar anodization conditions was reported previously [91]. Such structures were not observed for the anodization of Al foils in sulphuric acid. Their appearance was explained by the formation and growth of voids inside the PAA pore walls. Evolution of such voids causes splitting of the pore walls and formation of nanotubes.

In general, the applicability of such alumina nanotube arrays as templates should be further investigated. One can expect that filling of the spaces between the alumina nanotubes with solution or melt will lead to the formation of nanostructures with uncertain shapes, which is unfavorable for most device applications.

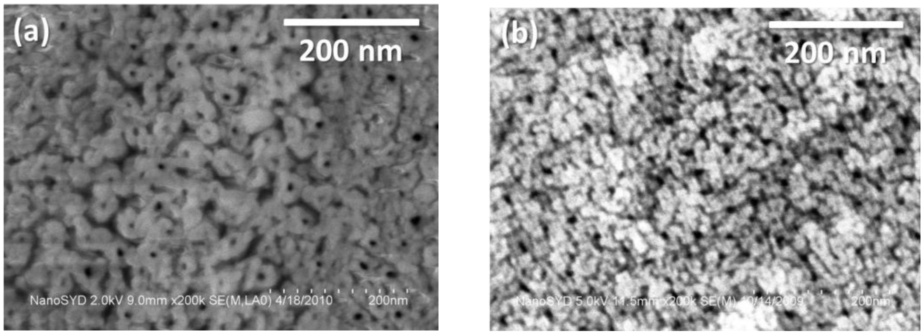

Figure 3.6. Thin PAA films on Si obtained by anodization of thin Al films in 10% sulphuric acid at 15 V (a) and 20 V (b).

Oxalic acid

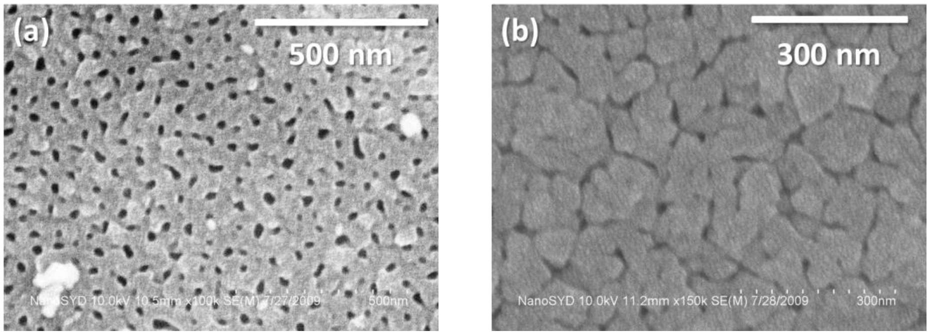

Figure 3.7. Thin PAA films on Si obtained by anodization of thin Al films with different surface morphology in 0.3M oxalic acid at 40 V. The PAA film shown in (b) was obtained by anodizing an Al film which had a higher grain size.

The anodization of thin Al films on Si in 0.3M oxalic acid at 30-60 V gives PAA films having pore diameters of 30-60 nm and interpore distances of about 100 nm (Fig. 3.7). That agrees well with the results obtained by other authors [18, 21]. The pores can be widened up to 80 nm by etching in phosphoric acid.

From cross-sectional SEM images of the PAA films, the pore growth rate was estimated. It was about 200-300 nm/min for the Al films deposited at 0.5 nm/s and anodized in 0.3M oxalic acid at 40 V and 10°C. This parameter was found to depend on the grain size of the Al film, as well as on the anodization voltage and temperature.

Phosphoric acid

Anodization of thin Al films in 0.1M phosphoric acid leads to the formation of PAA films having pore diameters of 100-150 nm and interpore distances of 200-300 nm (Fig. 3.8). These results are in agreement with the data published previously for the anodization of both Al foils and thin Al films [9, 29].

A short-time (5 min) anodization (Fig. 3.8a) gives a disordered PAA film with pores having irregular shapes and wide distribution of diameters. As can be seen from the tilted-view SEM image (Fig. 3.8b), the surface of the PAA film is rather rough and preserves some of the features (grooves and hillocks) of the initial Al surface. However, a longer-time (60 min) anodization results in a quite good pore ordering (Fig. 3.8c). Most of the pores are round and their tops are funnel-shaped. As can be seen from a lower-magnification image (Fig. 3.8d), the hexagonal pore ordering is obtained within 2-3 μm wide surface domains. The pore channels are straight and almost parallel to each other (Fig. 3.8e, cross-sectional view). Each pore ends up with U-shaped barrier alumina. The higher-magnification cross-sectional view (Fig. 3.8f) reveals that the barrier layer has the same or higher thickness if compared to the pore walls.

The typical rate of pore growth, estimated from cross-sectional SEM images, was about 80 nm/min. Thus the pore growth in phosphoric acid proceeds about 3 times slower than in oxalic acid under the common anodization conditions. In some cases, this difference can make the use of phosphoric acid advantageous over the use of oxalic acid as electrolyte. Since the degree of pore ordering depends mostly on the processing time

[9, 36], anodization of an Al film of given thickness in phosphoric acid should result in a better pore ordering.

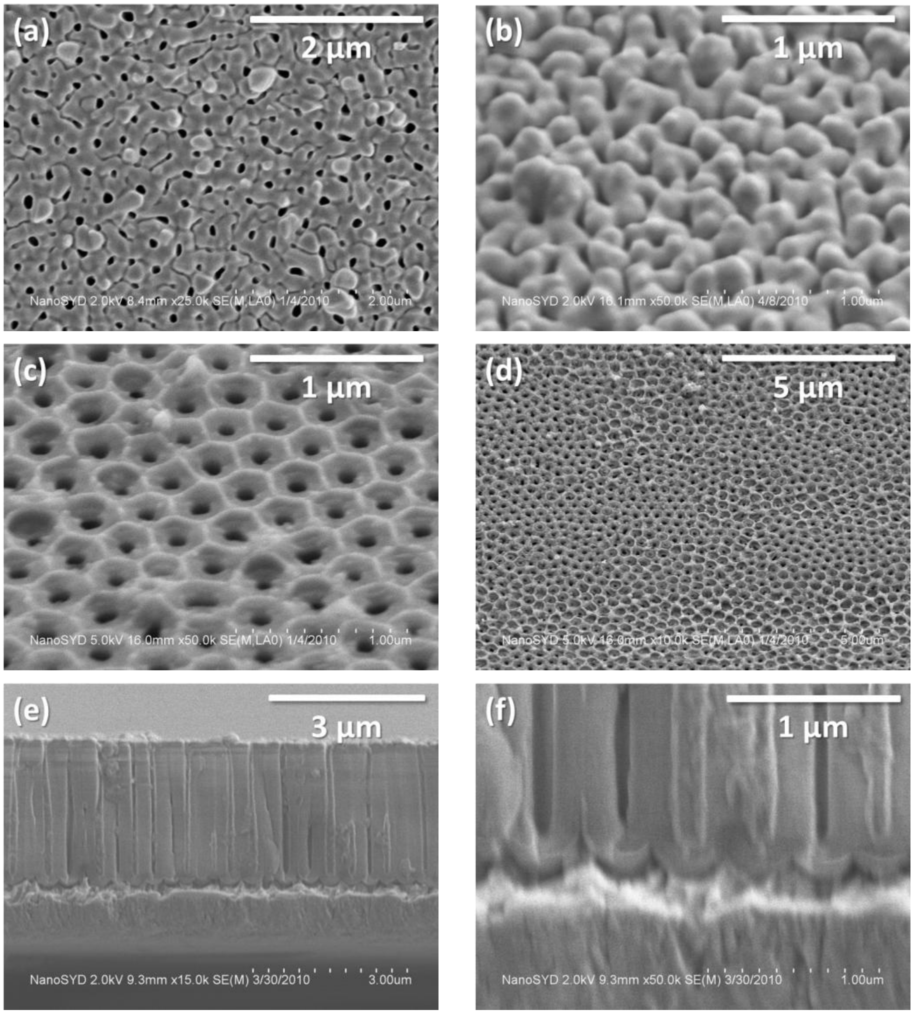

Figure 3.8. SEM images of thin PAA films on Si prepared by anodization of thin Al films in 0.1M phosphoric acid for 5 min. (a, b) and 60 min. (c-f)

3.4.3. Thin PAA films: effects of the Al films surface morphology

Fig. 3.9a is a top-view SEM image of 2 μm thick Al film on Si. The deposition rate for the film was about 2 nm/s. The surface of the film is rough and grainy; the typical size of the grains is 300-500 nm. Fig. 3.9b shows the surface of the PAA film obtained by anodizing the meant Al film in 0.3M oxalic acid at 40 V. It can be seen that the overall surface morphology of the Al film is still preserved for the PAA film. The pore ordering is very poor and the distribution of the pore diameters is wide. The bigger pores are densely grouped along the grooves between the grains. On the surface of the grains, the pore density is smaller. It can be also seen that the pores started growing almost perpendicular to the facets of the grains.

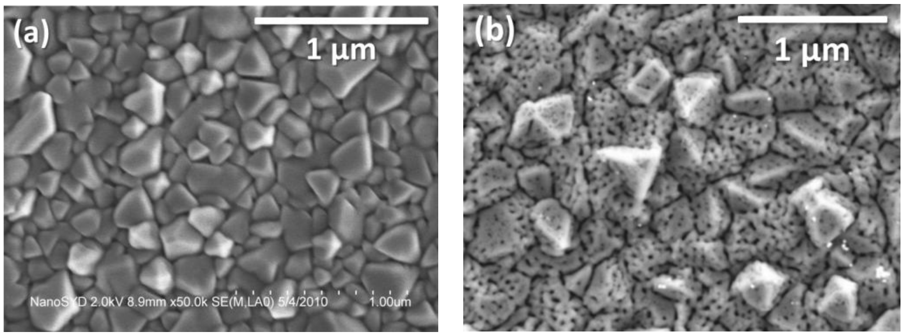

Figure 3.9. SEM images: 2 μm thick Al film evaporated onto Si substrate at 2 nm/s (a) and thin PAA film obtained by anodization of this Al film in 0.3M oxalic acid at 40 V (b). *Image (b) is made by S. Habouti (IMST)*

According to the commonly assumed mechanism [6, 31-33], the pore nucleation starts at local concaves on the Al surface, where the local electric field turns to be higher. One can expect that in the case of thin evaporated Al films which have columnar structure, the pores should nucleate first of all at the “triple points” between the neighboring grains. The growth of these pores dominates over the growth of the other pores, which were randomly nucleated at the surface of the grains. As a result, a highly disordered PAA structure is obtained. Such PAA films cannot be used as templates for the further nanowire/nanotube growth, and their structure should be improved.

500 nm thick Al films deposited at 0.5 nm/s exhibit lower grain size

and lower surface roughness. Actually the difference should be explained not only by the lower deposition rate but also by the lower thickness. The result of the anodization of such a film in 0.3M oxalic acid at 40 V is shown in Fig. 3.10. Here, the pore ordering is much better and the surface of the PAA film is smoother, if compared to the previous sample. However, at some points the pores are connected by well-pronounced grooves which correspond to the voids between the grains of the Al film.

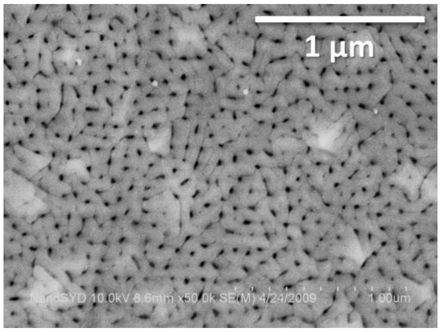

Figure 3.10. SEM image of a thin PAA film obtained by anodization of 500 nm thick Al film in 0.3M oxalic acid at 40 V. The Al film was deposited at 0.5 nm/s.

Lowering of the deposition rate for Al down to 0.05-0.1 nm/s results in a very smooth Al film with low grain size (Fig. 3.11a). Here, again, the thickness of the film is 500 nm. The PAA film formed under the same anodization conditions also exhibits a very smooth surface which is free from grooves or hillocks (Fig. 3.11b).

As was mentioned in Section 2.3.4, uncontrolled heating of the substrate during the Al deposition results in the formation of rough Al films having big grains. Fig. 3.12a, shows the surface of a 500 nm thick Al film on mica formed under intensive heating from the evaporation source. The deposition rate for Al was about 0.2 nm/s. The anodization of such a film gives a very rough and disordered PAA structure (Fig. 3.12b). The surface morphology of this film resembles the one which is seen in Fig. 3.12b: the pores are concentrated in the grooves between the grains, and the pore density on the grains is low.

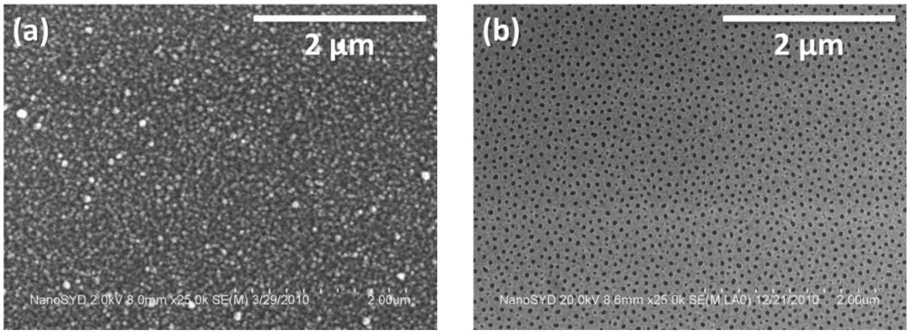

Figure 3.11. SEM images: 500 nm thick Al film evaporated onto Si substrate at 0.05-0.1 nm/s (a) and thin PAA film obtained by anodization of this Al film in 0.3M oxalic acid at 40 V (b).

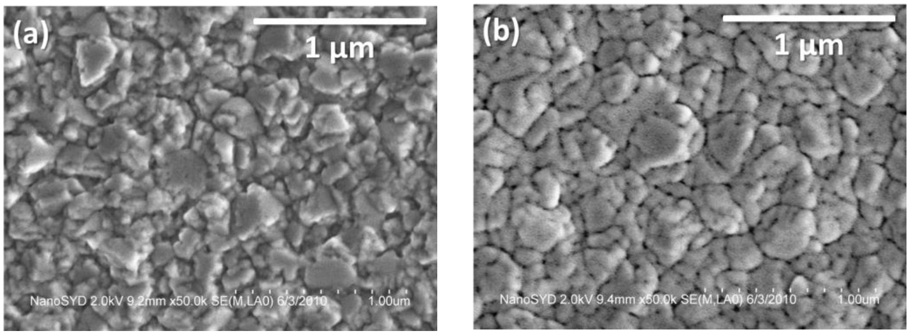

Figure 3.12. SEM images: 500 nm thick Al film evaporated onto mica substrate at 0.2 nm/s at elevated temperature (a) and thin PAA film obtained by anodization of this Al film in 0.3M oxalic acid at 40 V (b).

The main combinations of thin Al film deposition parameters and anodization conditions, which were utilized in the present work, are summarized in Table 3.1. The grain size ranges stated in the table were estimated from high-magnification SEM images of the respective Al films. The “expected” interpore distance is the typical distance between the neighboring pores, which is obtained for long-time anodization of Al at the same conditions [9, 36].

As can be seen from the presented data, the PAA film morphology which can be obtained for the given anodization conditions depends on

Table 3.1. Effect of the Al thin film deposition and subsequent anodization parameters on the final morphology of PAA films

Al film: substrate, thickness, deposition rate	Estimated grain size for the Al film (nm)	Anodization: electrolyte, voltage (V)	Expected interpore distance (nm)	Pore ordering, surface morphology
Si, glass, mica; 200 nm, 0.05-0.1 nm/s	20-40	0.3M oxalic acid, 30-40 V	80-100	Good, smooth
Si, glass, mica; 500 nm, 0.1-0.2 nm/s	50-100	0.3M oxalic acid, 40-60 V	~100	Good, smooth
Si, 500 nm, 0.5 nm/s	50-150	0.3M oxalic acid, 40-60 V	~100	Acceptable, small grooves and hillocks
		0.1M phosphoric acid, 170 V	200-300	Acceptable, small grooves and hillocks
Si, 1-2 μm, 0.5 nm/s	50-200	0.3M oxalic acid, 40-60 V	~100	Poor, small grooves and hillocks
		0.1M phosphoric acid, 170 V	200-300	Good, small hillocks
Si, 2-5 μm, 2 nm/s	100-300	0.3M oxalic acid, 40-60 V	~100	Very poor, big hillocks
		0.1M phosphoric acid, 170 V	200-300	Good, regular funnel-shaped pore openings
Si, 5 μm, 2-4 nm/s	100-400	0.3M oxalic acid, 40-60 V	~100	Very poor, big hillocks

the grain size of the Al film. For example, anodization in oxalic acid can only result in well-ordered and smooth PAA films if the grain size of the Al film does not exceed 100 nm. For the anodization in phosphoric acid, a quite good pore ordering can be obtained even for rough Al surfaces (see also Fig. 3.4).

As mentioned above, it is first of all the “triple points” between the Al grains which act as pore nucleation sites during anodization. The average distance between the neighboring “triple points” or pronounced concave features on the Al surface depends on the grain size. On the other hand, the interpore distance realized during the self-ordering of PAA is determined by the anodization voltage. If these two values match each other, or if the grain size is smaller than the expected interpore distance, a PAA structure with a good pore ordering can be obtained.

In fact, a similar trend is observed for the anodization of thin Al films which were pre-patterned by mechanical stamping [8, 92, 93]. If the distance between the “artificial” concave patterns was close to that of a self-organized PAA structure at a given anodization voltage, highly ordered PAA films could be obtained. If this distance was significantly higher, additional randomly organized pores were found between the “main” ones.

3.4.4. Thin PAA films on conductive underlayers

For the fabrication of 1D nanostructures via electrochemistry-based techniques (electrochemical and electrophoretic deposition into the pores of a template), one needs to have PAA structures standing on conductive supports. Even if the 1D nanostructures are fabricated by other techniques (for example, by template wetting) it might be necessary to have them in contact with a conductive support or underlayer. The typical example is the fabrication of P3HT nanotubes on ITO coated glass substrates for the further implementation in organic bulk heterojunction (BHJ) solar cells (this procedure will be described in detail in Chapter 5). In any case, the critical point is that the bottoms of the PAA pores are fully opened and reach the underlying conductive layer.

The anodization of Al films in phosphoric acid results in a barrier layer which is thicker than the pore walls and cannot be selectively penetrated (see Section 3.4.2.). Therefore in the procedure described below, only oxalic acid was used as an electrolyte.

In the present work, the formation of PAA films on Au underlayers and ITO coated glass substartes was investigated. The schematic of the fabrication procedure is shown in Fig. 3.13.

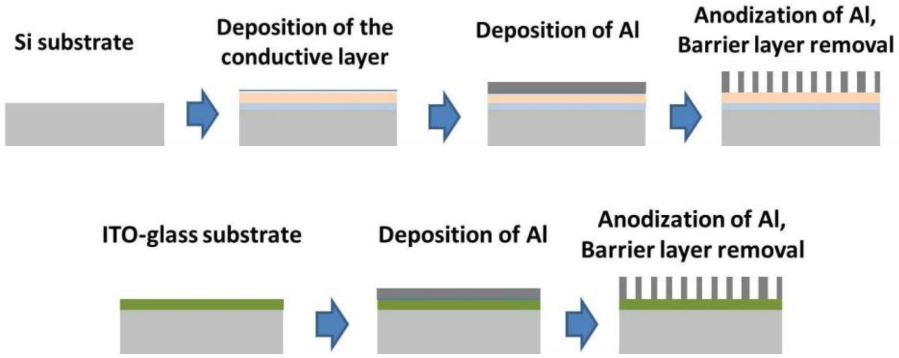

Figure 3.13. Fabrication of thin-film PAAs on Au underlayers and ITO-coated glass substrates.

The Au layer (typically 50-100 nm thick) was fabricated by e-beam evaporation. To provide a good adhesion to both the Si substrate and the Al film deposited above, thin (5-15 nm) Ti layers were applied.

For the preparation of thin PAA films on ITO, commercial ITO-coated glass slides were employed. A thin (typically 1-2 nm) adhesion layer was evaporated onto the ITO, and the Al film was deposited on top.

The thickness of the Ti adhesion layer between the Al film and the conductive layer is very critical. It was reported [27, 28] that the presence of a 2-10 nm thick Ti layer below the Al film leads to the formation of a thick barrier layer during the anodization. The reason for this is that Ti is oxidized and converted to TiO_2 which then depletes the electric field needed for the barrier layer thinning. As a result, the barrier layer turns to be thicker than the pore walls and therefore cannot be penetrated selectively. Such a situation can be seen in Fig. 3.14a, which shows a

PAA film formed on 100 nm Au layer with a 5 nm thick Ti film in between, after the standard pore widening in phosphoric acid for 45 min. On the bottom of each pore, an inverted U-shaped barrier layer is seen.

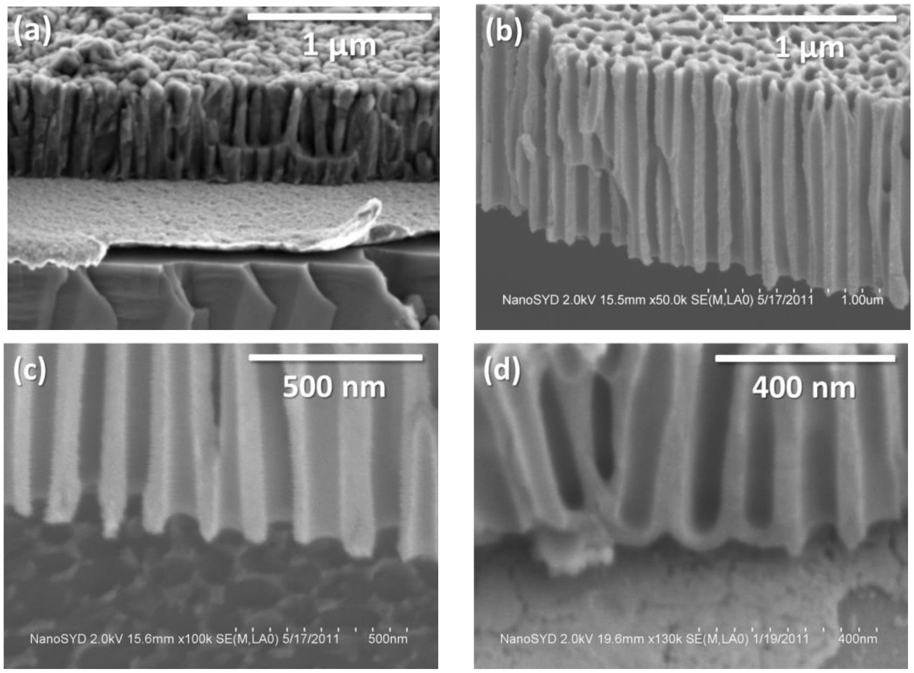

Fugure 3.14. SEM images: thin PAA film on 100 nm thick Au underlayer supported by Si substrate (a); thin PAA film obtained on ITO-glass by anodization in 0.3M oxalic acid, after pore widening (b); the high-magnification view of the pore bottoms, confirming that the barrier layer was penetrated (c); the bottom of the same PAA film in the region where the barrier layer could not be penetrated (d). *Image (a) is made by S. Habouti (IMST).*

The recommended thickness of the Ti layer for the considered procedure according to [27] is 0.2-0.5 nm. However, in the present work it was found that such ultrathin Ti layers cannot provide a proper adhesion between Al and ITO or between Al and Au. The Al films started flaking and detaching from the substrate right after the beginning of the anodization. Increasing the thickness up to 1-2 nm did not change the situation.

Quite good results were achieved after making low-temperature post-depositional annealing of the as-prepared Al films. The annealing was performed in a rough vacuum chamber (pressure about $3 \cdot 10^{-2}$ mbar) at about 150°C for 5 hours. The annealing helped to significantly improve the adhesion of the Al films to the ITO-glass substrates and made it possible to carry out the anodization at the normal conditions. Fig. 3.14b, shows PAA film on ITO-glass obtained by anodization of as-prepared Al film in 0.3M oxalic acid and subsequent widening of the pores in 5% phosphoric acid for 45 min. As can be seen from this picture and from the higher-resolution image (Fig. 3.14c), all the pores are open-through and reach the underlying ITO layer.

In some regions, small groups of pores with remained barrier layer can still be found (Fig. 3.14d). Most probably, these are tilted pores which nucleated at hillocks on the Al surface. The growth of these pores could be hindered by the evolution of the neighboring pores which were formed on smoother regions. As a result, the alumina remained under the bottoms of these tilted pores turned to be thicker and could not be fully dissolved.

It should be noted that increasing the annealing temperature up to 200°C lead to partial detachment and flaking of the Al films during the annealing. When the annealing procedure described above was applied to Al films on Au underlayers, it did not give satisfactory results, i.e. the Al films got detached during the anodization. Thus the optimal annealing and anodization conditions for Al films on Au have to be further studied.

The anodization of thin Al films on conductive supports can be effectively controlled by observing the current-time curve [14]. The drastic decrease of the anodization current corresponds to the point when the Al film is fully oxidized and the bottoms of the pores have reached the underlying conductive layer.

Fig. 3.15 shows current-time curves for the anodization of 500 nm thick Al film on a 100 nm Au film supported by Si. The anodization was made in 0.3M oxalic acid at 10°C, at voltages from 40 to 60 V. It can be seen that the steady-state anodization current density increases from about 30 A/m^2 at 40 V to almost 150 A/m^2 at 60 V. At 60 V, the anodization proceeds almost 4 times faster than at 40 V.

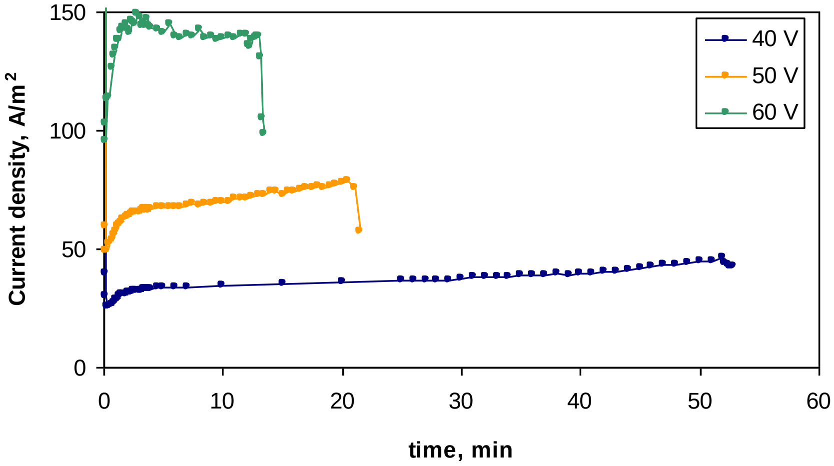

Figure 3.15. Current-time curves for the anodization of 500 nm thick Al films on Au underlayer supported by Si substrate in 0.3M oxalic acid at 10°C, for different voltages.

Since thin PAA films are transparent, the anodization can also be controlled by visual observation. When the Al film is fully converted to PAA, the underlying Au film can be easily seen. In the case of Al films on ITO-glass substrates, a transparent “window” is obtained.

When the anodization was carried out at lower voltages (30-35 V) the minimum of the curve corresponded to the full consumption of the Al over the whole exposed sample area. For the anodization at higher voltages (50-60 V) the full consumption of the Al was observed only within small restricted areas. These areas were surrounded by bigger regions where non-transparent Al could be seen, i.e. where the PAA did not reach the conductive layer. Retaining the voltage at the same level resulted in partial detachment of the PAA film. The uniformity of the PAA film thickness could only be improved by lowering the voltage down to 30 V after observing the minimum on the curve, and retaining it for 1-2 min. In that case, the rest of the Al was fully oxidized without film detachment.

3.5. SUMMARY AND OUTLOOK

In this chapter, different aspects of the fabrication of thin-film PAA templates were considered. Based on the obtained results, the following conclusions can be made:

1. 2-step anodization of Al foils in 0.1M phosphoric acid at 170 V without common pre-treatments (thermal annealing and electropolishing) leads to the formation of PAA films with acceptable pore ordering. For the preparation of highly ordered PAA structures, the common pre-treatment procedures should be employed.

2. Anodization of thin Al films in 10% sulphuric acid at 15-20 V results in the formation of alumina nanotubes. The inner diameters of the nanotubes are about 15-20 nm and the nanotube wall thickness is about 20 nm. The applicability of such structures as templates should be further investigated.

   Anodization of thin Al films in 0.3M oxalic acid at 30-60 V leads to the formation of thin PAA films with pore diameters of 30-60 nm and interpore distances of 80-100 nm.

   Anodization of thin Al films in 0.1M phosphoric acid at 170 V results in the formation of thin PAA films with pore diameters of 100-150 nm and interpore distances of about 300 nm.

   Since the rate of PAA pore growth during anodization is about 3 times lower in phosphoric acid than in oxalic acid under typical conditions, the use of phosphoric acid as an electrolyte allows the fabrication of better-ordered PAA structures for a given thickness of the Al film.

3. The structure of thin Al films used for the anodization determines the morphology of the formed PAA films to a large extent.

Adjusting the anodization conditions (in particular the electrolyte and the anodization voltage) against to the average grain size in the Al film allows the fabrication of well-ordered PAA structures. On the other hand, using Al films with a definite grain size is the way to obtain highly ordered PAAs at given anodization conditions.

4. Open-through PAA films on conductive underlayers (Au or ITO) can be obtained by anodizing thin Al films in 0.3M oxalic acid at 40-60 V and subsequent etching of the barrier layer in 5% phosphoric acid for 45-50 min. It is critical that the thickness of the Ti adhesion layer between the Al film and the conductive underlayer does not exceed 1-2 nm. A proper adhesion of the Al film to the substrate can be achieved by post-depositional thermal annealing at 100-150°C for a few hours. The procedure does not work well for the Al films on Au; for that case, the optimal fabrication conditions still have to be found.

5. Anodizing Al at low voltages (30-35 V) allows the fabrication of PAA films with more uniform thickness which is important for their use as templates. The thickness uniformity for higher voltages (50-60 V) can be improved by lowering the voltage down to 30 V at the end of the anodization and retaining it at this value for 1-2 min.

Chapter 4. Thin-Film PAA Templates on Free-Standing Thin-Film Substrates

4.1. INTRODUCTION

In general, PAAs can be obtained in two forms in terms of thickness: as thick (from tens to hundreds of micrometers) porous membranes and thin (from tens of nanometers to a few micrometers) porous films supported on a rigid substrate like silicon or glass. Thick AAO membranes are usually made by anodization of annealed and electropolished Al foils. After etching away the host aluminum and removing the barrier layer from the bottom of each pore, a free-standing thick PAA membrane can be obtained. On the other hand, thin-film PAAs are made by anodization of thin Al films initially deposited on rigid substrates by means of evaporation or sputtering. Such structures can be further integrated into various micro- and nanoscaled devices.

For some applications, it would be highly favorable to make free-standing PAAs or thin-film PAA structures on flexible thin-film supports. The idea of making free-standing PAA templates (eventually with open-through pores) has been realized in different ways. The most widely used method is chemical dissolution [9-11]. In this method, an Al foil is partly anodized and the remaining metal is dissolved in $HgCl_2$ or $CuCl_2$/HCl solution. Other techniques involve voltage reduction [94], applying voltage pulse [95] and voltage reversal [96] during the final step of the anodization; they result in the detachment of the PAA structure from the Al host. After releasing the PAA, the barrier layer can be optionally dissolved and the pores can be slightly widened by etching in phosphoric acid. These procedures lead to free-standing PAA structures. However, the brittleness of such unsupported structures for the thicknesses below a few tens of microns makes them almost useless for practical applications. Thin PAA films are normally used on the same supports which they were initially fabricated on. Recently partially free-standing thin-film PAAs were realized via making through holes in a Si substrate by etching it from the bottom side [97]. Fully free-standing thin PAA films were also made by the so-called “double-layer anodization” [98]. In this method, the anodization of the sacrificial metal layer introduced below the Al films allowed facile detachment of the PAA film.

Recently, an elegant approach for the fabrication of thin-film PAA templates on flexible PDMS substrates was also proposed [99]. The procedure involved pulsed anodization of a thin Al film on top of a multi-layered structure fabricated on a PDMS layer. The PDMS layer was initially formed on a thick Al sacrificial layer supported by a Si wafer. After the anodization, the Al sacrificial layer was selectively dissolved and a PAA structure on a conductive Au film supported by a flexible PDMS substrate was obtained.

In this chapter, a novel method for the fabrication of thin-film PAA templates on free-standing thin-film substrates is described. The method involves the use of water-soluble NaCl release layer produced by means of e-beam evaporation in high vacuum. The PAA templates are fabricated via anodization of thin Al films supported by thin layers of e-beam evaporated silicon oxide or aluminum oxide.

4.2. EXPERIMENTAL DETAILS

4.2.1. Deposition of thin films

Silicon (Si (100), resistivity 1-100 Ohm·cm^{-1}) substrates were pre-cleaned by ultrasonication in acetone and ethanol (5 min. in each solvent) followed by oxygen plasma etching (5 min. at 300 W, Branson IPC 3000 barrel plasma system).

Sodium chloride (NaCl) films with thickness from 20 nm to 5 μm were deposited on unheated Si or mica substrates using a NaCl “ingot” placed into a tungsten crucible liner. The “ingot” was made by putting small portions of a saturated NaCl solution into the crucible liner and slowly evaporating it until about 80% of the liner volume got filled by

NaCl. The evaporation rate was adjusted in the range between 0.1 and 2 nm/s by changing the e-beam current. All the subsequent films were deposited in the same vacuum chamber without breaking the vacuum.

Silicon oxide (SiO_x) films with a thickness of 4-5 μm were deposited on top of the NaCl film by e-beam evaporation from silicon oxide flakes placed into a molybdenum crucible liner. The deposition rate was kept in the range between 10 and 20 nm/s. Alternatively, aluminum oxide (Al_2O_3) films with a thickness of about 500 nm were deposited on top of the NaCl film by e-beam evaporation from Al_2O_3 pellets placed into a molybdenum crucible liner. The deposition rate for Al_2O_3 was about 0.2 nm/s.

Finally, Al films with a thickness from 500 nm to 2 μm were deposited from an intermetallic (BN-TiB_2) crucible liner. The evaporation rate for Al was adjusted in the range between 0.1 and 2 nm/s. In some of the experiments, the Al film was evaporated directly onto the NaCl film without any intermediate layers.

The pressure in the chamber during deposition was better than $1 \cdot 10^{-5}$ mbar. The acceleration voltage of the electron gun was fixed at 4.76 kV and the e-beam current was kept in the range between 1 and 80 mA, depending on the target material, the required evaporation rate and the load of the crucible.

4.2.2. Anodization of Al

The obtained multi-layered structure was put into a Petri dish filled by deionized water at room temperature and the Al film on the supporting layer was lifted off by dissolution of the NaCl release layer. After the detachment, a floating thin Al film on a supporting layer was obtained. A small mica sheet was put below the floating film and the film was carefully transferred onto it. After wiping the water away and drying, the film got firmly attached to the mica sheet. The mica sheet with the film attached to it was placed onto the sample holder of the anodization setup. To prevent the penetration of the electrolyte beneath the film, it was glued to the mica sheet by nail polish applied along its edge. Thus the mica sheet acted as a flat and rigid support for the thin Al film during the anodization. The electrical contact between the positive terminal of the DC power supply and the aluminum film was made with the help of conductive silver paint.

The anodization of the Al film was performed either in 0.3M oxalic acid at 40 V or in 0.1M phosphoric acid at 170 V at 5°C. The area of the Al film surface exposed to the electrolyte was about 8 x 8 mm^2. In that way, a PAA structure on a supporting layer with a thin intermediate layer of unoxidized Al was obtained. For the PAA film obtained in oxalic acid, the pores were further widened by soaking the samples in 5% phosphoric acid at room temperature for 45 min.

Finally, the mica sheet with the supported PAA film on it was dipped into deionized water. That resulted in the fast detachment of the supported PAA film from the mica sheet. At the same time, the PAA film was rinsed to remove the remaining electrolyte. The supported PAA film was kept at 150°C on a hotplate for 5 minutes in order to remove the water which could remain in the pores.

The SEM imaging of the fabricated structures was performed in a commercial instrument (Hitachi S-4800) with an accelerating voltage of 2 kV. In order to avoid charging, all of the samples were sputter-coated with Au-Pd (2-3 nm) prior to observation.

4.3. RESULTS AND DISCUSSION

The schematic of the fabrication of thin-film PAA templates on thin-film substrates with the use of NaCl release layers is shown in Fig. 4.1. In brief, the procedure includes the fabrication of a multilayered thin-film structure on a rigid substrate, the lift off of this structure by dissolving the NaCl layer and the anodization of the Al film. The individual stages of this procedure and the related issues will be discussed in detail below.

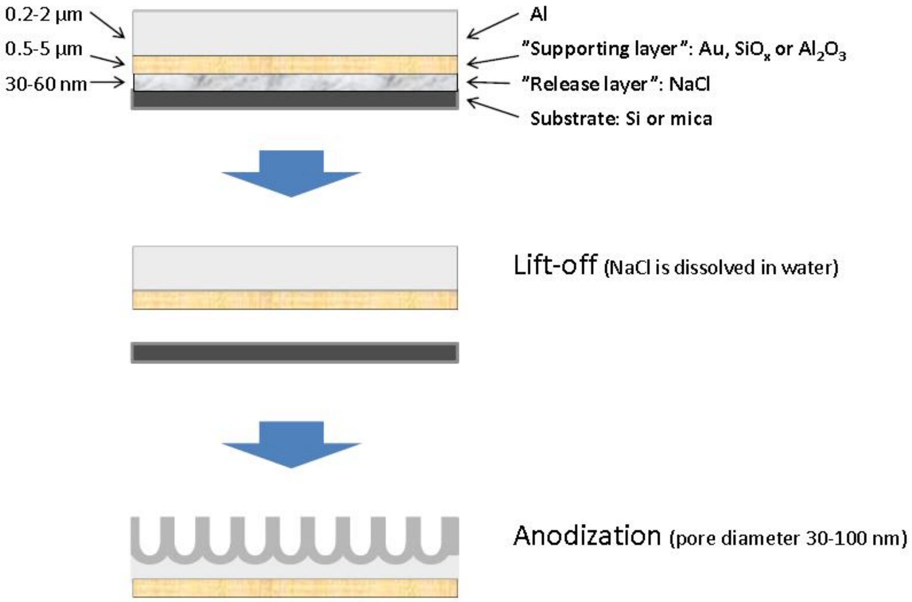

Figure 4.1. Schematic of the fabrication of thin-film PAA templates on free-standing thin-film supports.

4.3.1. Selection of the release layer

In principle, there are a number of different materials which could be used as release layers in thin-film fabrication. Relatively thick (a few microns) evaporated Al films can be used and further dissolved in NaOH [99]. However, this technique is not applicable in the case of supported PAA templates since the PAA is also dissolved by NaOH. In addition to that, multilayered structures obtained on such thick Al films might have unacceptably high surface roughness. Another modification of this technique involves electrochemical dissolution of Al layer in a NaCl solution [100, 101]. That requires making electrical contact to the Al layer which might be difficult for multilayered structures. Recently the use of water-soluble organic polymers as release layers in microfabrication was also reported [102, 103]. However, the adhesion of inorganic thin films to such layers might be poor and the application of such layers requires fine optimization of the spin-coating parameters and the composition of the precursor solutions.

Evaporated NaCl films have been widely used for producing free-standing thin films [104-107]. NaCl has the following advantages: it is cheap and readily available, it can be easily applied by e-beam or thermal evaporation, and it is very quickly dissolved in water. It is also important that a NaCl release layer can be deposited in the same vacuum chamber just before the deposition of the other films, without breaking the vacuum. That helps to avoid possible contamination of the fabricated structures.

4.3.2. Optimization of the deposition parameters for NaCl

In the present work, thin NaCl films were produced both by thermal and e-beam evaporation. The latter method is more convenient, since it allows a more accurate control of the deposition rate. The NaCl deposition conditions have been optimized assuming three main requirements to the release layer.

First, the release layer should be continuous and it should fully cover the underlying substrate. If the layer has holes going down to the substrate, the subsequent thin films will be in contact with the substrate and the complete lift off of the films will be impossible.

Second, the release layer should have a low surface roughness. A high roughness of this layer will lead to the roughening of the subsequently deposited films which is unfavorable.

Finally, the release layer should be quickly dissolved allowing fast lift-off of the subsequently deposited films.

In order to determine the optimal deposition conditions, NaCl films were evaporated at different rates ranging from 0.1 to 2 nm/s. Films with thickness from 20 nm to 5 μm were deposited. In Fig. 4.2a, SEM image of 5 μm thick NaCl films on Si deposited at 2 nm/s is shown. It can be seen, that the film has a rough grainy surface. The grain size varies from about 500 nm to 1-2 μm. At some points between the grains, large (around 1 μm) voids can be seen. Lowering the evaporation rate down to 0.5 nm/s results in a film with a similar grain size distribution, but in that case only a few small voids are observed (Fig. 4.2b). Thus in order to get continuous NaCl films, lower deposition rates should be employed. 5 μm thick NaCl films on Si are lusterless, which is also indicative of high surface roughness value. 600 nm thick NaCl film deposited at approximately the same rate (0.4-0.5 nm/s) has a reflective surface and is also much smoother on the microscopic scale (Fig 4.2c). Most of the grains are less than 500 nm in size, although a few grains of bigger size (1-2 μm) can also be seen.

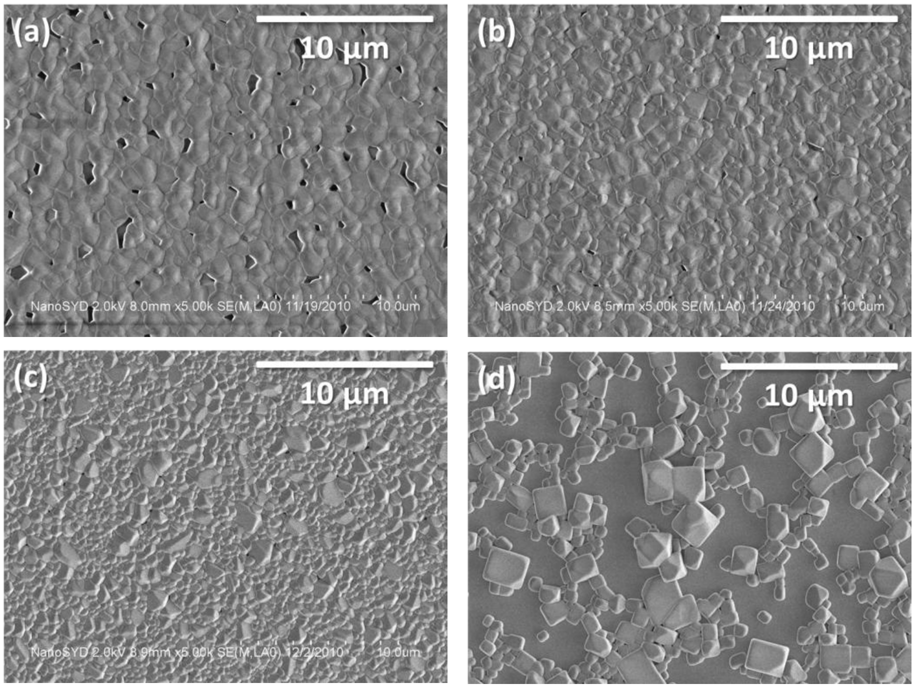

Figure 4.2. SEM images: 5 μm thick NaCl films on Si deposited at 2 nm/s (a) and 0.5 nm/s (b); 600 nm thick NaCl film on Si deposited at 0.5 nm/s (c), the same film partly dissolved and recrystallized after keeping in ambient air for a few hours (d).

It should be noted that post-depositional SEM observations of thin evaporated NaCl films are problematic since such films can easily get dissolved in humid air. Fig 4.2d shows a 600 nm thick NaCl film which was partly dissolved and recrystallized after keeping it in ambient air for a few hours. To avoid the dissolution of the films during the time between the deposition and the SEM imaging, they were stored in sealed boxes with silica gel. However such precautions did not help for the films having lower thicknesses (below 100 nm). Therefore in the present work SEM imaging was not performed for the films thinner than 100 nm.

From the obtained results, it can be concluded that the surface roughness of thin evaporated NaCl films increases with increase of both the deposition rate and the thickness. Thus in order to obtain smooth NaCl release layers, these parameters should be kept as low as possible. The minimum rate, which could be retained constant in the employed deposition machine, was about 0.1 nm/s.

To determine the lowest thickness of a NaCl film which would allow the complete and fast detachment of the thin films deposited above, a few more NaCl films of different thicknesses, starting from 20 nm, were deposited onto Si substrates. On top of each film, a thin (200-300 nm) Al layer was evaporated. The Al films were lifted off by putting the samples in a Petri dish with deionized water. For the 20-40 nm thick NaCl films, the detachment of the Al layer took too much time and the Al layer got partly broken. For the 60 nm thick NaCl film, the complete detachment of the Al film took about 2 minutes for a 1 x 1 cm^2 sample and the Al film remained undamaged.

Thus, the rate of 0.1 nm/s and the thickness of 60 nm were assumed to be the optimal parameters for depositing NaCl release layers.

4.3.3. Selection of the supporting layer

In some of the experiments, thin Al films were deposited directly onto NaCl release layers. After the lift-off, the obtained free-standing Al films were anodized to form PAA films. It was found that a self-standing Al film should have a thickness of at least 3-4 μm, preferably 5-10 μm. Thinner films can easily get broken and cannot be held without supports. As a consequence, two main difficulties appear in this approach.

First, few-micrometers thick Al films usually have very high surface roughness which will lead to a poor pore ordering in the finally obtained PAA films.

Second, producing thick Al films is problematic in most laboratory-scale evaporation systems because of the small crucible size and because of the spreading of the molten Al over the crucible walls.

If the thickness of the Al is reduced, the use of a supporting layer for the Al film should be considered. There are a few main requirements for such a supporting layer.

First, taking the deposited NaCl films out of the vacuum chamber will lead to their partial dissolution and therefore should be avoided. This means that the supporting layer should be made by some common deposition technique in the same deposition chamber without breaking the vacuum.

Next, it should be possible to produce few-micrometers thick supporting layers within acceptable time, i.e. the deposition rate for the respective material should be rather high.

Finally, the supported layer should have a smooth top surface and provide a good adhesion to the Al film deposited above.

There are two materials which meet (fully or partly) all of the mentioned requirements: evaporated silicon oxide (SiO_x) and evaporated aluminum oxide (Al_2O_3).

Both materials are readily available and can easily be deposited by e-beam evaporation. In the present work, deposition rates for SiO_x as high as 10-20 nm/s were obtained at intermediate (20-30 mA) beam currents. The maximum deposition rate obtained for Al_2O_3 was 0.2 nm/s. However, this value could be increased by placing the substrates more close to the deposition source. It is important that both materials form smooth amorphous films. In general, an amorphous supporting layer should be better than a polycrystalline one, since it will not introduce additional roughness to the subsequently deposited Al film by a grainy structure. Finally, both SiO_x and Al_2O_3 are known to provide good adhesion to Al films. Thus it is not necessary to introduce an adhesion layer between the supporting layer and the Al film.

4.3.4. Fabrication of PAA structures

The typical thickness of a SiO_x supporting layer was 4-5 μm. On top of the SiO_x, a 0.5-1 μm thick Al film was deposited. The typical thickness of an Al_2O_3 supporting layer was 500 nm because of lower deposition rate. The lower thickness of the supporting layer was compensated by depositing a thicker (about 2 μm) Al film.

The Al film on the supporting layer was lifted off by dissolving the NaCl release layer in water. After the lift-off, the Al film on the supporting layer was laminated onto a mica sheet (sometimes this technique is referred to as "lift-off lamination") and fixed on the sample holder of the anodization setup. The mica sheet acted as a flat and rigid support for the Al film during the anodization. After the anodization, the formed PAA film on a supported layer could be easily delaminated from the mica sheet by dipping the sample into water. In such a way the PAA film on a supported layer can be again transferred to some other substrate, if needed.

The as-prepared supported Al films were anodized either in 0.3M oxalic acid at 40 V or in 0.1M phosphoric acid at 170 V at 5°C. As a result, a PAA structure on a supporting layer with a thin intermediate layer of unoxidized Al was obtained.

Fig. 4.3a shows the top surface of a thin PAA film on a SiO_x supporting layer obtained by anodization in 0.1M phosphoric acid at 170 V. The pores are about 100-150 nm wide and the interpore distances are about 300 nm. The film has a typical morphology which is expected for the employed anodization conditions (compare, for example, to Fig. 3.8). In Fig. 4.3b, the cross-sectional view image of the fabricated structure is shown. It can be seen that the SiO_x layer is homogeneous and rather smooth. The presence of hillocks on the surface of the PAA film is explained by the high-rate deposition of the Al and also by the heating of the Al from the evaporation source during the deposition. Between the PAA and the SiO_x, a thin layer of unoxidized Al can be seen.

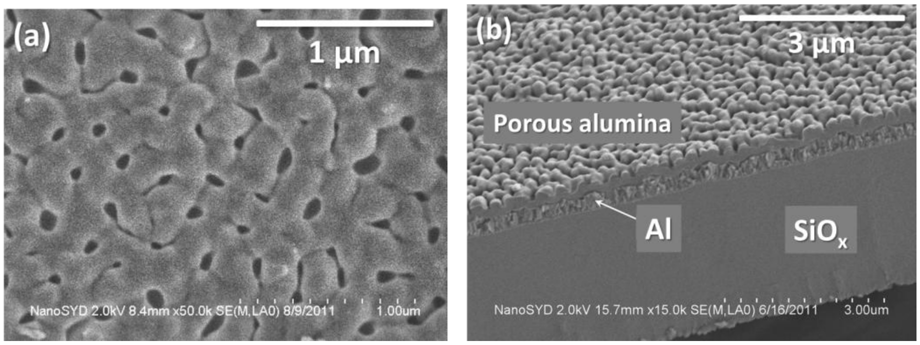

Figure 4.3. SEM images: top surface of a thin PAA film on a SiO_x supporting layer obtained by anodization in 0.1M phosphoric acid at 170 V (a), cross-sectional view of the same structure (b)

In Fig. 4.4a, the top surface of a thin PAA film on an Al_2O_3 supporting layer, obtained by anodization in 0.3M oxalic acid at 40 V, is shown. The pores are about 30 nm wide and the interpore distance is about 50-70 nm. Here, again, the “usual” PAA morphology, which is expected for the anodization of an Al film in oxalic acid, is obtained. Fig. 4.4b shows the cross-sectional view of the same structure. On the bottom of the structure, the Al_2O_3 supporting layer is seen. Above the Al_2O_3, a thick layer of unoxidized Al is located. Within this layer, three sub-layers with a bit different grain sizes can be noticed. The reason for their appearance is that the Al deposition was terminated two times and the chamber was opened for the refilling of the crucible. Thus the growth of Al columnar grains was terminated at some point and a thin native aluminum oxide film was formed.

The figure also shows the top view (Fig. 4.4c) and the cross-sectional view (Fig. 4.4d) of the same structure after the standard pore widening in phosphoric acid. It can be seen that the pore diameters increased to about 60-80 nm and the surface between the pores was smoothened. The hillocks on the PAA surface, which can be noticed in Fig.4.4b, correspond to the big grains of the Al film.

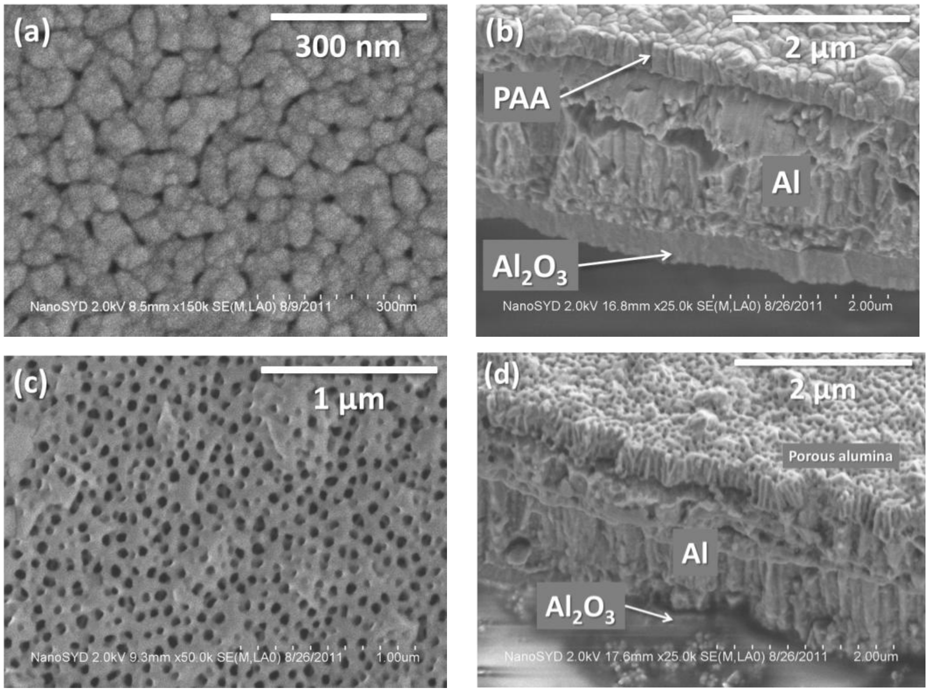

Figure 4.4. SEM images: top surface of a thin PAA film on an Al_2O_3 supporting layer obtained by anodization in 0.3M oxalic acid at 40 V (a); cross-sectional view of the same structure (b); top view and cross-sectional view of the same structure after pore widening in 5% phosphoric acid for 45 min.

4.4. SUMMARY AND OUTLOOK

In summary, thin-film PAA templates on free-standing thin-film SiO_x or Al_2O_3 supporting layers were successfully fabricated by a novel technique, which employed the use of water-soluble NaCl release layers.

It was found that the evaporation rate of 0.1 nm/s and the thickness of 60 nm are the optimal parameters for the deposition of NaCl release layers. The as-deposited NaCl films allow the fast and reliable lift-off of the subsequently deposited thin films.

Films of evaporated SiO_x and Al_2O_3 can act as appropriate supporting layers for thin Al films and subsequently fabricated PAA structures.

Some steps of the described procedure can be further improved. In particular, the Al thin films should be deposited at a lower rate (0.1-0.2 nm/s) and with a proper cooling of the substrate. This will allow the preparation of smooth Al films with small grains and PAA structures with good pore ordering.

As an option, the anodization of the Al could be made for the initial multilayered structure, i.e. without dissolving the NaCl layer. In such a case, the formed PAA template could be used for the fabrication of nanostructures and then lifted off at the very end by dissolving the NaCl layer. However, it is problematic to effectively isolate the NaCl layer from the electrolyte and to avoid its local dissolution during the anodization.

The fabricated PAA films on supporting layers can in principle be transferred to other substrates by lift-off lamination. As a temporary support, a thin mica sheet can be used.

Applying a thin conductive film between the Al and the supporting layer in the same manner as was described in Section 3.4.4 would make it possible to fabricate PAA templates on conductive thin-film substrates. Such templates could in turn be used, e.g. for the fabrication of metallic nanowire arrays on thin-film supports via electrochemical deposition. Furthermore, the fabricated nanowire arrays could be transferred to another substrate via lift-off lamination.

The application of the as-prepared PAA templates for the fabrication of organic nanotubes by means of template wetting will be described in detail in Chapter 6.

Chapter 5. Nanowires and Nanotubes from π-Conjugated Organic Materials Fabricated by Template Wetting

5.1. INTRODUCTION

1D nanostructures from π-conjugated organic molecules are known to possess interesting optical, electrical and optoelectronical properties, namely emission of light following electrical or optical excitation, waveguiding and lasing. They have already been used successfully as active layers in field effect transistors, light emitting diodes, full colour displays, organic semiconductor lasers and solar cells [108-111]. Mutual alignment and orientation of such nanostructures may influence the device performance. Therefore, it is important to synthesize well aligned nanoaggregates, having high aspect ratios, in a controllable manner.

The use of PAA's as templates is a versatile approach to the preparation of 1D nano- and microstructures. Wetting of PAA templates with solutions or melts allows fabrication of nanowires and nanotubes from a wide variety of materials. The diameters and lengths of such 1D structures correspond to those of the templates, which in turn can be readily tuned within a wide range by adjusting the anodization conditions.

In the present chapter, the fabrication of 1D nanostructures (nanowires and nanotubes) from poly(3-hexylthiophene) (P3HT), poly(9,9-dioctylfluorene-2,7-diyl) (PF8), 2,7-diphenylcarbazole (DPC), zinc phthalocyanine (ZnPc) and perylene-tetracarboxydiimide (PTCDI) by means of wetting of PAA templates, is considered.

The investigation of the formation of 1D nanostructures form these materials (as well as from the other derivatives bearing the same molecular structure units) is important since they are promising candidates for different electronic device applications. P3HT is employed as active material in BHJ solar cells [112]. Polyfluorenes, polycarbazoles as well as phthalocyanines and perylene derivatives are also considered as active layer materials for different optoelectronic devices [54-56, 113-115].

Since the DPC nanowires are obtained for the first time by the mentioned technique, their morphology and optical properties are systematically studied and compared to those of the DPC nanoaggregates obtained by organic molecular beam deposition (OMBD) on mica substrates. The fabrication of P3HT nanostructures for the further implementation in bulk heterojunction solar cells will be described in details in Chapter 6.

5.2. MECHANISMS OF TEMPLATE WETTING

The morphology of 1D nanostructures and microstructures obtained by wetting of porous templates is determined by the wetting mechanism involved [51-53].

It is considered that wetting of pores by liquids consisting of molecules with low molecular weight starts with the formation of a wetting layer on their walls, which is similar to the formation of precursor films on smooth substrates. However, curved liquid films are susceptible to instabilities. Occurrence of instabilities leads to the formation of menisci and can eventually lead to a complete filling of the pore volume, if more liquid moves into the pore. In such a case, nanowires can be obtained (Fig. 5.1a).

In the case of a melt containing sufficiently mobile macromolecules whose characteristic dimensions are larger than the pore diameter, a mesoscopic wetting layer is rapidly formed on the pore walls. If such a layer is kinetically stable, nanotubes can be obtained after solidifying the polymer (Fig. 5.1b). As this mechanism involves the formation of a precursor film, it can be referred to as “precursor wetting”. A prerequisite for “precursor wetting” is a sufficiently high surface energy of the pore walls which is realized for PAA templates.

If templates are wetted with polymers at temperatures slightly above their solidification temperatures or by microphase-separated block copolymer melts, individual macromolecules cannot easily be removed from the bulk. In such a case, rapid formation of a precursor film is suppressed. The pore volume is entirely filled by the material and nanowires are obtained (Fig. 5.1c). As this mechanism is driven by classical capillarity, it may be referred to as “capillary wetting”. The same mechanism governs infiltration if the initially polar pore walls are converted into a non-polar surface with low surface energy, for example by silanization. Then, there is no more driving force for the rapid formation of a precursor film [51-53].

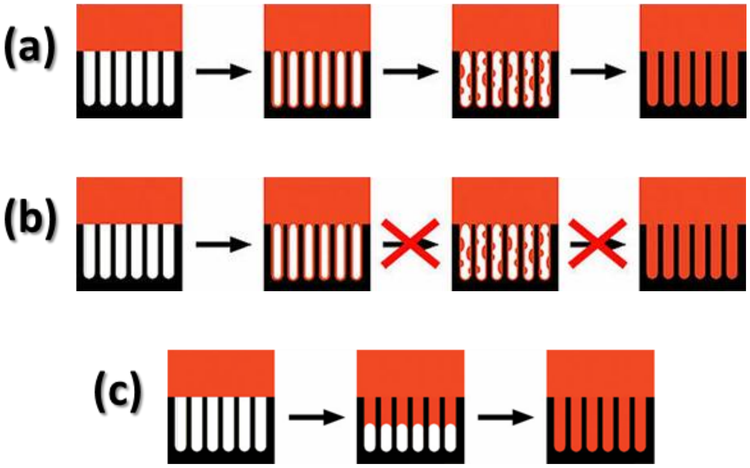

Figure 5.1. Mechanisms of template wetting [116].

5.3. EXPERIMENTAL DETAILS

5.3.1. P3HT nanotubes

P3HT (regioregular, semiconductor grade) was purchased from Rieke Metals. For the fabrication of nanostructures by means of template wetting, commercial membrane filters (Anodisc™), having mean pore diameters of 200 nm and thickness of 60 µm, were used. The P3HT was inserted into the pores of the template by both solution- and melt-assisted wetting. In the case of solution-assisted wetting, two solutions of P3HT in chlorobenzene having different concentrations (a saturated solution and a

1 mg/ml solution) were used. A drop of P3HT solution was placed on top of a membrane and the membrane was sandwiched between two glass slides. The membrane was left covered for 10-12 hours to allow slow evaporation of the solvent. In the case of melt-assisted wetting, a thin P3HT film was formed on a glass microscope slide by spin-coating from a saturated solution in chlorobenzene (at 600 rpm for 60 s). A porous membrane was placed onto the P3HT film and heated on a hotplate to 250°C for 15 min. In both cases, a sticky carbon pad was attached to one side of the membrane, while the other side was cleaned from the excess polymer by scratching with a scalpel. The nanotube arrays were freed by dissolving the membrane in a 2M NaOH solution for 5 hours.

5.3.2. PF8 nanowires and nanotubes

Regioregular PF8 was purchased from Sigma-Aldrich. For the fabrication of nanofibers by means of template wetting, commercial membrane filters (Anodisc™) mentioned above, were employed. The PF8 was introduced into the pores of the template by both solution- and melt-assisted wetting. In the case of solution-assisted wetting, two solutions of PF8 in toluene having different concentrations (a saturated solution and a 1 mg/ml solution) were used. A drop of a PF8 solution was placed on top of a membrane and the membrane was sandwiched between two glass slides. The membrane was left covered for about 10 hours to allow slow evaporation of the solvent. In the case of melt-assisted wetting, a thin PF8 film was formed on a glass slide by spin-coating from a saturated solution in toluene (at 600 rpm for 60 s). A porous membrane was placed onto the PF8 film and heated on a hotplate to 180°C for 15 min. A sticky carbon pad was attached to one side of the membrane, while the other side was cleaned from the excess polymer by scratching with a scalpel. The nanowire/nanotube arrays were released by dissolving the membrane in a 2M NaOH solution.

5.3.3. DPC nanowires

The DPC was synthesized by I. Wallmann et al. following the procedure described in details elsewhere [117]. For the fabrication of nanowires by means of template wetting, commercial membrane filters (Anodisc™) mentioned above, were employed. Two solutions of DPC in DMSO having different concentrations (a saturated solution and a 0.02M solution) were used. The DPC was introduced into the pores by means of so called "drip-and-dry" method. This method involved placing the template on a 50°C hot plate and slowly dripping the precursor solution onto it. After each drop was added, the solvent was allowed to evaporate. After a prescribed number of "drip-and-dry" cycles (typically 20), a piece of the membrane was attached to an adhesive carbon pad and excess material was removed from the top of the membrane using a scalpel. Supported DPC nanofibers were obtained by selective dissolution of the supported membrane in 2M NaOH solution. Another piece of the same membrane was left unsupported and freed from excess material on both sides. In that case, nanofibers were freed by dissolution of the membrane (2M aqueous NaOH, 5 hours), rinsed several times in deionized water and collected by centrifugation.

5.3.4. ZnPc and PTCDI nanowires

ZnPc and PTCDI (semiconductor grade) were purchased from Sigma-Aldrich. Both materials were introduced into the pores by means of so called "dip-and-dry" method. In that technique, the porous membrane was dipped into the respective solution for 2 minutes. After dipping, the membrane was put on a 50°C hot plate and the solvent was allowed to evaporate. 5 mg/ml solution of ZnPc in N,N'-dimethylacetamide and saturated solution of PTCDI in chloroform were used. After 20 "dip-and-dry" cycles, a sticky carbon pad was attached to one side of the membrane, while the other side was cleaned from the excess polymer by scratching with a scalpel. The nanowire arrays were released by soaking the membrane in a 2M NaOH solution for 5 hours.

5.3.5. Characterization of the nanostructures

Optical images of nanowire/nanotube arrays and single nanowires/nanotubes were obtained by a fluorescence microscope (Nikon Eclipse). Polarization measurements (for DPC nanowires) were performed using the same microscope with a rotational stage mounted on its sample holder. Temperature dependent fluorescence spectra of the DPC samples between room temperature and 6 K were performed in a He-cryostat with the pressure in the sample chamber being lower than $5 \cdot 10^5$ mbar. Fluorescence of the DPC samples was excited by a He-Cd laser (λ = 325 nm) and the spectra were acquired using a spectrograph coupled to a cooled CCD camera.

Scanning electron microscopy (SEM) images of all nanowire/nanotube arrays were acquired using a Hitachi S-4800 instrument operating at beam voltages of 2–3 kV. In order to facilitate SEM imaging, all of the samples were coated with Au/Pd (2 nm) by magnetron sputtering (Cressington HR 208 sputter coater). Atomic force microscopy (AFM) was performed with an apparatus from JPK Instruments operating in tapping mode.

5.4. RESULTS AND DISCUSSION

5.4.1. P3HT nanowires and nanotubes

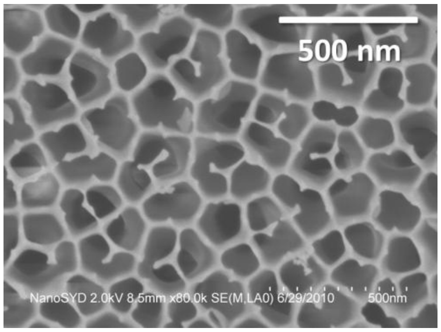

Figure 5.2. Top-view SEM image of a commercial PAA membrane (Anodisc™)

A top-view SEM image of a commercial PAA membrane (Anodisc™) is shown in Fig. 5.2. On the image, individual pore openings are clearly seen. The pores have irregular shape and are not well arranged, which is a characteristic of a single-step anodization process. The pore openings are funnel-shaped. Over the pore openings a very thin porous layer with lower pore diameters and interpore distances can be seen. Such a complex structure of the membrane arises, probably, from some specific manufacturing conditions (changing the anodization voltage, etc.).

SEM images of P3HT nanotubes fabricated by template wetting are presented in Fig. 5.3. Fig. 5.3a shows a bundle of P3HT nanotubes obtained after the wetting of a template by 1 mg/ml P3HT solution. Fig. 5.3b shows an array of P3HT nanotubes obtained by wetting of a template by a P3HT melt. The nanotubes have the same diameters as those of the template pores (about 250 nm). The endings of the nanotubes are grown together and are funnel-shaped. Thus the formed P3HT nanotubes represent a replica of the structure of the PAA template. Most of the nanotubes are bent showing mechanical flexibility.

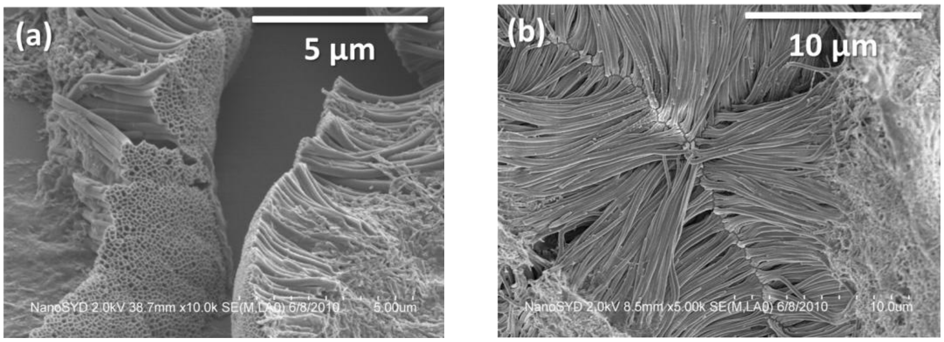

Figure 5.3. SEM images of P3HT nanotubes obtained by wetting of a PAA template: by a saturated solution of P3HT in chlorobenzene (a) and by P3HT melt (b).

It should be noted that for P3HT, both solution- and melt-assisted wetting leads to the formation of nanotubes, not nanowires. That can be explained by the “precursor wetting” mechanism described above. This mechanism involves the formation of kinetically stable precursor film on the walls of the PAA template. The evaporation of the solvent (in the case of P3HT solution) and solidification of the polymer after cooling it below the melting point (in the case of P3HT melt) leads to the formation of nanotubes in the pores of the PAA template.

5.4.2. PF8 nanowires and nanotubes

SEM images of PF8 nanostructures prepared by template wetting are presented in Fig. 5.4. Fig. 5.4a shows a bundle of PF8 nanotubes obtained after the wetting of a template by a 1 mg/ml PF8 solution. The nanotubes has the same diameters as the pores of the membrane (about 250 nm). The shapeless residue between the nanotubes is probably the alumina which was not removed completely during the PAA template dissolution. In Fig. 5.4b, the opening of a single nanotube is shown. The nanotube wall thickness, as can be estimated from the picture, is about 50 nm. Figures 5.4c and 5.4d show arrays of PF8 nanowires obtained by wetting of a template by a saturated PF8 solution and PF8 melt, respectively. Many of the nanowires are bent, showing some degree of flexibility.

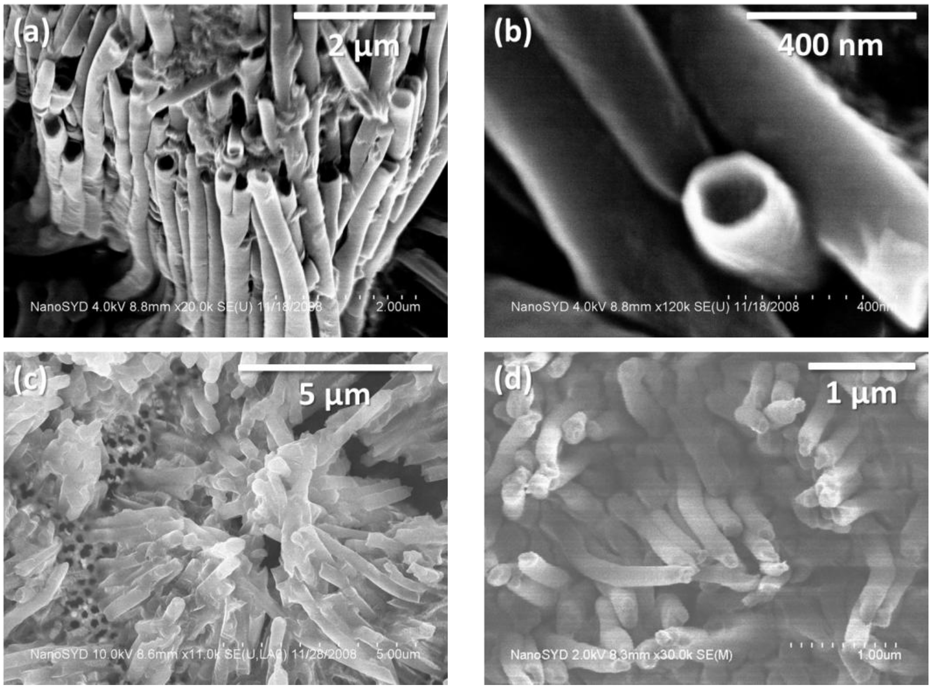

Figure 5.4. SEM images of PF8 nanotubes obtained via wetting of a PAA template by PF8 solutions in toluene having different concentrations: (1 mg/ml (a, b), saturated solution (c)) and by PF8 melt (d).

It should be noted that for the 1 mg/ml PF8 solution, mostly nanotubes are formed, while for the saturated solution and melt only nanowires can be obtained. This fact can be explained by the “precursor wetting” mechanism which is described above for P3HT. However, in the case of PF8 the formed precursor film is not stable. The template pores can be completely filled if the amount of material is sufficient, which is the case for concentrated solutions and melts of PF8.

5.4.3. DPC nanowires

Since the DPC nanosturctures were obtained for the first time by template wetting technique, their morphology and optical properties were studied in more detail. The results were compared to those for DPC nanoaggregates grown on mica by organic molecular beam deposition (OMBD). These structures were fabricated by A. Ghazal in his Bachelor Thesis [118]. The detailed analysis of the results for these two types of DPC nanostructures is given in [119].

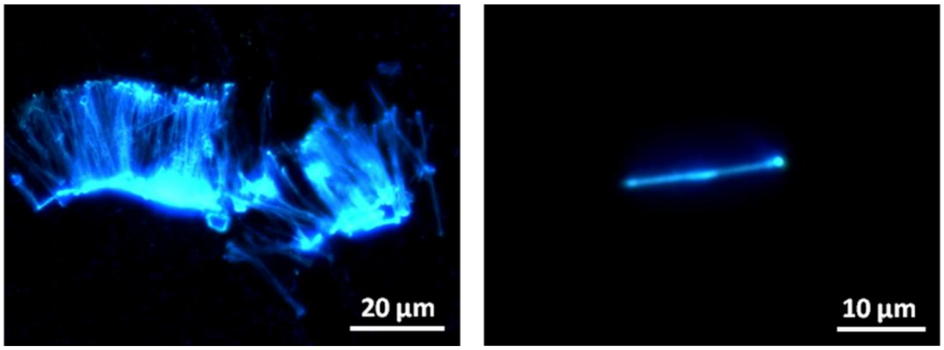

Figure 5.5. Fluorescence microscopy images of DPC nanowires obtained by wetting of a PAA template: bundle of nanowires lying on a carbon pad (a) and a single nanowire isolated via centrifugation (b).

Fluorescence microscopy images of the DPC nanowires obtained by wetting of a PAA template by a saturated solution of DPC in DMSO are shown in Fig. 5.5. Fig. 5.5a shows a bundle of blue-emitting nanowires remained on the surface of a carbon pad after complete dissolution of the porous template. It can be seen that the ends of the nanowires are merged together. Bright blue emitting regions on the image correspond probably to some excess of the DPC which did not go into the pores of the template. In Fig. 5.5b a single DPC nanowire (or a small bundle of nanowires) isolated by centrifugation is displayed. The mean nanowire length estimated from the fluorescence microscopy images is about 30 µm which is two times less than the pore depth of the PAA template (60 µm). Probably, the employed number of “drip-and dry” cycles was not enough to fill all the pores of the template completely. Some of the nanowires (or bundles of nanowires) could also get broken during the template removal procedure.

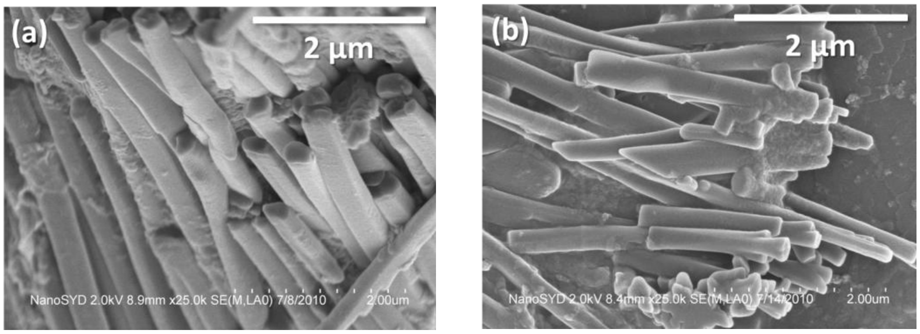

Figure 5.6. SEM images of DPC nanowires obtained by wetting of a PAA template: by a saturated solution of DPC (a) and by a diluted (0.02M) solution of DPC (b).

SEM images of DPC nanowires fabricated by template wetting are presented in Fig. 5.6. Fig. 5.6a shows a bundle of DPC nanowires obtained after the wetting of a template by a saturated DPC solution. The nanowires have the same diameters as those of the template pores (about 250 nm). Some of them are slightly bent showing some degree of flexibility. The shapeless residue which can be seen in between the wires is most likely the alumina which was not dissolved completely during the template removal. In the Fig. 5.6b DPC nanowires obtained by wetting of a template by a diluted (0.02M) DPC solution are shown. The as-prepared nanowires are quite short (less than 2 µm) if compared to those obtained with the use of a saturated DPC solution. Apparently, in the case of lower concentrations the lack of material inside the template pores does not allow the formation of longer structures. The tips of the wires show a characteristic funnel-like shape originating from the initial surface morphology of the porous template (see Fig. 5.2).

Fig. 5.7 shows an AFM scan of a single DPC wire by template wetting, lying on a glass substrate. It can be seen that the shape of the wire is not perfectly cylindrical but exhibits a few facets. On the surface of the wire some small grains are also seen. Most probably these features originate from the morphology of the PAA templates. The width of the wire measured by AFM is about 350 nm, i.e. higher than the value which can be obtained from SEM images. However the substrate below the wire might not be perfectly flat and the wire itself can be slightly bent and raised above the substrate surface; therefore it is hard to extract the real dimensions of the wire from the presented image. Thus for the case of single nanowires obtained by the wetting technique and transferred to another substrate, only quantitative characterization can be made by AFM. The wire dimensions should be estimated from SEM images.

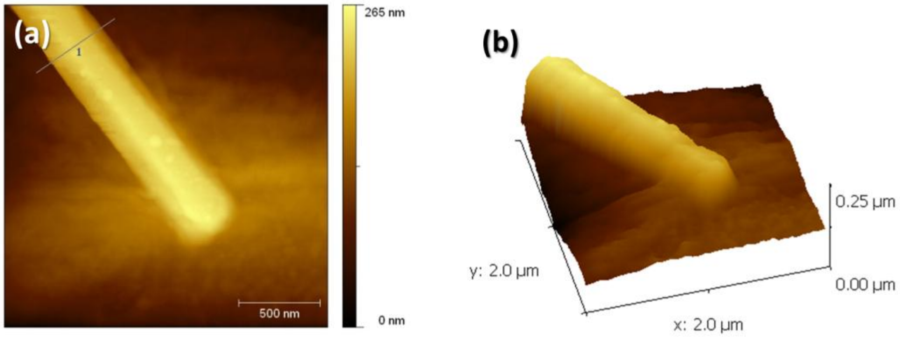

Figure 5.7. 2D (a) and 3D (b) AFM image (2 x 2 μm^2) of a single DPC nanowire obtained by template wetting.

Polarization properties of DPC nanostructures

Polarization measurements performed on the as-fabricated DPC nanowires reveal their strong polarization anisotropy. The dependence of the fluorescence intensity on the polarization angle for single DPC nanoaggregates obtained by OMBD and template wetting are shown in Figures 5.8 and 5.9, respectively.

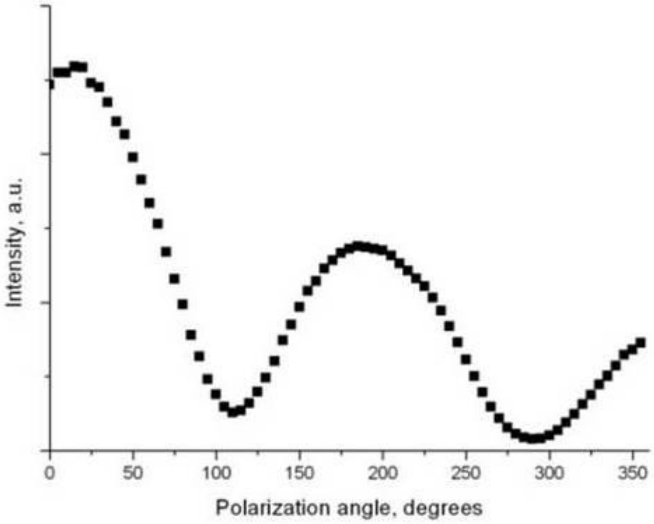

Figure 5.8. Dependence of the fluorescence intensity on the polarization angle for a single DPC nanofiber obtained by OMBD at substrate temperature 330 K.

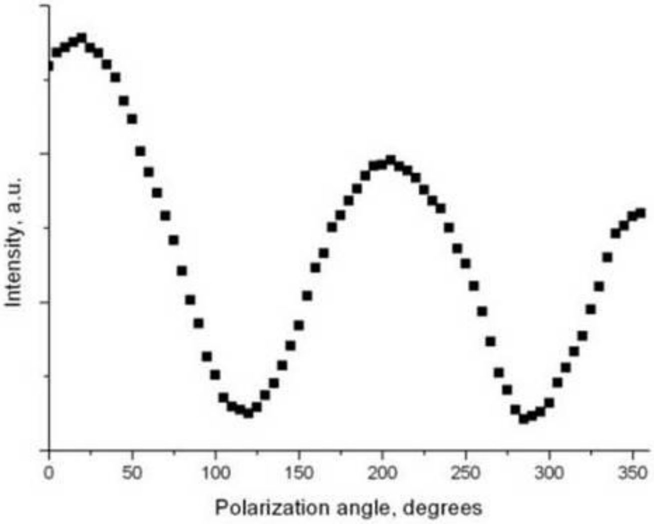

Figure 5.9. Dependence of the fluorescence intensity on the polarization angle for a single DPC nanowire obtained by template wetting.

It can be seen that the intensity in the second maximum is lower than in the first one, i.e. the nanowires undergo bleaching when being irradiated by UV light in air. Since the observed dependence is highly distorted by the bleaching, only the first S-shaped branch of the curve was used to determine the polarization ratio. For this purpose, a fit of this branch for each case by a $\sin^2$ was made.

The measured polarization ratio $\rho = (I_{\max} - I_{\min})/(I_{\max} + I_{\min})$ of the maximum ($I_{\max}$) and minimum ($I_{\min}$) intensities is 0.86 ± 0.02 for a single nanowire obtained by OMBD and 0.49 ± 0.02 for a single nanowire obtained by template wetting. The difference in these values can be explained by the higher degree of molecular alignment within the nanoaggregates made by OMBD. As it has been shown by scanning near-field optical microscopy (SNOM) and polarized linear fluorescence measurements for p-6P nanofibers grown on mica by OMBD [120, 121], deviations from the mean polarization angle can be caused by inhomogeneities within individual nanoaggregates, i.e. each nanowire can consist of domains having different molecular orientations. Thus the difference in the polarization ratios found for the two methods can also be explained by a wider distribution of orientations of such domains within individual wires made by template wetting. In addition, some of the observed wires may actually consist of several individual aggregates which cannot be resolved by the microscope. That should also lead to the lowering of the observed polarization ratio.

For both methods of fabrication, the maximum fluorescence intensity is observed for the orientation of the polarizer being almost perpendicular (88°) to the nanowires' long axes. This is in agreement with the results obtained for p-6P nanofibers on mica [120, 122]. Thus it can be concluded that for DPC nanowires obtained by both techniques the main linear transition dipole moment is oriented nearly perpendicular to the wire axes.

Low-temperature photoluminescence of DPC nanostructures

Temperature dependent PL spectra for bulk DPC as well as for DPC nanostructures obtained by template wetting and OMBD at two different substrate temperatures are presented in Appendix B (pages 127-130).

Since all the measurements were performed in vacuum (pressure lower than $5\cdot10^5$ mbar), no changes in the PL spectra due to bleaching were observed. As can be seen from the picture, the shape of the spectra changes significantly with decreasing the temperature from 298 K to 6 K. The structure of the spectra is also different for all the samples under investigation. In particular, the spectral features are significantly different for DPC nanowires obtained by wetting if compared to the case of OMBD; for OMBD they also differ for two substrate temperatures. It should be also noted that with decreasing the temperature, the overall intensity of all PL spectra increases significantly, i.e. the fluorescence yield increases.

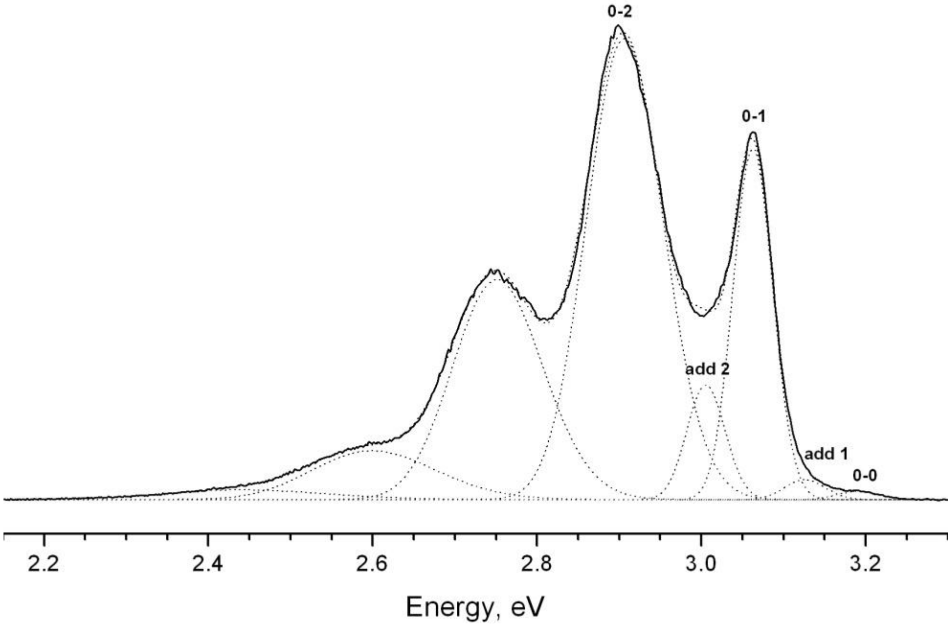

Figure 5.10. PL spectrum of bulk DPC measured at 60 K (solid line), fit of the spectrum by Gaussian peaks (dotted lines).

For the quantitative analysis, all of the spectra were fit with a set of Gaussian curves. An example of such a fitting is shown in Fig. 5.10. From the fitting procedure individual peak positions, linewidths

(FWHMs) and relative intensities were determined. The three most pronounced vibronic peaks are 0-0, 0-1 and 0-2. The intensity of the 0-0 peak for the bulk DPC is negligible, that can be explained by a strong self absorption.

In Fig. 5.11, shifts of the 0-0 and 0-1 peaks with respect to the room temperature spectrum for bulk DPC and DPC nanowires obtained by template wetting and by OMBD at two substrate temperatures are shown. It can be seen that the 0-0 and 0-1 peaks for all samples show a blue shift with decreasing temperature. The position of the 0-2 peak (not shown on the picture) does not present any distinct trend. The blue shift in low temperature PL spectra was also observed for p-6P nanofibers [122, 123]. It was attributed to exciton-phonon interactions, the probability of which decreases with decreasing temperature.

In Fig. 5.12, widths of the 0-0 and 0-1 peaks for all PL spectra are presented. The peak widths decrease monotonically with decreasing temperature, pointing to an inhomogeneous broadening mechanism [123]. For the 0-2 peak in the spectra of bulk DPC and DPC nanowires obtained by template wetting (not shown) the same trend is observed. For the nanowires obtained by OMBD, the width of this peak slightly increases between 298 K and 210 K and then decreases again. It should be noted, however, that the structure of PL spectra observed at relatively high temperatures (above 200 K) is not well pronounced, which makes the quantitative analysis rather difficult. In particular, the exact widths and relative intensities of the 0-2 peak and peaks corresponding to higher order transitions are hard to determine.

With decreasing the temperature, a redistribution of relative peak intensities is observed for all samples. In particular, the relative intensity of the 0-0 peak decreases, becoming negligible (less then 1%) at temperatures below 90 K. The relative intensity of the 0-1 peak slightly increases between 298 K and 230 K and then decreases again.

For the temperatures below 90 K, the PL spectra cannot be fitted with the same set of peaks which is used for higher temperatures. Additional peaks have to be introduced between 0-0 and 0-1 peaks and also between 0-1 and 0-2 peaks (see Fig. 5.10, the corresponding peaks are labeled as

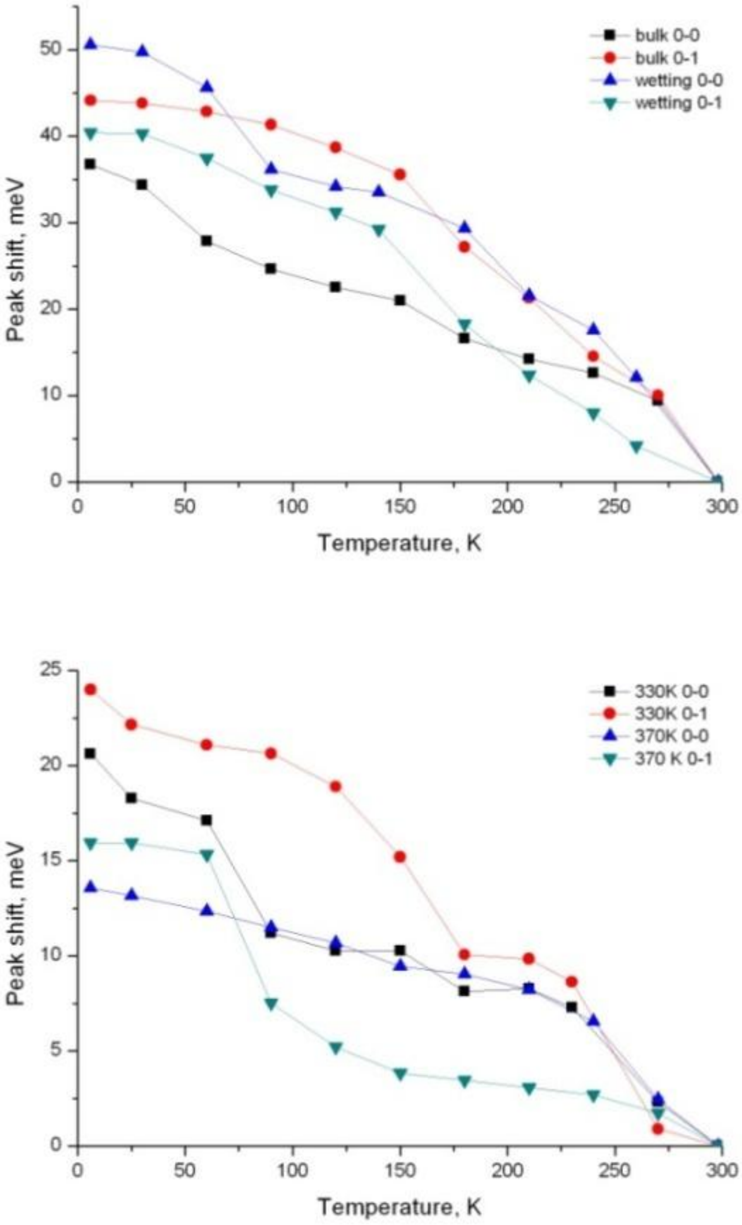

Figure 5.11. Peak shifts with respect to the room temperature spectrum for bulk DPC and DPC nanowires obtained by template wetting (a) and for DPC nanowires obtained by OMBD at two substrate temperatures (b).

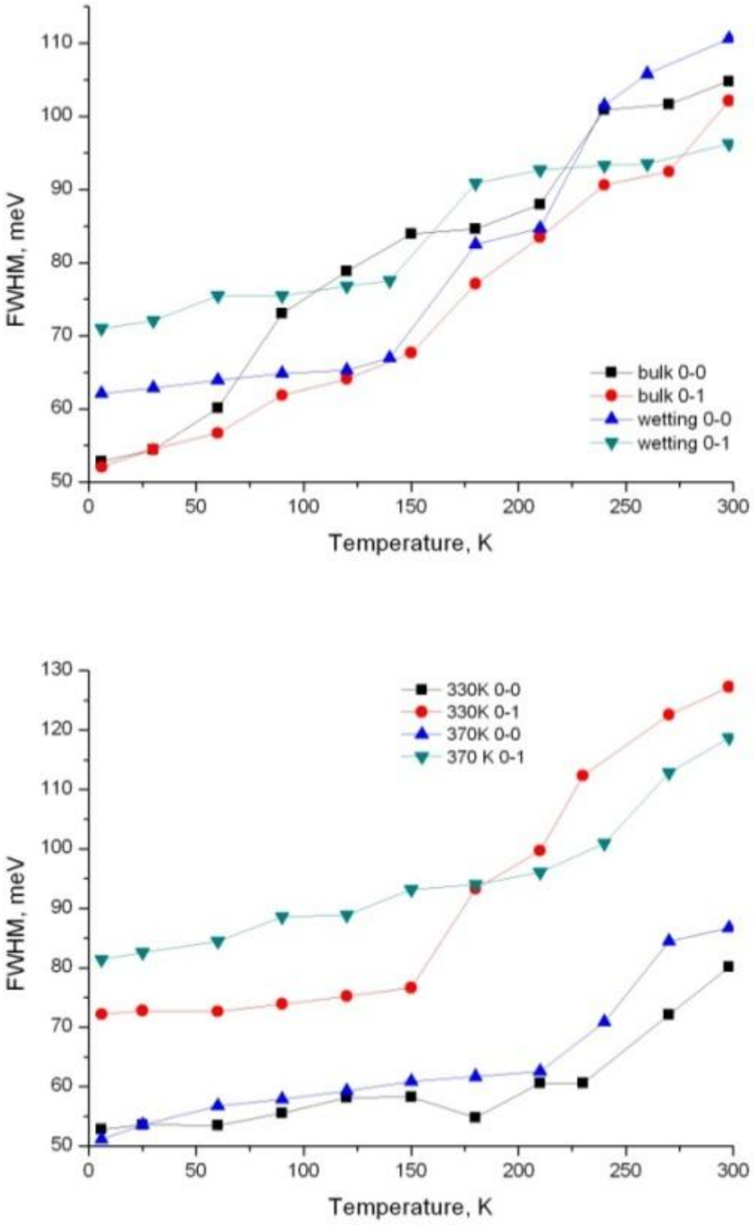

Figure 5.12. Peak widths in PL spectra of bulk DPC and DPC nanowires obtained by template wetting (a) and of DPC nanowires obtained by OMBD at two substrate temperatures (b).

“add 1” and “add 2”). These additional peaks show the same behaviour as 0-0 and 0-1 peaks, namely they shift to the blue with decreasing the temperature and their linewidths also decrease. Furthermore, the relative intensities of these peaks increase when decreasing the temperature from 90 K to 6 K. The appearance of additional peaks in the high-energy part of a PL spectrum was reported for p-6P nanowires [122, 123]. The nature of these peaks is still unclear. They can be assigned e.g. to another molecular species in the deposited film [123].

5.4.4. PTCDI nanowires

PTCDI was introduced into the template pores by means of so-called “dip-and-dry” method. This method involved dipping a PAA template into a saturated PTCDI solution in chloroform a number of times and letting the solvent fully evaporate each time. The “drip-and-dry” technique used for DPC could not be employed for the case of PTCDI. Because of its very high volatility, chloroform would fully evaporate before the solution could fill the template pores completely. As a result, the PTCDI would crystallize just on top of the template, and not inside the pores.

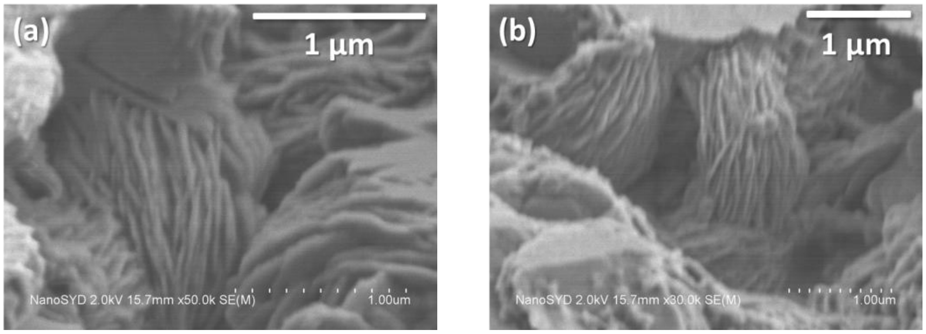

Figure 5.12. PTCDI nanowires obtained by wetting of a PAA template with a saturated solution of PTCDI in chloroform.

PTCDI nanowires obtained by wetting of a PAA template with a saturated solution of PTCDI in chloroform are shown in Fig. 5.12. The tips of the nanowires are connected to big unstructured pieces of PTCDI which was not completely removed before the template dissolution. The nanowire diameters are about 100 nm which is much lower than the template pore diameter (250 nm).

In fact, it is unclear from the obtained SEM images, if the PTCDI forms only nanowires, and not nanotubes, under these particular conditions. To determine the morphology of the PTCDI nanostructures obtained by template wetting, further studies have to be conducted.

5.4.5. Nanostructures from ZnPc

ZnPc was inserted into the template pores by means of so-called "dip-and-dry" method. That was made by dipping a PAA template into a 5 mg/ml solution of ZnPc in N,N'-dimethylacetamide a number of times and letting the solvent fully evaporate in each cycle. As in the case of PTCDI, dripping the ZnPc solution onto the template would lead to the crystallization just on top of the template, because of the fast evaporation of the solvent.

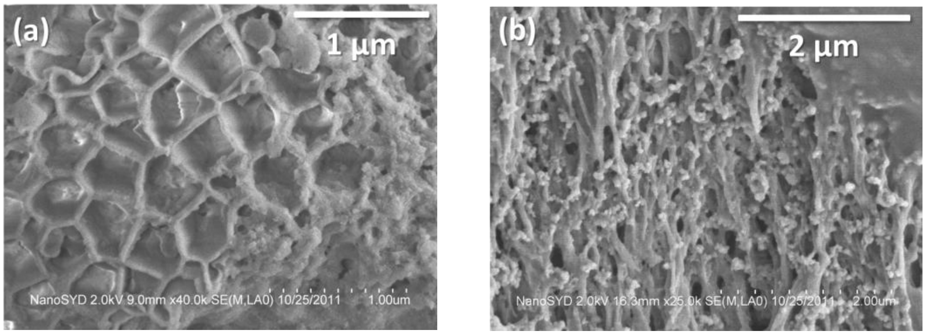

Figure 5.13. Pores of the PAA membrane filled with ZnPc (a) and ZnPc aggregates formed after crystallization of ZnPc in the template pores (b).

This approach failed to give any pronounced 1D nanostructures form ZnPc. As can be seen from Fig. 5.13a, the pores of the PAA template were at least partly filled by ZnPc after the employed wetting procedure. Fig. 5.13b shows ZnPc nanoaggregates formed in the template pores close to the pore openings. In the upper part of the picture, unstructured ZnPc film which covered the PAA template can be seen. The SEM images confirm that the ZnPc solution entered the pores during the wetting procedure. Apparently, the amount of material crystallized inside the template pores was not enough to form pronounced nanowires. Probably, long nanoaggregates could be formed after employing a big number of dip-and-dry cycles. However, the need to employ too many of such cycles would make the approach itself unfeasible. As an alternative, electrophoretic deposition of ZnPc into the template pores could be used. This technique has been successfully used to prepare nanowire arrays from other phthalocyanines [46-49].

5.5. SUMMARY AND OUTLOOK

In this chapter, the template fabrication of 1D nanostructures from P3HT, PF8, DPC, PTCDI and ZnPc is described. It is shown that all of the mentioned materials, except from ZnPc, form nanowires and/or nanotubes when being introduced into the pores of a PAA template in the form of solution or melt. The results are summarized in Table 5.1 and compared to the data obtained by other authors for the same molecules or chemically analogous derivatives.

Nanostructures form the polymers P3HT and PF8 can be obtained by both solution- and melt-assisted template wetting. For these materials, the so-called “precursor wetting” is realized. For P3HT, the precursor film formed on the pore walls is kinetically stable, and therefore this material can only form nanotubes – for wetting with both solutions and melts. For PF8, the formed precursor film is not stable and the morphology of the obtained nanostructures depends on the amount of material introduced into the pores. For solutions with lower concentrations, mostly nanotubes are obtained. For highly concentrated solutions and melts, the pore volume can be filled completely, and the formation of nanowires is dominating.

Table 5.1. 1D nanostructures from π-conjugated organic materials fabricated via template-based techniques.

Material	Reference	Method of fabrication	Fabrication conditions	Morphology of the obtained nanostructures
P3HT	[124]	MAW	250°C, vacuum	Nanohillocks
	[125]	NIL with PAA film on Si as a stamp	125°C	Nanohillocks
	Present work	SAW	1 mg/ml solution	Nanotubes
		SAW	Saturated solution	Nanotubes
		MAW	250°C, vacuum	Nanotubes/ hollow nanohillocks
PF8	[56]	SAW	40 mg/ml PF8 solution	Nanotubes
	[54, 55]	SAW	60 mg/ml PF8 solution	Nanowires
	Present work	SAW	1 mg/ml PF8 solution	Nanotubes
		SAW	Saturated solution	Nanotubes
		MAW	180°C	Nanowires
Carbazole	[103]	PVD into PAA template	150°C	Nanotubes
DPC	Present work	SAW, “dip-and-dry”	Saturated solution	Nanowires
PDD	[50]	ED into PAA template	CF_3COOH as protonating agent	Nanowires
PTCDI-C8	Present work	SAW, “drip-and-dry”	Saturated solution	Nanowires
CuPc, $EuPc_2$, $GdPc_2$, $HErPc_2$	[46-49]	ED into PAA template	CF_3COOH as protonating agent	Nanowires
ZnPc	Present work	SAW, “drip-and-dry”	5 mg/ml solution	Small nanoaggregates

Abbreviations: PDD – “perylene-diimide derivative”, CuPc – copper phthalocyanine, $EuPc_2$ – europium bisphthalocyanine, $GdPc_2$ – gadolinium bisphthalocyanine, $HErPc_2$ – erbium bisphthalocyanine; MAW – melt-assisted wetting, SAW – solution-assisted wetting, NIL – nanoimprint lithography, PVD – physical vapor deposition, ED – electrochemical deposition.

The small molecules DPC, PTCDI and ZnPc can be introduced into a PAA template by wetting it with a corresponding solution a number of times and letting the solvent fully evaporate after each wetting approach (“dip-and-dry” and “drip-and-dry” techniques). These techniques result in the crystallization of the corresponding material inside the template pores and its accumulation with each wetting-drying cycle.

For DPC, it was demonstrated, that the length of the nanowires depends on the concentration of the wetting solution (for the same number of “drip-and-dry cycles”). For a saturated solution of DPC, the pores are filled almost completely, while for a diluted (0.02 M) solution only few-μm long wires could be obtained. The obtained nanowires show strong polarization anisotropy. The polarization ratio was found to be 0.49 ± 0.02, indicating a rather low degree of mutual alignment of DPC molecules (and/or molecular domains) in the nanowires. Detailed analysis of the temperature dependent PL spectra from the as-prepared DPC nanowires reveals many of the trends reported for p-6P nanofibers [123], namely blue shifts and narrowing of the spectral peaks with decreasing temperature and redistribution of peak intensities.

For PTCDI, the wetting of a template with a saturated solution gives few-μm long nanowires whose widths are lower than the pore diameters (around 100 nm).

For ZnPc, introducing a 5 mg/ml solution into the template pores gave only small aggregates. Therefore, template wetting cannot be considered as the optimal technique for the fabrication of ZnPc nanowire arrays. Instead, electrophoretic deposition of ZnPc into the template pores could be used.

Chapter 6. Template Fabrication of Nanostructures for Bulk Heterojunction Solar Cells

6.1. ARCHITECTURE OF BHJ SOLAR CELLS

The ideal structure of a BHJ solar cell is schematically shown in Fig. 6.1. The phases of donor and acceptor within the BHJ have to be interspaced with an average length scale of around 10-20 nm, i.e. equal to or less than the exciton diffusion length. The two phases should form percolated highways to ensure high mobility charge carrier transport with reduced recombination. Furthermore, a pure donor phase at the hole collecting electrode and a pure acceptor phase at the electron collecting electrode should be placed. That will minimize the losses by recombination of the wrong sign charges at the wrong electrode. A pure donor or acceptor phase will also act as a diffusion barrier for the wrong sign charge carriers at the respective electrode [126, 127].

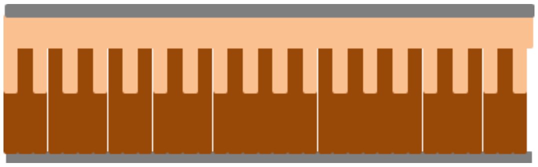

Fig. 6.1. The ideal structure of a BHJ solar cell [127].

Self-organization of organic semiconductors has been introduced by e.g. an amphiphilic primary structure like di-block copolymers resulting in a self-organized phase [128] or liquid crystalline self-organizing columns of donor-acceptor phases [129]. In the mentioned devices, the device architectures were not optimal in terms of their nano-scale morphology. Further improvements were needed to obtain devices of higher efficiency.

A promising approach for the realization of the architecture mentioned above is filling of PAA pores with semiconducting polymers. This idea has been realized by different authors for P3HT and PCBM as the active layer materials [124, 125, 130-134]. In most approaches, 1D nanostructures from P3HT were fabricated on ITO electrode and the space between them was filled by PCBM. The P3HT was introduced into PAA pores by melt-assisted wetting [124, 132, 134] and also by nanoimprint lithography, using PAA templates as mechanical stamps [125]. P3HT-PCBM blends were also used [133], in that case 1D core-shell structures were obtained in the template pores. PCBM was applied on top of the P3HT nanostructures by lift-off lamination [125].

It has been demonstrated that the hole mobility in regioregular P3HT can be enhanced by a factor of 20 by infiltrating it into straight nanopores of a PAA template. Furthermore, optical characterization of the formed P3HT nanowires showed that the polymer chains are partially aligned in the charge-transport direction [131]. It was reported [124] that in a photovoltaic device utilizing P3HT nanorods as donor and C_{60} as acceptor, a seven-fold efficiency increase, compared to a device with a planar bilayer, is achieved. Thus PAA template-based nanostructuring of active layers in BHJ solar cells was proved to be effective for improving their performance.

This chapter describes the fabrication of P3HT nanostructures for the further implementation in organic BHJ solar cells. Different aspects of using thin-film PAA templates for this purpose are discussed in detail.

6.2. EXPERIMENTAL DETAILS

6.2.1. Fabrication of P3HT nanotubes – "Procedure 1"

The schematic of the fabrication procedure is shown in Fig. 6.2.

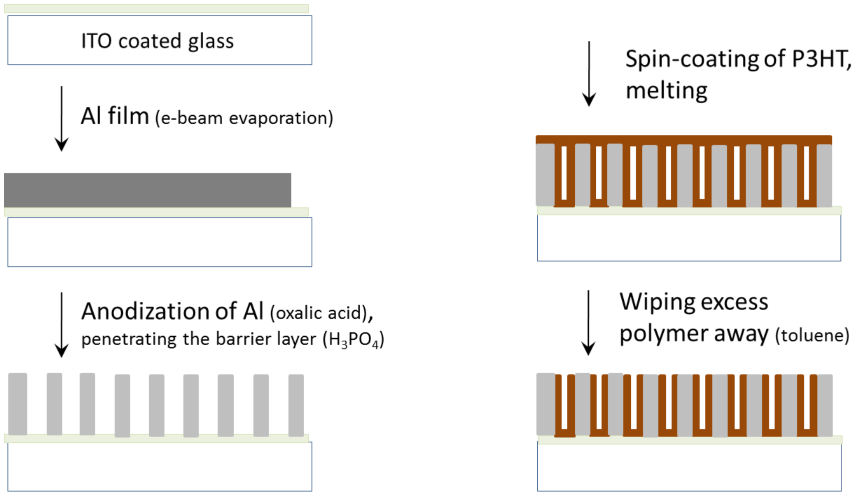

Figure 6.2. Template fabrication of P3HT nanotubes on ITO coated glass substrates (“Procedure 1”).

PAA template preparation

ITO-coated glass slides were cleaned by ultrasonication in isopropanol for 5 min. followed by oxygen plasma etching (5 min. at 100 W, Branson IPC 3000 barrel plasma system). Thin Al films (thickness 500-800 nm) were produced on ITO-coated glass slides by e-beam evaporation. The deposition rate was 0.1-0.2 nm/s. The substrates were kept in contact with a water-cooled stage at temperature about 10°C. To improve the adhesion of Al to ITO, a thin (1-2 nm) Ti layer was formed on top of ITO by e-beam evaporation, prior to the deposition of Al.

The as-prepared thin Al films were anodized in 0.3M oxalic acid at 40-60 V at 5°C. After the anodization, the barrier oxide was penetrated and the pores were slightly widened by soaking the sample in 5% H_3PO_4 at room temperature for 45 min. Afterwards the PAA templates were rinsed 3 times in deionized water, dried on a hot plate at 150°C for 15 min. and cleaned by oxygen plasma etching (5 min. at 300 W, Branson IPC 3000 barrel plasma system).

Fabrication of P3HT nanotubes

A thin P3HT film was made on the top of a PAA template by spin-coating from a saturated P3HT solution in chlorobenzene at 900 rpm for 60 s. The formed P3HT film was baked at 70°C for 30 min. in air to let the remaining solvent fully evaporate. Afterwards the PAA template with a thin P3HT film on top was placed into a vacuum chamber and heated up to 250-270°C for 30 min to allow the melt-assisted wetting of the PAA template. The pressure in the chamber was about 10^{-2} mbar. After the heating was turned off, the sample was left for cooling down to the room temperature at the same pressure. The excess of the P3HT was fully removed from the top of the PAA template by gently wiping it with a soft tissue wetted by toluene. In some of the experiments, the P3HT nanotubes were partly released by etching the PAA template in 2M NaOH for 10-30 min. or fully released by soaking in a stirred 2M NaOH for 2 hours at room temperature.

6.2.2. Fabrication of P3HT nanotubes – "Procedure 2"

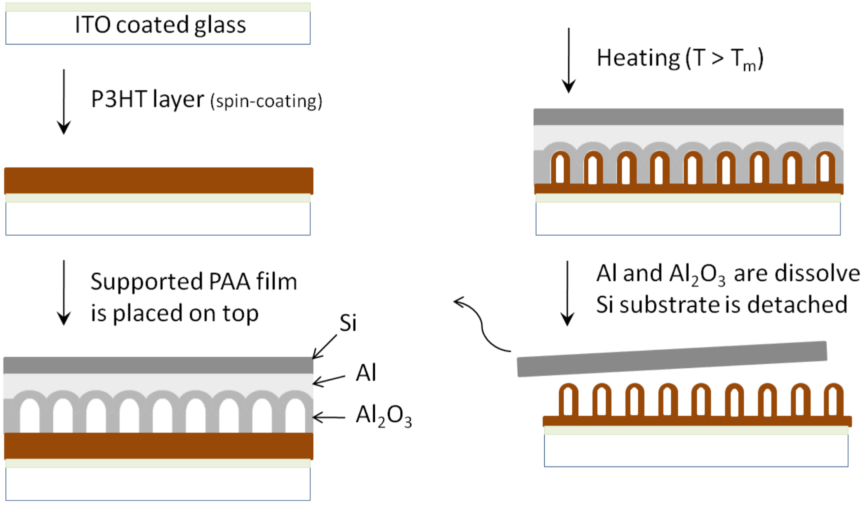

Figure 6.3. Template fabrication of P3HT nanotubes on ITO coated glass substrates ("Procedure 2").

The schematic of the fabrication procedure is shown in Fig. 6.3.

PAA template preparation

Silicon (Si (100), *p*-type, resistivity 1-100 Ohm·cm^{-1}) substrates were pre-cleaned by ultrasonication in acetone and ethanol (5 min. in each solvent) followed by oxygen plasma etching (5 min. at 300 W, Branson IPC 3000 barrel plasma system). Thin Al films (thickness 500-1000 nm) were produced on Si substrates by e-beam evaporation. The deposition rate was 0.1-0.2 nm/s. The substrate temperature during deposition was about 10°C. To improve the adhesion of Al to Si, a thin (5 nm) Ti layer was deposited by e-beam evaporation, prior to the deposition of Al.

The as-prepared thin Al films were anodized in 0.1M H_3PO_4 at 170 V at 5°C. The obtained PAA templates were rinsed 3 times in deionized water, dried on a hot plate at 150°C for 15 min. and cleaned by oxygen plasma etching (5 min. at 300 W, Branson IPC 3000 barrel plasma system).

Fabrication of P3HT nanotubes

ITO-coated glass slides were cleaned by ultrasonication in isopropanol for 5 min. followed by oxygen plasma etching (5 min. at 100 W, Branson IPC 3000 barrel plasma system). A thin P3HT film was made on the top of ITO-coated glass slide by spin-coating from a saturated P3HT solution in chlorobenzene at 600 rpm for 60 s. In some of the experiments, a thin P3HT film was made both on ITO-glass and on top of the PAA template used for wetting. In such cases, the spinning rate was 900 rpm for both substrates. The formed P3HT films were baked at 70°C for 30 min. in order to remove the remaining solvent.

For some of the samples, a thin layer of PEDOT:PSS was formed on ITO-glass prior to the application of P3HT. PEDOT:PSS was applied by spin-coating a filtered solution at 3000 rpm for 60 s. The formed PEDOT:PSS thin film was baked at 110°C for 50 min.

PAA template was placed on top of P3HT film on ITO-glass upside down and the two structures were firmly fixed together by metallic clamps. The “sandwiched” samples were placed into a vacuum chamber and heated up to 250-270°C for 30 min as described above for “Procedure 1”. The P3HT nanotube- or nanohillock-arrays on ITO glass were released by etching the PAA template and the remaining Al in 2M NaOH for 5-24 hours (depending on the sample size) at room temperature and lifting off the Si substrate.

In some of the experiments, thin PAA films on Al supports prepared by two-step anodization of Al foils were used as templates. The two-step anodization of Al foils was made as described in Section 3.4.1. The procedure for the P3HT nanotubes preparation was similar to the one described above

6.2.3. Fabrication of P3HT nanotubes – "Procedure 3"

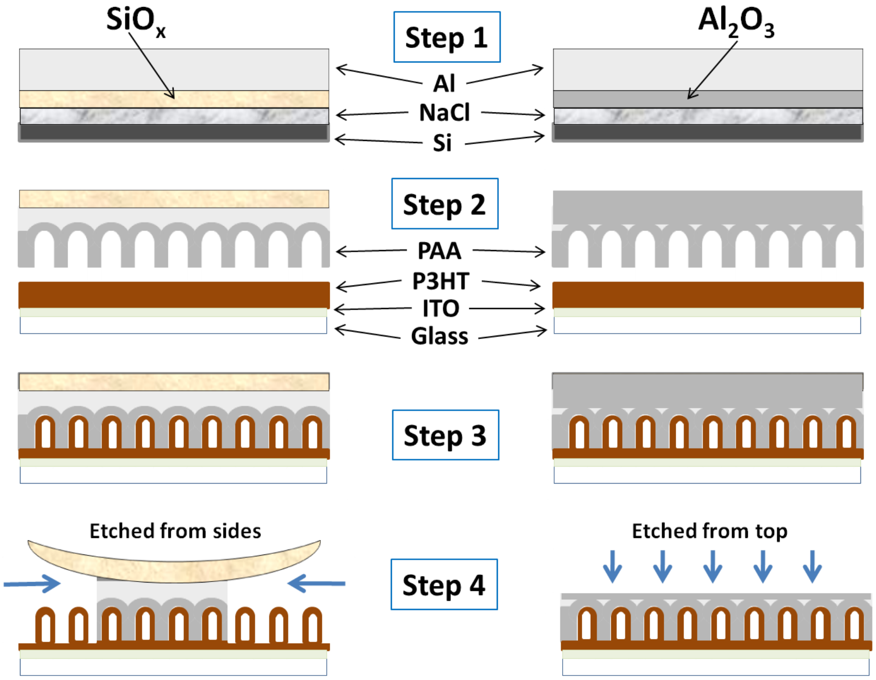

Figure 6.4. Template fabrication of P3HT nanotubes on ITO coated glass substrates with the use of NaCl release layer ("Procedure 3"):

Step 1 – NaCl release layer, SiO_x or Al_2O_3 supporting layer and thin Al film are deposited onto a Si substrate;

Step 2 – thin Al film on supporting layer is detached from the Si substrate and anodized to form PAA template, the PAA template is placed upside down onto a thin P3HT film on ITO-glass;

Step 3 – as a result of melt-assisted wetting, P3HT nanotubes are formed in the pores of the PAA template;

Step 4 – the PAA template is removed by etching in NaOH.

The schematic of the fabrication procedure is shown in Fig. 6.4.

PAA template preparation

The procedure for the fabrication of PAA templates on thin-film supports, which was used in “Procedure 3”, is described in detail in Chapter 4.

Fabrication of P3HT nanotubes

The ITO-coated glass slides were pre-cleaned as described above for “Procedure 2”. A thin P3HT film was made on the top of ITO-coated glass slide by spin-coating from a saturated P3HT solution in chlorobenzene at 600 rpm for 60 s and the formed films were baked at 70°C for 30 min.

Thin-film supported PAA template was placed on top of P3HT film on ITO-glass upside down and made in a firm contact with the ITO-glass by gently pressing it from the top. The “sandwiched” samples were heated up to 250°C for 5 min. The P3HT nanotube- or nanohillock-arrays on ITO glass were released by etching the PAA template and the remaining Al in stirred 2M NaOH solution for 10-50 min. (depending on the sample size and the supporting layer of the PAA template) at room temperature.

6.3. RESULTS AND DISCUSSION

6.3.1. “Procedure 1”

In “Procedure 1”, the PAA template is made on ITO-coated glass and the pores are subsequently filled with P3HT melt to form P3HT nanotubes staying in contact with the ITO electrode (see Fig. 6.2).

For the efficient work of a solar cell, it is critical that the P3HT nanotubes stay in electrical contact with the bottom electrode (i.e. ITO layer) while the complementary material (typically PCBM) fills the free spaces between the P3HT nanotubes. It is important that the PCBM does not have any contact with the ITO electrode.

Fig. 6.5a, shows a PAA template filled with P3HT according to “Procedure 1”.

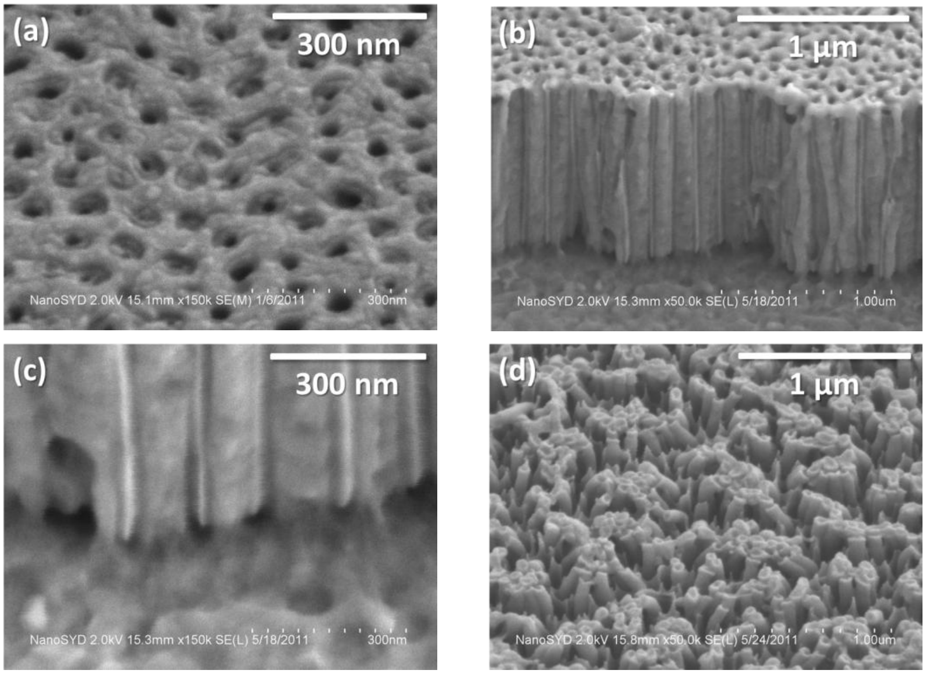

Figure 6.5. SEM images: PAA template filled with P3HT via melt-assisted wetting (a), cross-sectional views of a P3HT-laden PAA template standing on ITO-glass (b, c), P3HT nanotubes partly released by etching the PAA template in 0.1M NaOH for 15 min. (d),

On the picture, tips of the P3HT nanotubes, sitting in the template pores, are seen. The outer diameter of the nanotubes is equal to the template pore diameter (about 80 nm). The nanotube wall thickness, as can be estimated from the image, is about 20-30 nm and is almost the same for all of the nanotubes. Some of the pores were merged together during the etching in H_3PO_4; thus, the respective nanotubes are also merged. Since the template pore diameter varies from about 60 to 100 nm, the inner diameter of the narrowest P3HT nanotubes can be as small as 5-10 nm. In principle, for narrower pores (less than 50 nm) only nanowires could be formed. In such a case the complementary material

(PCBM) could not be inserted into the tubes and the area of the interface between the two phases would be much smaller. As was mentioned above, the P3HT and PCBM should be interspaced with an average length scale of around 10-20 nm, i.e. equal to or less than the exciton diffusion length. Therefore the optimal template pore diameter is considered to be higher than 60 nm, preferably in the range between 60 and 100 nm. These diameters are typically obtained after controlled etching of the PAA prepared by anodization of Al in oxalic acid at 60 V. The nanotubes are in contact with the underlying ITO layer, as can be seen form Fig. 6.5 (b, c).

There is one more reason why the use of oxalic acid at this particular voltage is favourable. The thickness of the barrier layer formed after anodization of Al in the other two common electrolytes, namely sulphuric acid and phosphoric acid, is higher than the PAA pore wall thickness. For such PAA films, the barrier layer cannot be removed without penetrating the pore walls. On the other hand, the barrier layer for the PAA films formed in oxalic acid at 60 V (i.e. close to the breakdown voltage) is thinner than the pore walls and can be easily penetrated by wet etching [27, 28].

One could assume that partial release of the P3HT nanotubes from the template pores would increase the area of the interface between P3HT and PCBM and increase the device performance. Fig. 6.5d, shows an array of P3HT nanotubes partly freed by soaking the sample in 0.1M NaOH at room temperature for 15 min. As can be seen from the picture, the pores of the remaining PAA film are significantly widened and there are gaps between the walls of the P3HT nanotubes and the PAA pore walls. It is known [3-4] that PAA films consist of two types of aluminum oxide which have different density. The outer part of a pore wall is built from a lower density oxide, while the inner part consists of oxide having higher density. As a result, the wet etching of PAA films is not isotropic. The outer parts of the pore walls are etched away significantly faster, leaving rod-like upright standing PAA fragments consisting of higher-density aluminum oxide. Such a situation is unfavourable for the fabricated solar cell device since the layer of electron acceptor (PCBM) applied at the next stage will fill the gaps between the P3HT nanotubes and the PAA pore walls and get in contact with the ITO electrode. In addition to this, the widened template pores will not serve as a mechanical support for the P3HT nanotubes any more.

Thus it can be concluded that for “Procedure 1” the further wet etching of the PAA template should not be made. In that case, the electron acceptor material should be applied on top of the P3HT-laden template.

6.3.2. “Procedure 2”

In “Procedure 2”, a thin P3HT film is formed on ITO-glass by spin-coating and a thin-film PAA template on a silicon substrate is placed upside-down on top of the P3HT film and firmly attached to it. Heating of the “sandwiched” structure above the melting point of P3HT leads to the wetting of the template by the P3HT melt. After solidification of the melt, P3HT nanotubes are formed in the template pores. The arrays of P3HT nanotubes (or hollow “nanohillocks”) upright standing on a thin P3HT film are released by dissolving the PAA and the remaining Al in NaOH and lifting off the silicon substrate.

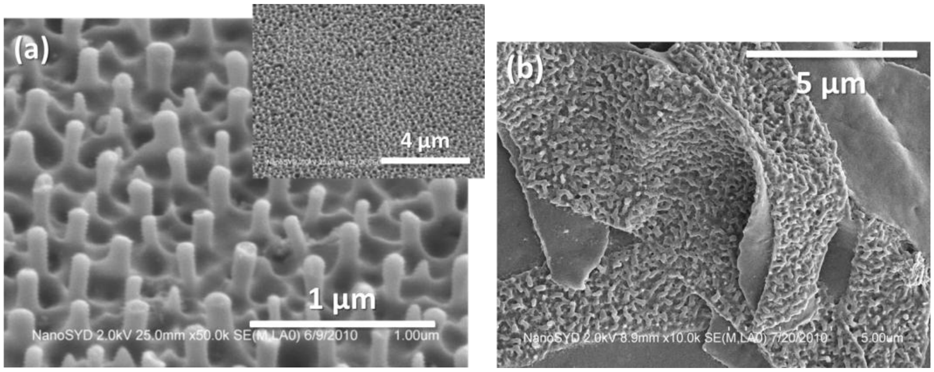

Figure 6.6. P3HT nanohillocks on a thin P3HT film made by template wetting. The P3HT film is formed directly on ITO-coated glass, without intermediate PEDOT:PSS layer (a). The structured P3HT film may get damaged and partly detached during the template removal procedure if a PEDOT:PSS layer is present below the P3HT film (b).

Fig. 6.6a shows an array of P3HT nanohillocks on a thin P3HT film, formed on ITO coated glass. The mean diameter of the nanohillocks is about 100 nm which is equal to the mean diameter of the pores of the PAA template used (see Fig. 3.8). The mean nanohillock height is equal to the mean depth of the PAA pores (400-500 nm). Between the hillocks, small ridges can be seen. The ridges are about 100-200 nm high and less than 50 nm wide. They result from the filling of the concave features of the PAA template surface (see also Fig. 3.8) by the P3HT melt. Thus the formed P3HT nanostructures form a replica of the surface of the PAA template employed.

In fact it is not possible to conclude from the presented SEM images, if nanotubes (or hollow nanohillocks) or nanowires were formed. However, SEM images of a similar PAA template wetted by P3HT melt under the same conditions (Fig. 6.5) confirm the formation of nanotubes. For this sample, the excess of P3HT was fully removed from the top of the template by wiping with a soft tissue wetted in toluene and the template pores could be directly observed. The nanotube wall thickness is estimated to be 20-30 nm. Thus it should be expected that the P3HT nanohillocks obtained in "Procedure 2" are hollow and have the wall thickness of about 20-30 nm. The inner volume of these hillocks is probably filled with air captured from the template pores on the stage of melt-assisted wetting.

It should be pointed out that the melt assisted wetting procedure described here is very different from the structuring of P3HT films by nanoimprint lithography using PAA templates as stamps. The latter procedure involves the pressing of the softened polymer into the template pores. In such a case, the polymer is heated up to a temperature which is far below its melting point. As a result, only nanowires (or filled nanohillocks) can be obtained. The melt assisted wetting involves the formation of P3HT precursor film on the walls of the template. In the case of P3HT, this film is kinetically stable, which leads to the formation of nanotubes after the solidification of the polymer.

It was found that the optimal aspect ratio of the PAA template pores, which allows the fabrication of upright standing nanotubes, is about 3 to

5. Nanostructures of higher aspect ratios tend to bend and merge together. The required aspect ratios can be obtained by carefully controlling the anodization time for the given electrolyte and voltage. For the anodization in 0.1M phosphoric acid at 170 V the needed time is 5 min. These parameters give PAA films with 100 nm wide and 300-500 nm deep pores. Anodization in 0.3M oxalic acid at 40-60 V is also an option. In that case the subsequent pore widening in H_3PO_4 will give 80 nm wide pores and low interpore distances (around 50-100 nm compared to 200-300 nm for the anodization in phosphoric acid).

The "surface quality" of the PAA template (i.e. pore ordering, absence of grooves between the pores) in "Procedure 2" is less critical than in "Procedure 1". On the opposite, the trenches between the formed P3HT nanohillocks, originating from the grooves between the PAA pores, increase the area of the interface between P3HT and PCBM. That should increase the overall device performance.

In general, the described procedure allowed the fabrication of upright standing P3HT nanohillocks on large areas (up to 1 X 1 cm^2). However, for bigger samples (2.5 X 2.5 cm^2), the etching of the PAA during the template removal step took an extremely long time (up to 48 hours), even under intensive stirring. The etching process was also hard to control because of the rigidness and opacity of the Si substrates.

The presence of a thin PEDOT:PSS films below the P3HT film introduced additional difficulties. The water based NaOH solution used to remove the PAA could also penetrate beneath the P3HT film and partly dissolve the PEDOT:PSS layer. That led to fragmentation and partial detachment of the P3HT film, as can be seen from Fig. 6.6b. Such a difficulty occurred even if the sides of the samples were covered by nail polish to prevent the dissolution of PEDOT:PSS.

The described problem was caused by the need to etch the PAA and the remaining Al from the sides of the sample and hence by the prolonged soaking of the samples in the etching solution. In order to reduce the etching time and to improve the control of the PAA removal, thin PAA films supported by Al foils were used as templates. These films were prepared by two-step anodization of Al foils and had approximately the same morphology (pore sizes and interpore distances) as the PAA films on Si substrates. These films were employed in the same manner as the ones fabricated on Si supports. The advantage of using PAA films on Al substrates was that the substrate could be also removed by wet etching. $CuCl_2$/HCl solution was used as etching solution for Al. This solution allowed very fast and selective (with respect to aluminum oxide) etching of the Al host. Complete removal of the Al support took typically 5-7 min. and after that the PAA was etched away by soaking the sample in 2M NaOH for 20 min.

Though the duration of the template removal step was reduced to about 30 minutes, this approach failed to give big arrays of P3HT nanotubes. The P3HT structures were found to form only on very small, restricted areas on the P3HT film.

Such a failure can be explained by the fact that thick Al foils have a rather big surface roughness on a big scale. In other words, the foils are "wavy" on the scale of tens or hundreds of microns. Therefore the area of contact between the PAA film on Al foil and the P3HT film during the wetting procedure can be restricted to a few small regions. The rest of the PAA template is not wetted by the P3HT melt.

In order to overcome the difficulties described above for "Procedure 2", thin-film PAA templates on thin-film supports were employed. The corresponding procedure is denoted as "Procedure 3".

6.3.3. "Procedure 3"

"Procedure 3" described below is the modified version of "Procedure 2". In this procedure, a thin PAA film supported on either a thin silicon oxide film or a thin aluminum oxide film is used as a template. Such free-standing thin-film PAA templates are prepared with the help of NaCl release layers, as described in detail in Chapter 4. These templates are employed in the same manner as the ones fabricated on rigid Si or Al supports.

Fig 6.7a shows an array of P3HT nanohillocks on a thin P3HT film on ITO-coated glass. These structures were obtained via melt-assisted wetting of a PAA template shown in Fig. 4.3. The template was prepared by anodizing thin Al film supported by 5 μm thick evaporated silicon oxide in 0.1M phosphoric acid at 170 V. The morphology of the nanostructured P3HT film represents the surface features of the employed PAA template. The hillocks have heights of 200-400 nm and diameters of 100-200 nm. The distance between neighbouring hillocks is 200-300 nm.

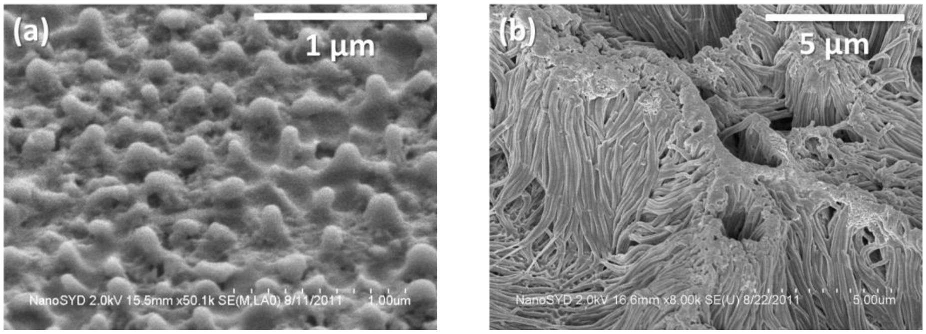

Figure 6.7. P3HT nanostructures obtained by wetting of free-standing thin-film PAA templates.

On Fig 6.7b, P3HT nanotubes supported by thin P3HT film on ITO-glass are shown. The structures were made by melt-assisted wetting of a PAA template shown in Fig. 4.4. The template was prepared by anodizing thin Al film supported by 500 nm thick evaporated aluminum oxide in 0.3M oxalic acid at 40 V. The pores were subsequently widened by wetting the sample in 5% phosphoric acid for 45 min. at room temperature. The obtained nanotubes are about 10 μm long and are merged together. The aspect ratios of these particular structures are not optimal for the considered solar cell architecture. However they can be readily decreased by tuning the anodization time.

Thin-film PAA templates on thin film supports have clear advantages over templates fabricated on rigid supports like Si and Al.

First, such templates are rather flexible which makes it possible to have a firm contact between a template and a spin-coated polymer film. Even in the case of a “wavy” polymer film surface, a flexible thin-film template will follow all of the surface features. That allows the fabrication of ordered 1D polymer nanostructures on large areas.

Second, the thin-film nature of the supporting layers facilitates significantly the PAA template removal. As the etching of the PAA proceeds, the flexible silicon oxide layer lifts off gradually. That makes the etching much faster. When the etching is completed, the silicon oxide film can be easily removed from the top of the nanostructured P3HT film without shifting or damaging it. If a PEDOT:PSS layer is formed below the P3HT film, the reduction of the etching time should help to prevent its dissolution.

If the supporting layer consists of aluminum oxide, it can be readily etched together with the PAA film. In such a case, the template removal procedure is even simpler and takes about 20 minutes.

The mentioned advantages makes “Procedure 3” a very effective procedure for the fabrication of P3HT nanostructures on P3HT thin films via template wetting.

6.4. SUMMARY AND OUTLOOK

In this chapter, different aspects of the realization of BHJ solar cells via template wetting approaches were considered.

P3HT nanotubes having diameters of 80 nm and wall thickness of 20-30 nm were successfully realized by melt-assisted wetting of thin-film PAA templates on ITO-glass substrates (“Procedure 1”). Structuring of a thin P3HT film on ITO-glass by applying a PAA template from top and heating up the “sandwiched” structure allows the fabrication of nanohillock arrays.

Using PAA templates on rigid substrates like Si (“Procedure 2”) is only suitable for small samples (less than 1 X 1 cm^2) because of difficulties with the template removal.

The use of thin-film PAA templates on thin-film supports (“Procedure 3”) facilitates the template removal procedure and allows effective formation of P3HT nanostructures over large areas. The use of this technique in the case of a PEDOT:PSS underlayer needs further optimization.

The next step in the realization of solar cell devices is the application of the electron acceptor material (typically PCBM). Finally Al top electrode is made on top by thermal evaporation and electrical contacts are made (Fig. 6.7).

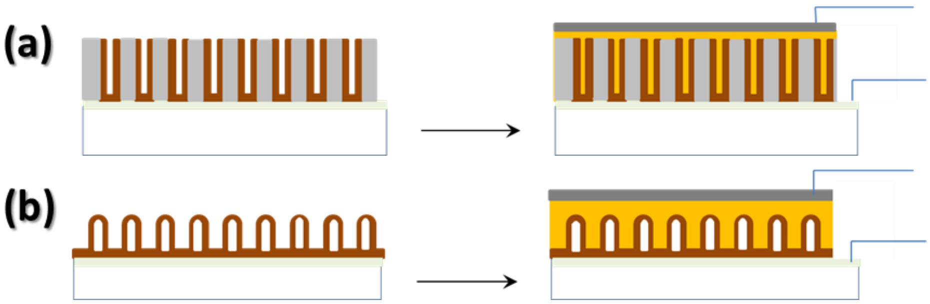

Figure 6.7. Fabrication of organic BHJ solar cells via template based approach: application of the electron acceptor material and fabrication of the top electrode for “Procedure 1” (a), “Procedure 2” and “Procedure 3” (b).

Applying the electron acceptor layer may not be straightforward. Fig. 6.8 shows arrays of P3HT nanotubes fabricated according to “Procedure 1“ and partly covered by PCBM by spin-coating. The spin-coating was made from a saturated solution of PCBM in dichloromethane at 900 rpm for 2 min. It can be seen that the PCBM film is not continuous and there are big areas on the PAA template surface which are not covered at all. It is also unclear whether the PCBM has filled the P3HT nanotubes or not. Apparently the time used for spin-coating was not enough to allow the filling of the P3HT nanotubes. Besides that, the amount of PCBM which was supplied from one droplet during the spin-coating was not enough to cover the surface of the PAA template completely. On the other hand, prolonged exposure of the P3HT nanotubes to the dichloromethane-based solution and/or applying PCBM from several droplets will most probably lead to the partial dissolution of these structures.

The alternative method of applying the electron acceptor material is vacuum evaporation. In such a case, fullerene C_{60} can be used instead of PCBM. If the aspect ratios of the P3HT nanotubes don't exceed 2 or 3, one could expect that the nanotubes as well as the space between them will be filled.

The performance of the solar cell architectures discussed in this chapter should be checked by conducting relevant electrical measurements on the samples having different sizes of the P3HT nanotubes and different spacing between them.

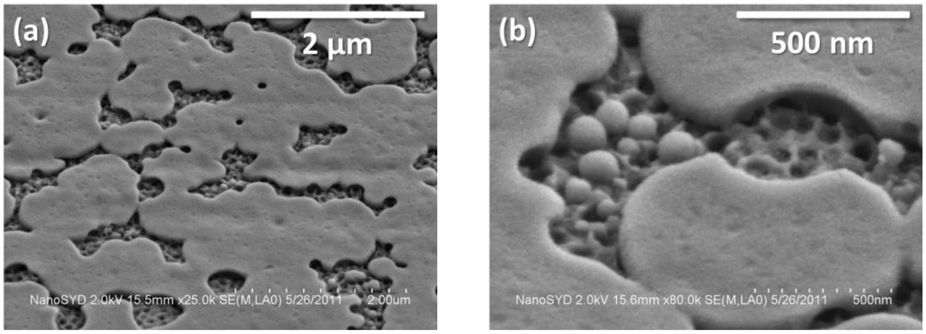

Figure 6.8. P3HT nanotube arrays fabricated according to "Procedure 1" and partly covered by PCBM by spin-coating.

7. Conclusions

This thesis is focused on the fabrication of thin-film porous anodic alumina (PAA) templates on different substrates. The influence of different parameters on the quality of the PAA templates was investigated. The preparation of organic nanowires and nanotubes via melt- or solution-assisted wetting of PAA templates was also studied.

The structure and surface morphology of thin evaporated Al films depend strongly on the deposition rate, temperature and type of the substrate. The overall surface roughness of the films increases monotonically with increasing the deposition rate from 0.1 to 2 nm/s. Heating of the substrate up to 350-450°C during the evaporation of Al results in the formation of big faceted Al grains. A similar structure is obtained if the substrate is placed very close to the evaporation source and is intensively heated by the radiation from the source. For low deposition rates (0.1-0.2 nm/s) the roughness of the films correlates well with the roughness of the bare substrates.

In general, maintaining low deposition rate, low substrate temperature and low residual gas pressure allows the fabrication of smooth Al films with low grain size.

The morphology of the thin-film PAA structures, obtained by anodization of either Al foils or thin Al films, depends on the anodization conditions, such as type of the electrolyte, voltage and time.

The structure of thin Al films used for the anodization determines the morphology of the formed PAA films to a large extent. Adjusting the anodization conditions (in particular the electrolyte and the anodization voltage) against to the average grain size in the Al film allows the fabrication of well-ordered PAA structures. On the other hand, using Al films with a definite grain size is the way to obtain highly ordered PAAs at given anodization conditions.

The critical point in the fabrication of thin-film PAA templates on conductive substrates is the thickness of the Ti adhesion layer between the Al and the ITO and the voltage during the anodization. The proper adhesion of Al to ITO with an ultra-thin (1-2 nm) Ti layer can be achieved by post-depositional thermal annealing at 100-150°C for a few hours. The thickness uniformity for PAA films prepared in oxalic acid at high voltages (50-60 V) can be improved by lowering the voltage down to 30 V at the end of the anodization.

Thin-film PAA templates on free-standing thin-film SiO_x or Al_2O_3 supporting layers were successfully fabricated by a novel technique, which employed the use of water-soluble NaCl release layers. Films of evaporated SiO_x and Al_2O_3 can act as appropriate supporting layers for thin Al films and subsequently fabricated PAA structures.

1D nanostructures from P3HT, PF8, DPC and PTCDI were obtained by solution- and/or melt-assisted wetting of PAA membranes. The morphologies of these nanostructures are different and depend on the type of material and the fabrication conditions. For DPC nanowires, which were obtained for the first time by this technique, it was demonstrated, that the length of the nanowires depends on the concentration of the wetting solution. The obtained nanowires show strong polarization anisotropy. Detailed analysis of the temperature dependent PL spectra from the as-prepared DPC nanowires reveals many of the trends reported for p-6P nanofibers, namely blue shifts and narrowing of the spectral peaks with decreasing temperature and redistribution of peak intensities.

The fabrication of P3HT nanostructures for the further implementation in organic BHJ solar cells was investigated. P3HT nanotubes having diameters of 80 nm and wall thickness of 20-30 nm were successfully realized by melt-assisted wetting of thin-film PAA templates on ITO-glass substrates. Structuring of a thin P3HT film on ITO-glass by applying a PAA template from top and heating up the “sandwiched” structure allows the fabrication of nanohillock arrays. The performance of the obtained structures in real solar cell devices should be checked by conducting relevant electrical measurements on the samples having different sizes of the P3HT nanotubes and different spacing between them.

References

1. G.E.J. Poinern, N. Ali and D. Fawcett. Progress in nano-engineered anodic aluminum oxide membrane development. *Materials* 4 (2011) 487-526.
2. J.W. Diggle, T.C. Downie, and C.W. Goulding. Anodic oxide films on aluminum. *Chem. Rev.* 69 (1969) 365-405.
3. M.M. Lohrengel. Thin anodic oxide layers on aluminum and other valve metals: high field regime. *Mater. Sci. Engin. R11 (1993) 243*-294.
4. E. Palibroda, A. Lupsan, S. Pruneanu, M. Savos. Aluminium porous oxide growth. On the electric conductivity of the barrier layer. *Thin Solid Films* 256 (1995) 101-105.
5. Y.-S. Kim, S.-I. Pyun, S.-M. Moon and J.-D. Kim. The effects of applied potential and pH on the electrochemical dissolution of barrier layer in porous anodic oxide film on pure aluminium. *Corrosion Science* 38 (1996) 329-336.
6. F. Li, L. Zhang, R.M. Metzger. On the growth of highly ordered pores in anodized aluminum oxide. *Chem. Mater.* 10 (1998) 2470-2480.
7. H. Masuda, K. Fukuda. Ordered metal nanohole arrays made by a two-step replication of honeycomb structures of anodic alumina. *Science* 268 (1995) 1466-1468.
8. H. Masuda, H. Yamada, M. Satoh, H. Asoh, M. Nakao, T. Tamamura. Highly ordered nanochannel-array architecture in anodic alumina. *Appl. Phys. Lett.* 71 (1997) 2770-2772.
9. PCT/EP2007/006768. A method of manufacturing a self-ordered porous structure of aluminum oxide, a nanoporous article and a nano object.
10. T.T. Xu, R.D. Piner, R.S. Ruoff. An improved method to strip aluminum from porous anodic alumina films. *Langmuir* 19 (2003) 1443-1445.
11. Y. Zhao, M. Chen, Y. Zhang, T. Xu, W. Liu. A facile approach to formation of through-hole porous anodic aluminum oxide film. *Mater. Lett.* 59 (2005) 40-43.
12. T. Xu, G. Zangari, and R.M. Metzger. Periodic holes with 10 nm diameter produced by grazing Ar^+ ion milling of the barrier layer in hexahonally ordered nanoporous alumina. *Nano Lett.* 2 (2002) 37-41.
13. M. Lillo, D. Losic. Ion-beam pore opening of porous anodic alumina: the

formation of single nanopore and nanopore arrays. *Mat. Lett.* 63 (2009) 457-460.

14. H. Asoh, M. Matsuo, M. Yoshihama, and S. Ono. Transfer of nanoporous pattern of anodic porous alumina into Si substrate. *Appl. Phys. Lett.* 83 (2003) 4408-4410.
15. P.K. Karahaliou, M. Theodoropoulou, C.A. Krontiras, N. Xanthopolos, S.N. Georga, M.N. Pisanias, M. Kokonou, A.G. Nassiopoulou, and A. Travlos. Transient and alternating current conductivity of nanocrystalline porous alumina thin films on silicon, with embedded silicon nanocrystals. *J. Appl. Phys.* 95 (2004) 2776-2780.
16. M. Kokonou, A.G. Nassiopoulou and K.P. Giannakopoulos. Ultra-thin porous anodic alumina films with self-ordered cylindrical vertical pores on a p-type silicon substrate. *Nanotechnology* 16 (2005) 103-106.
17. H. Shiraki, Y. Kimura, H. Ishii, S. Ono, K. Itaya, M. Niwano. Investigation of formation processes of an anodic porous alumina film on a silicon substrate. *Appl. Surf. Sci.* 237 (2004) 369-373.
18. B. Das. Investigation of nanoporous thin-film alumina templates. *J. Electrochem. Soc.* 151 (2004) D46-D50.
19. PCT/US2002/037732. Thick porous anodic alumina films and nanowire arrays grown on a solid substrate.
20. H. Asoh, K. Sasaki, S. Ono. Electrochemical etching of silicon through anodic porous alumina. *Electrochemistry Communications* 7 (2005) 953-956.
21. A. Vlad, M. Mátéfi-Tempfli, S. Faniel, V. Bayot, S. Melinte, L. Piraux and S. Mátéfi-Tempfli. Controlled growth of single nanowires within a supported alumina template. *Nanotechnology* 17 (2006) 4873-4876.
22. M. Kokonou, K.P. Giannakopoulos, A.G. Nassiopoulou. Few nanometer thick anodic porous alumina films on silicon with high density of vertical pores. *Thin Solid Films* 515 (2007) 3602-3606.
23. M. Kokonou, A.G. Nassiopoulou. Nanostructuring Si surface and Si/SiO$_2$ interface using porous-alumina-on-Si template technology. Electrical characterization of Si/SiO$_2$ interface. *Physica* E 38 (2007) 1-5.
24. S. Ono, A. Oide, H. Asoh. Nanopatterning of silicon with use of self-organized porous alumina and colloidal crystals as mask. *Electrochim. Acta.* 52 (2007) 2898-2904.
25. F. Zacharatos, V. Gianneta and A.G. Nassiopoulou. Highly ordered hexagonally arranged nanostructures on silicon through a self-assembled

silicon-integrated porous anodic alumina masking layer. *Nanotechnology* 19 (2008) 1-4.

26. M. Kokonou, C. Rebholz, K.P. Giannakopoulos, C.C. Doumanidis. Low aspect-ratio porous alumina templates. *Microelectron. Eng.* 85 (2008) 1186-1188.
27. T.R.B. Foong, A. Sellinger, and X. Hu. Origin of the bottlenecks in preparing anodized aluminum oxide (AAO) templates on ITO glass. *ACS Nano* 2 (2008) 2250-2256.
28. P. Liu, V.P. Singh and S. Rajaputra. Barrier layer non-uniformity effects in anodized aluminum oxide nanopores on ITO substrates. *Nanotechnology* 21 (2010) 1-8
29. J.J. Hill, K. Haller, and K.J. Ziegler. Direct fabrication of high-aspect ratio anodic aluminum oxide with continuous pores on conductive glass. *J. Electrochem Soc.* 158 (2011) E1-E7.
30. M.M. Couse, A.E. Miller, D.T. Crouse, and A.A. Ikram. Nanoporous alumina template with in situ barrier oxide removal, synthesized from a multilayer thin film precursor. *J. Electrochem Soc.* 152 (2005) D167-D172.
31. O. Jessensky, F. Müller, and U. Gösele. Self-organized formation of hexagonal pore arrays in anodic alumina. *Appl. Phys. Lett.* 72 (1998) 1173-1175.
32. K. Nielsch, J. Choi, K. Schwirn, R.B. Wehrspohn, and U. Gösele. Self-ordering regimes of porous alumina: the 10% porosity rule. *Nano Lett.* 2 (2002) 677-680.
33. Z. Su, G. Hähner and W. Zhou. Investigation of the pore formation in anodic aluminium oxide. *J. Mat. Chem.* 18 (2008) 5787-5795.
34. M.A. Kashi and A. Ramazani. The effect of temperature and concentration on the self-organized pore formation in anodic alumina. *J. Phys. D: Appl. Phys.* 38 (2005) 2396-2399.
35. M.A. Kashi, A. Ramazani, M. Rahmandoust and N. Noormohammadi. The effect of pH and composition of sulphuric-oxalic acid mixture on the self-ordering configuration of high porosity alumina nanohole arrays. *J. Phys. D: Appl. Phys.* 40 (2007) 4625-4630.
36. A. Belwalkar, E. Grasing, W. Van Geertruyuden, Z. Huang, W.Z. Misiolek. Effect of processing parameters on pore structure and thickness of anodic aluminum oxide (AAO) tubular membranes. *Journal of Membrane Science* 319 (2008) 192-198.

37. A. Rauf, M. Mehmood, M.A. Rasheed, M. Aslam. The effects of electropolishing on the nanochannel ordering of the porous anodic alumina prepared in oxalic acid. *J. Solid State Electrochem.* 13 (2009) 321-332.
38. D. Ma, S. Li, C. Liang. Electropolishing of high-purity aluminium in perchloric acid and ethanol solutions. *Corrosion Science* 51 (2009) 713-718.
39. C.R. Martin. Membrane-based synthesis of nanomaterials. *Chem. Mater.* 8 (1996) 1739-1746.
40. G. Cao, D. Liu. Template-based synthesis of nanorod, nanowire, and nanotube arrays. *Advances in Colloid and Interface Science* 136 (2008) 45-64.
41. R.O. Al-Kaysi, T.H. Ghaddar, and G. Guirado. Fabrication of one-dimensional organic nanostructures using anodic aluminum oxide templates. J. Nanomat. (2009) 1-14.
42. S. Shingubara, Y. Murakami, K. Morimoto, T. Takahagi. Formation of aluminum nanodot array by combination of nanoindentation and anodic oxidation of aluminum. *Surf. Sci.* 532-535 (2003) 317-323.
43. A. Yamaguchi, K. Hotta, and N. Teramae. Optical waveguide sensor based on a porous anoduc alumina/aluminum multilayer film. *Anal. Chem.* 81 (2009) 105-111.
44. F. Trivinho-Strixino, H.A. Guerreiro, C.S. Gomes, E.C. Pereira, and F.E.G. Guimaraes. Active waveguide effects from porous alumina: an optical sensor proposition. Appl. Phys. Lett. 97 (2010) 011902.
45. G. Kartopu, M. Es-Souni, A.V. Sapelkin, and D. Dunstan. Large-scale, reliable and robust SERS-active nanowire substrates prepared using porous alumina templates. *Journal of Nanoscience and Nanotechnology* X (2007) 1-5.
46. H.-B. Xu, H.-Z. Chen, W.-J. Xu, M. Wang. Fabrication of organic copper phthalocyanine nanowire arrays via a simple AAO template-based electrophoretic deposition. *Chem. Phys. Lett.* 412 (2005) 294-298.
47. R. Bai, H.-Z. Chen, H.-B. Zhou, M.-M. Shi, M. Wang. Formation and characterization of europium bisphthalocyanine nanowires by electrophoretic deposition. *J. Cryst. Growth* 285 (2005) 183-190.
48. H.-Z. Chen, L. Cao, H.-B. Zhou, Y. Rong, M. Wang. Fabrication of gadolinium biphthalocyanine nano/microwires by electrophoretic deposition. *J. Cryst. Growth* 281 (2005) 530-537.

49. R. Bai, M. Shi, M. Ouyang, Y. Cheng, H. Zhou, L. Yang, M. Wang, H.-Z. Chen. Erbium bisphthalocyanine nanowires by electrophoretic deposition: morphology control and optical properties. *Thin Solid Films* 517 (2009) 2099-2105.
50. R. Bai, M. Ouyang, R.-J. Zhou, M.-M. Shi, M. Wang, and H.-Z. Chen. Well-defined nanoarrays from an n-type organic perylene-diimide derivative for photoconductive devices. *Nanotechnology* 19 (2008) 055604.
51. M. Steinhart, R.B. Wehrspohn, U. Gösele, J.H. Wendorff. Nanotubes by template wetting: a modular assembly system. *Angew. Chem. Int. Ed.* 43 (2004) 1334-1344.
52. M. Steinhart, J.H. Wendorff, A. Greiner, R.B. Wehrspohn, K. Nielsch, J. Schilling, J. Choi, U. Gösele. Polymer nanotubes by wetting of ordered porous templates. *Science* 296 (2002) 1997.
53. S. Schlitt, A. Greiner, and J.H. Wendorff. Cylindrical polymer nanostructures by solution template wetting. *Macromolecules* 41 (2008) 3228-3234.
54. D. O’Carrol and G. Redmond. Highly anisotropic luminescence from poly(9,9-dioctylfluorene) nanowires doped with orientationally ordered *β*-phase polymer chains. *Chem. Mater.* 20 (2008) 6501-6508.
55. D. O’Carrol, D. Iacopino, A. O’Riordan, P. Lovera, E. O’Connor, G.A. O’Brien, and G. Redmond. Poly(9,9-dioctylfluorene) nanowires with pronounced *β*-phase morphology: synthesis, characterization, and optical properties. *Adv. Mater.* 20 (2008) 42-48.
56. S. Moynihan, D. Iacopino, D. O’Carrol, P. Lovera, and G. Redmond. Template synthesis of highly oriented polyfluorene nanotube arrays. *Chem. Mater.* 20 (2008) 996-1003.
57. L. Zhao, W. Yang, Y. Ma, J. Yao, Y. Li, and H. Liu. Perylene nanotubes fabricated by the template method. *Chem. Commun.* (2003) 2442-2443.
58. C. Barret, D. Iacopino, D. O’Carrol, G. De Marzi, D.A. Tanner, A.J. Quinn, and G. Redmond. Synthesis of pentacene nanotubes by melt-assisted template wetting. *Chem. Mater.* 19 (2007) 338-340.
59. X.-P. Shen, G. Yin, C. Gao, Z. Xu. Construction and fluorescence of organic nanotube arrays by template-based physical vapor deposition method. *Mat. Chem. Phys.* 113 (2009) 202-207.
60. F. Ericson, N. Kristensen, J.-Å. Schweitz, U. Smith. A transmission electron microscopy study of hillocks in thin aluminum films. *J. Vac. Sci.*

Technol. B 9 (1991) 58-63.

61. G. Hass and J.E. Waylonis. Optical constants and reflectance and transmittance of evaporated aluminum in the visible and ultraviolet. *J. Opt. Soc. Am.* 51 (1961) 719-722.
62. K. Guenther, I. Penny, R.R. Willey. Corrosion-resistant front surface aluminum mirror coatings. *Optical Engineering* 32 (1993) 547-552.
63. C.W. Hollars and R.C. Dunn. Evaluation of thermal evaporation conditions used in coating aluminum on near-field fiber-optic probes. *Rev. Sci. Instrum.* 69 (1998) 1747-1752.
64. V. Starý. Epitaxial growth of Al thin films on mica and investigation of film structure. *Czech. J. Phys. B* 26 (1976) 882-889.
65. P.A. Flinn, D.S. Gardner, and W.D. Nix. Measurement and interpretation of stress in aluminum-based metallization as a function of thermal history. *IEEE Trans. Electron Devices*, V. ED-34, No.3, March 1987.
66. M. Higo, X. Lu, U. Mazur, and K.W. Hipps. Preparation of atomically smooth aluminium films: characterization by transmission electron microscopy and atomic force microscopy. *Langmuir* 13 (1997) 6176-6182.
67. P. Quintana, A.I. Oliva, O. Ceh, and J.E. Corona. Thickness effects on aluminum thin films. *Superficies y Vacio* 9 (1999) 280-282.
68. N.G. Semaltianos. Thermally evaporated aluminium thin films. *Appl. Surf. Sci.* 183 (2001) 223-229.
69. H. Qui, F. Wang, P. Wu, L. Pan, L. Li, L. Xiong, Y. Tian. Effect of deposition rate on structural and electrical properties of Al films deposited on glass by electron beam evaporation. *Thin Solid Films* 414 (2002) 150-153.
70. M. Aguilar, P. Quintana, and A.I. Oliva. Thickness-stress relations in aluminum thin films. *Materials and Manufacturing Processes* 17 (2002) 57-65.
71. M. Higo, K. Fujita, M. Mitsushio, T. Yoshidome, T. Kakoi. Epitaxial growth and surface morphology of aluminum films deposited on mica studied by transmission electron microscopy and atomic force microscopy. *Thin Solid Films* 516 (2007) 17-24.
72. S.-J. Hwang, J.-H. Lee, C.-O. Jeong, and Y.-C. Joo. Effect of film thickness and annealing temperature on hillock distributions in pure Al films. *Scripta Materialia* 56 (2007) 17-20.
73. G. Guisbiers, O. Van Overschelde, M. Wautelet, Ph. Leclère, and R.

Lazzaroni. Fractal dimension, growth mode and residual stress of metal thin films. *J. Phys. D: Appl. Phys.* 40 (2007) 1077-1079.

74. S. Hosseinabadi, A. Mortezaaliand, A.A. Masoudi. Investigating aluminum thin films properties by stochastic analysis. *Surf. Interface Anal.* 40 (2008) 71-75.
75. F.M. D'Heurle. Aluminum films deposited by RF sputtering. *Metallurgical Transactions* 1 (1970) 725-732.
76. A.G. Blachman. DC bias-sputtered aluminum films. *J. Vac. Sci. Technol.* 10 (1973) 299-302.
77. M. Furukawa, Y. Yamamoto, H. Ikakura, N. Tanaka, M. Hashimoto, A. Sano, and S. Shingubara. Surface morphologies of sputter-deposited aluminum films studied using a high-resolution phase-measuring laser interferometric microscope. *Appl. Opt.* 35 (1996) 701-707.
78. D.L. Rode, V.R. Gaddam, and J.H. Yi. Subnanometer surface roughness of DC magnetron sputtered Al films. *J. Appl. Phys.* 102 (2007) 024303.
79. J. Podbrdský, V. Drahoš. Electron microscope study of aluminium films evaporated on air-cleaved sodium chloride. *Czech. J. Phys. B* 19 (1969) 217-221.
80. D.J. Semin, and K.L. Rowlen. Influence of vapor deposition parameters on SERS active Ag film morphology and optical properties. *Anal. Chem.* 66 (1994) 4324-4331
81. M. Higo, K. Fujita, Y. Tanaka, M. Mitsushio, T. Yoshidome. Surface morphology of metal films deposited on mica at various temperatures observed by atomic force microscopy. *Appl. Surf. Sci.* 252 (2006) 5083-5099.
82. K. Cai, M. Müller, J. Bossert, A. Rechtenbach, K.D. Jandt. Surface structure and composition of flat titanium films as a function of film thickness and evaporation rate. *Appl. Surf. Sci.* 250 (2005) 252-267.
83. Metals Hanbook: Volume 5. Surface cleaning, finishing and coating. American Society for Metals, 1982, 715 p.
84. Gwyddion – Free SPM data analysis software, http://gwyddion.net/
85. B.A. Movchan, A.V. Demchishin. Poluchenie pokrytij pri vakuumnoj kondensatsii metallov i splavov. *Phys. Met. Metallogr.* 28 (1969) 83-90.
86. J.A. Thornton. High rate thick film growth. *Ann. Rev. Mat. Sci.* 7 (1977) 239-260.
87. J.A. Thornton. The microstructure of sputter-deposited coatings. *J. Vac. Sci. Technol. A* 4 (1986) 3059-3065.

88. K.L. Westra, D.J. Thomson. The microstructure of thin films observed using atomic force microscopy. *Thin Solid Films* 257 (1995) 15-21.

89. D.L. Smith. Thin-film deposition: principles and practice. McGraw-Hill, Inc., New York, 1995. 616 p.

90. S. Sellner, A. Gerlach, S. Kowarik, F. Schreiber, H. Dosch, S. Meyer, J. Pflaum, G. Ulbricht. Comparative study of the growth of sputtered aluminum oxide films on organic and inorganic substrates. *Thin Solid Films* 516 (2008) 6377-6381

91. Y.F. Mei, X.L. Wu, X.F. Shao, G.S. Huang, G.G. Siu. Formation mechanism of alumina nanotube array. *Phys. Lett.* A 309 (2003) 109-113.

92. H. Masuda, H. Asoh, M. Watanabe, K. Nishio, M. Nakao, and T. Tamamura. Square and triangular nanohole array architectures in anodic alumina. *Adv. Mater.* 13 (2001) 189-192.

93. H. Asoh, S. Ono, T. Hirose, M. Nakao, H. Masuda. Growth of anodic porous alumina with square cells. *Electrochim. Acta* 48 (2003) 3171-3174.

94. R.C. Furneaux, W.R. Rigby, and A.P. Davidson. The formation of controlled-porosity membranes from anodically oxidized aluminum. *Nature* 337 (1989) 147-149.

95. J.H. Yuan, W. Chen, R.J. Hui, Y.L. Hu, and X.H. Xia. Mechanism of one-step voltage pulse detachment of porous anodic alumina membranes. *Electrochim. Acta* 51 (2006) 4589-4595.

96. M. Tian, S. Xu, J. Wang, N. Kumar, E. Wertz, Q. Li, P.M. Campbell, M.H.W. Chan, and T.E. Mallouk. Penetrating the oxide barrier in situ and separating freestanding porous anodic alumina films in one step. *Nano Lett.* 5 (2005) 697-703.

97. C.-S. Toh, B.M. Kayes, E.J. Nemanick, and N.S. Lewis. Fabrication of free-standing nanoscale alumina membranes with controllable pore aspect ratios. *Nano Lett.* 4 (2004) 767-770.

98. X. Jiang, N. Mishra, J.N. Turner, and M.G. Spencer. Freestanding alumina membrane by double-layer anodization. *IEEE Trans. Nanotechnol.* 6 (2007) 328-333.

99. S. Mátéfi-Tempfli, and M. Mátéfi-Tempfli. Vertically aligned nanowires on flexible silicone using a supported alumina template prepared by pulsed anodization. *Adv. Mater.* 21 (2009) 1-6.

100. S. Metz, A Bertsch, and P. Renaud. Partial release and detachment of microfabricated metal and polymer structures by anodic metal dissolution.

Journal of microelectromechanical systems 14 (2005) 383-391.

101. E. Patrick, V. Sankar, W. Rowe, S.-F. Yen, J.C.Sanchez, and T. Nishida. Flexible polymer substrate and tungsten microelectrode array for an implantable neural recording system. 30th Annual International IEE EMBS Conference. Vancouver, British Columbia; Canada, August 20-24, 2008.
102. V. Linder, B.D. Gates, D. Ryan, B.A. Parviz, and G.M. Whitesides. Water-soluble sacrificial layers for surface micromachining. *Small* 1 (2005) 730-736.
103. US 2009/0236310 A1. Adjustable solubility in sacrificial layers for microfabrication.
104. A.H.F. Muggleton. Deposition techniques for the preparation of thin film nuclear tatgets. *Vacuum* 37 (1987) 785-817.
105. T. Tepper, D. Shechtman, D. Van Heerden, D. Josell. fcc titanium in titanium/silver multilayers. *Mater. Lett.* 33 (1997) 181-184.
106. US 7943194 B2. Process for preparing flake-form pigments based on aluminum and on SIOZ(Z=0,7-2,0) comprising forming a layer of separating agent.
107. P. Bujard and H. Hoppe. SiO_2 as gas barrier and nano holes in SiO_2 flakes. *J. Phys.: Conference Series* 61 (2007) 166-169.
108. S.R. Forrest. The path to ubiquitous and low-cost organic electronic applications on plastic. *Nature* 428 (2004) 911–918.
109. A.P.H.J. Schenning, E.W. Meijer. Supramolecular electronics: nanowires from self-assembled p-conjugated systems. *Chem. Commun*. (2005) 3245–3258.
110. J.H. Schön, A. Dodabalapur, C. Kloc, B. Batlogg. A Light-Emitting Field-Effect Transistor. *Science* 290 (2000) 963 – 965.
111. N. Tessler. Lasers based on semiconducting organic materials. *Adv. Mater*. 11 (1999) 363-370.
112. M.T. Dang, L. Hirsch, and G. Wantz. P3HT:PCBM, best seller in polymer photovoltaic research. *Adv. Mater.* 23 (2011) 3597-3602.
113. J. Li and A.C. Grimsdale. Carbazole-based polymers for organic photovoltaic devices. *Chem. Soc. Rev.* 39 (2010) 2399-2410.
114. J. Li, F. Dierschke, J. Wu, A.C. Grimsdale and K. Müllen. Poly(2,7-carbazole) and perylene tetracarboxydiimide: a promising donor/acceptor pair for polymer solar cells. *J. Mater. Chem.* 16 (2006) 96-100.
115. J.Y. Kim, A.J. Bard. Organic donor/acceptor heterojunction photovoltaic

devices based on zinc phthalocyanine and a liquid crystalline perylene diimide. *Chem. Phys. Lett.* 383 (2004) 11-15.

116. http://www.mpi-halle.mpg.de
117. I. Wallmann, G. Schnakenburg, A. Lützen, Synthesis of functionalized oligophenylenes and oligoarylenes bearing heteroaryl groups, *Synthesis* 1, (2009) 79-84.
118. A. Ghazal. Organic Molecular Nanotechnology. Bachelor Thesis. University of Southern Denmark, 2009.
119. K. Bordo, M. Schiek, A. Ghazal, I. Wallmann, A. Lützen, F. Balzer, and H.-G. Rubahn. Parallelly and normally surface-aligned organic nanofiber arrays. *J. Phys. Chem. C*, 115 (2011) 20882-20887.
120. J. Beermann, S.I. Bozhevolnyi, V.G. Bordo, H.-G. Rubahn. Two-photon mapping of local molecular orientations in hexaphenyl nanofibers. *Opt. Commun.* 237 (2004) 423-429.
121. J. Beermann, S.I. Bozhevolnyi, F. Balzer, H.-G. Rubahn. Two-photon near-field mapping of local molecular orientations in hexaphenyl nanofibers. *Laser Phys. Lett.* 2 (2005) 480-484.
122. S. Guha, J.D. Rice, Y.T. Yau, C.M. Martin, M. Chandrasekhar, H.R. Chandrasekhar, R. Guentner, P. Scanduicci de Freitas, and U. Scherf. Temperature-dependent photoluminescence of organic semiconductors with varying backbone conformation. *Phys. Rev.* B 67 (2003) 125204.
123. F. Balzer, A. Pogantsch, H.-G. Rubahn. Temperature dependent analysis of three classes of fluorescence spectra from p-6P nanofiber films. *Journal of Luminescence* 129 (2009) 784-7.
124. J.S. Kim, Y. Park, D.Y. Lee, J.H. Lee, J.H. Park, J.K. Kim, and K. Cho. Poly(3-hexylthiophene) nanorods with aligned chain orientation for organic photovoltaics. *Adv. Funct. Mater.* 20 (2010) 540-545.
125. W. Wiedermann, L. Sims, A. Abdelilah, A. Exner, R. meier, K.P. Musselman, J.L. MacManus-Driscoll, P. Müller-Buschbaum, G. Scarpa, P. Lugli, and L. Schmidt-Mende. Nanostructured interfaces in polymer solar cells. *Appl. Phys. Lett.* 96 (2010) 263109.
126. C.J. Brabec, N.S. Sariciftci, and J.C. Hummelen. Plastic solar cells. *Adv. Funk. Mater.* 11 (2001) 15-26.
127. S. Günes, H. Neugebauer, and N.S.Sariciftci. Conjugated polymer-based organic solar cells. *Chem. Rev.* 107 (2007) 1324-1338.
128. S. Jenekhe, X.L. Chen. Self-assembled aggregates of rod-coil block copolymers and their solubilization and encapsulation in fullerenes.

Science 279 (1998) 1903-1907.

129. A. Tracz, J. Jeszka, M. Watson, W. Pisula, K. Mullen, T. Pakula. Uniaxial alignment of the columnar super-structure of a hexa (alkyl) hexa-*peri*-hexabenzocoronene on untreated glass by simple solution processing. *J. Am Chem. Soc.* 125 (2003) 1682-1683.
130. US 6946597 B2. Photovoltaic devices fabricated by growth from porous template.
131. K. Coakley, B. Srinivasan, J. Ziebarth, C. Goh, Y. Liu, and M.D. McGehee. Enhanced hole mobility in regioregular polythiophene infiltrated in straight nanopores. *Adv. Funct. Mater.* 15 (2005) 1927-1932.
132. G. O'Brien, A. Quinn, D. Iacopino, N. Pauget and G. Redmond. Polythiophene mesowires: synthesis by template wetting and local electrical characterization of single wires. *J. Mater. Chem.* 16 (2006) 3237-3241.
133. H.-S. Wang, L.-H. Lin, S.-Y. Chen, Y.-L. Wang and K.-H. Wei. Ordered polythiophene/fullerene composite core-shell nanorod arrays for solar cell applications. *Nanothechnology* 20 (2009) 075201.
134. A. Santos, P. Formentin, J. Pallares, J. Ferre-Borrull, L.F. Marsal. Quasi-ordered P3HT nanopillar-nanocap structures with controlled size. *Mater. Lett.* 64 (2010) 371-374.

Appendix A. List of publications

I. Journal articles, to be submitted:

1. K. Bordo, M. Schiek and H.-G. Rubahn, “Thin-film porous anodic alumina templates on free-standing thin-film substrates”. In preparation.
2. K. Bordo, M. Schiek and H.-G. Rubahn, “Nanowires and nanotubes from conjugated organic materials fabricated by template wetting”. In preparation.

II. Journal articles, peer reviewed:

1. K. Bordo and H.-G. Rubahn, “Effect of deposition rate on structure and surface morphology of thin evaporated Al films on dielectrics and semiconductors”. *Materials Science (Medžiagotyra)* (in press).
2. K. Bordo, M. Schiek, A. Ghazal, I. Wallmann, A. Lützen, F. Balzer, and H.-G. Rubahn, “Parallelly and normally surface-aligned organic nanofiber arrays”. *J. Phys. Chem. C,* 115 (2011) 20882-20887.
3. J. Kjelstrup-Hansen, L. Tavares, R.M. de Oliveira-Hansen, X. Liu, K. Bordo and H.-G. Rubahn, “Optical properties of microstructured surface-grown and transferred organic nanofibers”. *J. Nanophoton.*, 5 (2011) 1-11.

III. Talks and poster presentations:

1. K. Bordo, M. Schiek, and H.-G. Rubahn. “Nanowires and Nanotubes by Template Wetting”. *CAU-SDU Workshop*. Sønderborg, Denmark, November 10, 2010.

2. K. Bordo, M. Schiek, M. Es-Souni, and H.-G. Rubahn. “Mesoporous thin film templates for the synthesis of nanowires and nanotubes”. *Workshop “Organic Materials for Flexible Devices”*. Sønderborg, Denmark, April 19, 2010.
3. K.V. Bordo, M. Es-Souni, S. Habouti, M. Schiek, H.-G. Rubahn. “Mesoporous thin film templates for the synthesis of nanowires and nanotubes”. *Advanced Materials and Technologies - the 12-th International Conference-School*. Palanga, Lithuania, August 27-31, 2010. Book of abstracts.
4. K.V. Bordo, M. Es-Souni, S. Habouti, M. Schiek, H.-G. Rubahn. “Mesoporous thin film templates for the synthesis of nanowires and nanotubes”. *Chemistry and Physics of Materials for Energetics. A European School in Materials Science.* Milano, Italy, September 14-19, 2009. Book of abstracts.
5. K.V. Bordo, S. Habouti, M. Schiek, H.-G. Rubahn, M. Es-Souni, “Mesoporous thin film templates for the synthesis of nanowires and nanotubes”. *3rd International Workshop on Smart Materials & Structures*. Kiel, Germany, August 19-21, 2009. Book of abstracts.

Appendix B. Temperature dependent PL spectra of DPC samples

1. PL spectra of bulk DPC

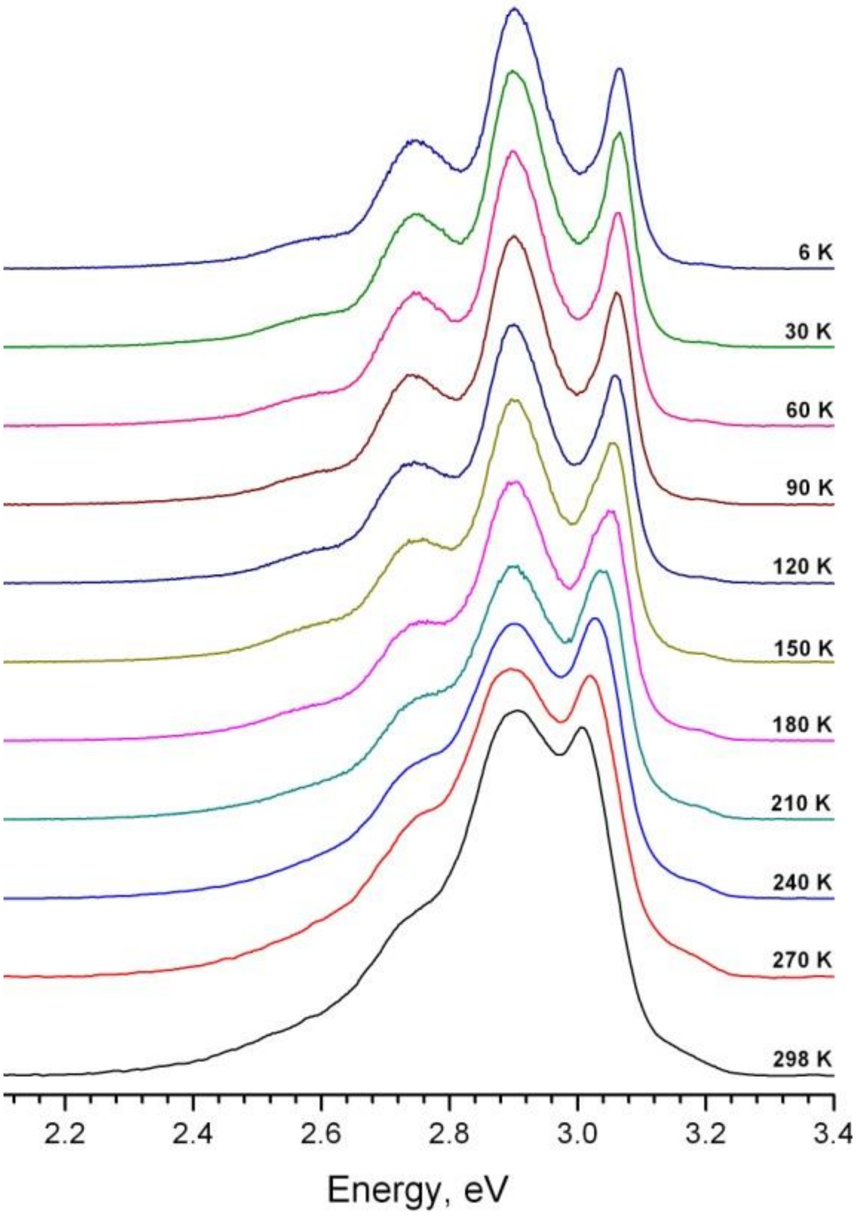

2. PL spectra of DPC nanowires obtained by template wetting

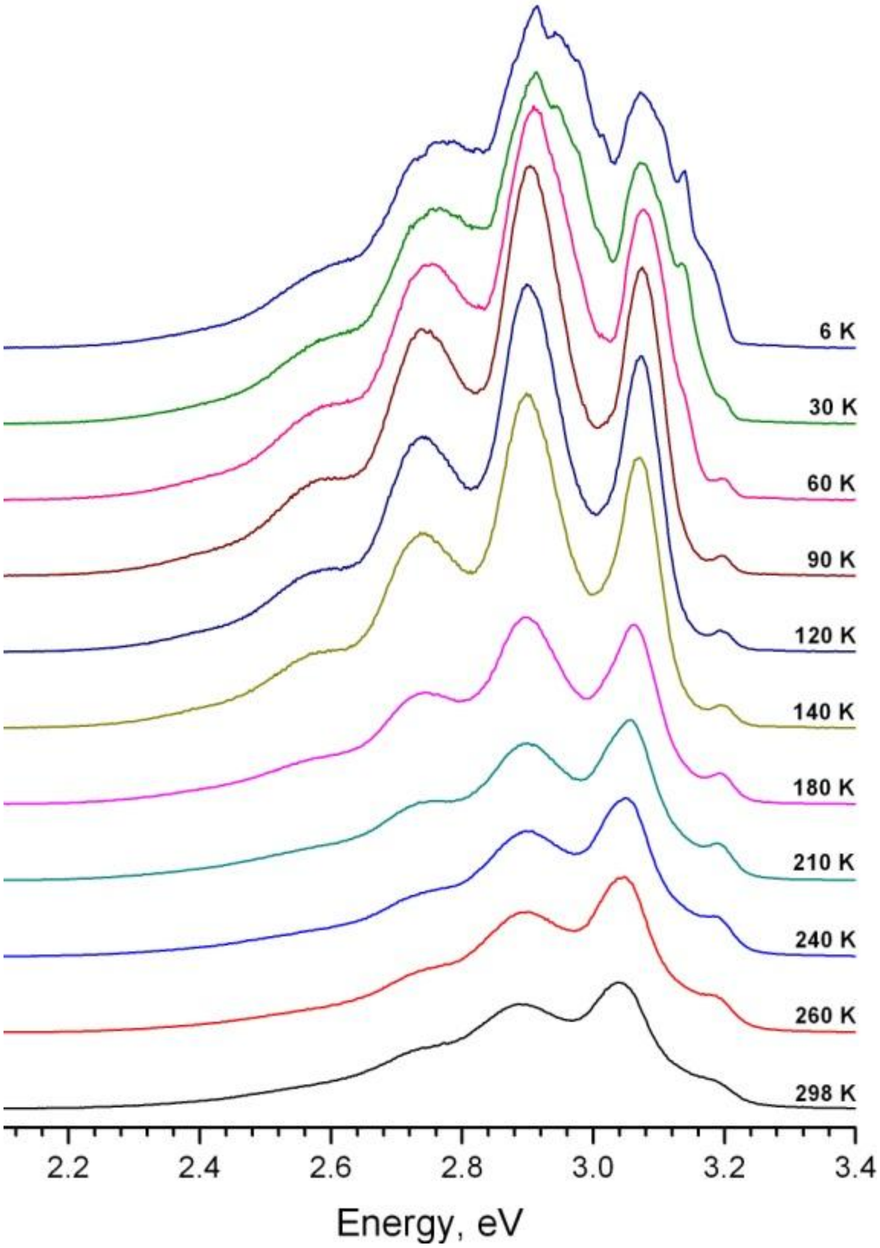

3. PL spectra of DPC nanoaggregates obtained by OMBD (substrate temperature 330 K)

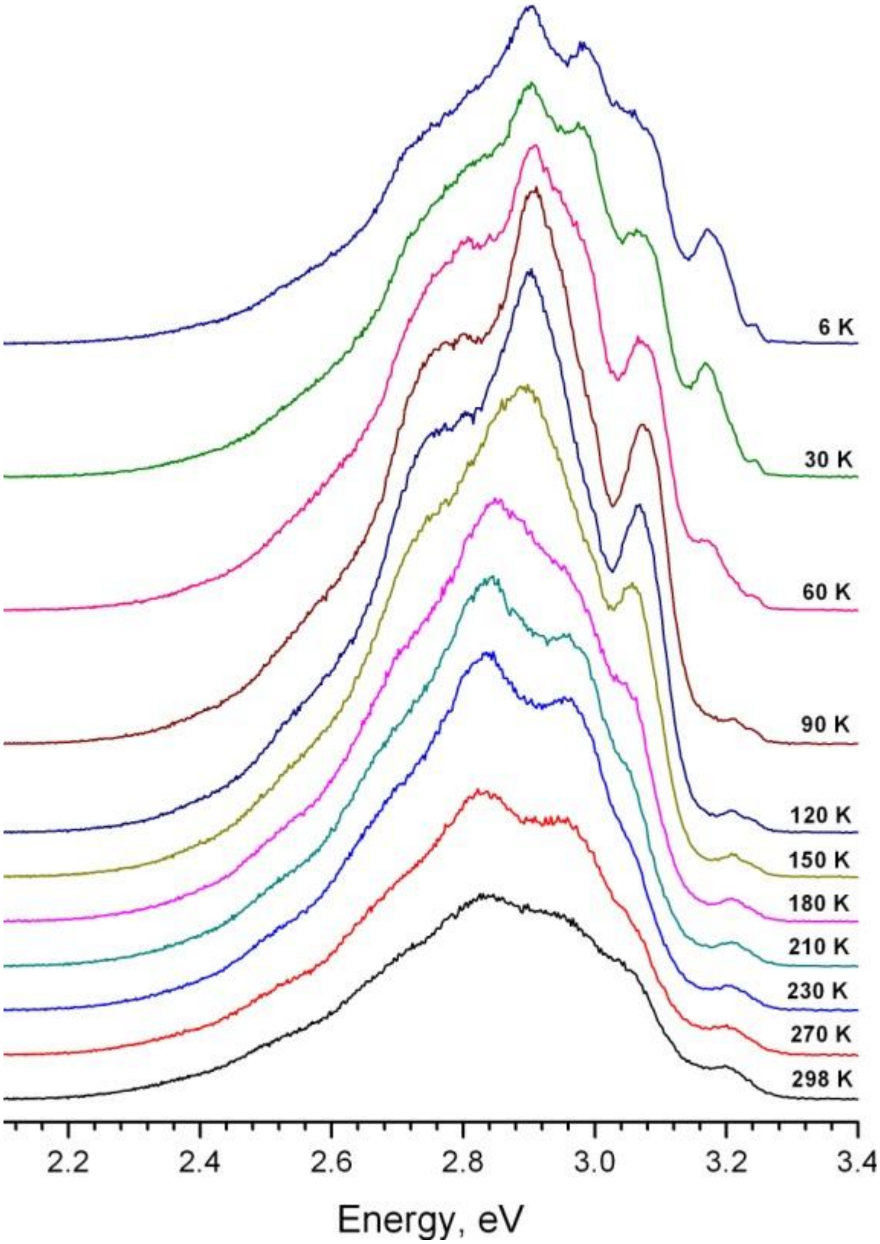

4. PL spectra of DPC nanoaggregates obtained by OMBD (substrate temperature 370 K)